INSTITUTE OF PAPER SCIENCE AND TECHNOLOGY
ATLANTA, GEORGIA

A STATISTICAL TREATMENT OF NON-NORMAL SEM DATA AND THE APPLICATION TO DESIGNED FIBER/FILLER/POLYMER STRUCTURES

Doctoral Dissertation
Submitted on December 13, 2004
Defended on November 24, 2004

Submitted to:

Dr. Timothy Patterson
Dr. Wayne Robbins
Dr. Robert Moran
Dr. Alan Rudie
Dr. Yulin Deng

Office of Academic Affairs, IPST

Submitted by:

Fern Sterling Peterson

A Statistical Treatment of non-Normal SEM Data and the Application to Designed Fiber/Filler/Polymer Structures

A Dissertation Submitted by
Fern Sterling Peterson

B.A. 1998, Saint Olaf College
Northfield, Minnesota

Masters of Science 2000, Institute of Paper Science and Technology
Atlanta, Georgia

Degree of Doctor of Philosophy 2004, Institute of Paper Science and Technology
Atlanta, Georgia

A Statistical Treatment of non-Normal SEM Data and the Application to Designed Fiber/Filler/Polymer Structures

Approved by:

_____

Dr. Timothy Patterson

_____

Dr. Wayne Robbins

_____

Dr. Robert Moran

_____

Dr. Alan Rudie

_____

Dr. Yulin Deng

Date Approved:_____

TABLE OF CONTENTS

TABLE OF FIGURES

TABLE OF TABLES

ACKNOWLEDGEMENTS

There are two groups of people I would like to thank; those who nurtured and helped me develop my intellectual capacity and academic know-how and my friends and family who let me choose my own path and supported me every step of the way.

I would like to thank the Institute of Paper Science and Technology and all the member companies for their support. Special thank you to Dr. H. Jeff Empie, who is responsible for introducing me to IPST back at Saint Olaf College. Thanks to all the research and academic faculty at IPST including Ted Jackson, Miranda Bliss, Dr. David Rothbard, and Chuck Courchene.

I greatly appreciate all the help and guidance given to us from Bowater Inc., IMERYS World Wide Paper Division and Ciba Specialty Chemicals Inc. Special thanks to Frank Foley, Leslie McLain and Paul Norton.

My committee members have been invaluable to me over the past four years. Dr. Yulin Deng was most accommodating when he agreed to fill a vacant position in the committee towards the end of the project. Dr. Robert Moran has been a great influence on this project. As an outside industry partner, his insights helped to ground this research in the real world. I truly do thank Dr. Wanye Robbins for being the first creator of the problem statement for the thesis. Without his guidance, this project would not have stayed on course and become a problem worthy of a doctorial degree. Dr. Alan Rudie has been my mentor and guiding light since I first became his intern the summer before I started here at IPST. He then became my Masters advisor and was a strong academic influence on my career here at IPST. Alan has been both a shoulder to cry on and a sounding board for issues both personal and academic. Dr. Timothy F. Patterson graciously took me and my project under his wing. When this project began, it was outside his immediate realm of interest but thanks to his knowledge and guidance, he now has his first Ph.D. student!

Last but never least I cannot possible thank my family and friends enough. They have supported me all my life and I am truly blessed to have such a wonderful family.

SUMMARY

The research pursued in this dissertation is related to a new piece of papermaking technology donated to the Institute of Paper Science and Technology (IPST) by the Procter and Gamble Company (P&) for further study. It was believed that the patentented proceses could greatly increase the filler loading of tissue sheets without reducing strength properties, bulk or softness. Unfortunately, this turned out not to be the case. Despite the technology not meeting expectations, there was still an important hypotesis contined in the patents: by manipulating the fiber/filler/polymer structure of a sheet, one could "design" the macroscopic physical properties of the sheet. A major hurdle in further testing this concept was that little was known about fiber/filler/ polymer structures. Therefore one of the primary objectives of this thesis was to design fiber/filler/polymer structures for newsprint and in the process develop a greater understanding of fiber/filler/ polymer structures. Five different designed structures were created for study. The designed structures were composed of virgin, hydrosulfite bleached, TMP southern pine, Georgian kaolin clay and various polymers. Five filler levels from 0% to 20% were employed with each of these different structures. Numerous physical tests were used to gather data which would help to develop an understanding for the macroscopic properties of the structures.

However, on a microscopic scale, there were no published techniques for getting quantitative data on the fibers, filler particles and polymers. This work developed a method for obtaining statistically significant, objective data from SEM images. The significant aspect of this method was that it greatly reduced the subjective qualities usually associated with microscopy observation. It employed statistical methods to determine the number and type of required SEM images and computer based image analysis techniques to quantify the size/shape characteristics of pertinent image features. With the knowledge of SEM and statistics, this method was the *first* to bridge the gap between them and extract quantitative data from SEM images. However, this was not an easy task because the image analysis data proved to be non-normal data with an unknown distribution. This specific application is imaging filler particles in paper, but the method could be applied to similar image types.

The method should be tested to show that it was a valid method. In order to test the method paper structures were creted and data from bulk physical tests and particle based SEM image analyses were compared Comparrisons were made using a statistical method called *Principal Component Analysis (PCA)* where the data is grouped and reduced to find data correlations not readily apparent in the raw data. There has not been a study previously where macroscopic properties (physical testing) were correlated with microscopic properties (image analysis). Several distinct correlations between selected physical testing data and image data were found. These correlations varied from designed structure designed to structure. Some of the macroscopic physical properties that correlated with the microscopic image data included:

- TAPPI and printing opacity
- Brightness
- Static and kinetic coefficient of friction
- Porosity
- Thickness
- Dry and wet tensile index
- Bending stiffness

Another imaging tool utilized for studying the designed structures was Transmission Electron Microscopy (TEM). TEM was used to visualize the polymers directly. A unique gold colloid technique was developed and preliminary results were obtained. Once this technique is fully developed, it should allow for direct visualization of polymers in paper sheets. This would identify the location of the polymers and complete the evaluation of the designed structures. Preliminary experimentsindicate some success with this method, although it was still in a very early stage of development.

1 INTRODUCTION

The ultimate goal of this work was to design fiber/filler/polymer (FFP) structures that would allow for greater levels of filler content in newsprint without significant quality reduction of sheet strength, optical properties or surface properties. When filler is introduced into a paper sheet, almost all strength properties decrease linearly with filler addition. Part of the reason for this phenomenon is because filler/fine material interrupts either fiber-to-fiber bonding, or physically lodges between fibers during the papermaking process (Scott, 1996). Often it is necessary to enhance the retention of the filler/fine material and prevent it from interfering with inter-fiber bonding through the addition of chemical polymers. Thus, it was the intent to design FFP structures that kept filler particles off the fibers, allowed for greater fiber-fiber bonded area, greater filler retention and thus enhanced sheet strength properties.

Fibers retain most of their original structure during the pulping and papermaking process and are the principal structural components of paper. As a result, their properties largely determine the properties of the finished paper sheet. Fiber properties affect the finished paper mainly in two respects; one being the formation and consolidation of the paper structure and the other being the properties of the dry paper (Retulainen, 1998).

Filler and polymers are materials added to the pulp to enhance various physical properties of the finished sheet, such as opacity and brightness. Adding filler to a sheet will decrease the size and distribution of pores, thereby increasing opacity and creating a smoother surface (Bristow, 1986). Filler material is also typically less expensive than fiber, a reality which has driven papermakers to create sheets with higher and higher filler content. Therefore, it remains an industry goal to find better fillers and methods of their incorporation into the paper structure that do not interfere with fiber to fiber bonding. Fillers are added to the sheet to improve opacity and brightness. Adding filler to a sheet will decrease the size and distribution of pores, thereby increasing opacity and creating a smoother surface (Bristow, 1986).

The actual mechanisms by which fibers, fillers and fines, and polymers interact in a paper sheet are poorly understood. Fibers have a negative surface charge in water and filler often has a negative charge in water as well. Fillers can be attached to fibers,

despite the negative charge on both constituents by using polymers and other retention mechanisms. Polymers adsorb onto cellulose and filler surfaces and variables that can affect this process include chain length, flexibility, charge distribution, acid/base equilibrium, conformation, hydrogen bonding, polymer concentration, contact time, and shear forces.

At the beginning of the project is was assumed that the patented P&G process offered new and unique retention chemistry resulting in a higher filler content and improved bulk and strength properties. What was unique about the process was the use of anionic PAM, which was originally added for softness not for retention chemistry. It was later realized that any bulk in the tissue sheet that was maintained was due to the yankee dryer creping process. As filler was added strength presumably dropped which was the reason for starch addition. There was no evidence of differences in filler location or filler particle size.

This dissertation represents a novel approach for investigating the relationship of the fiber/filler structure of several designed FFP structures formed in the laboratory. Typically a particular paper is characterized by bulk properties which provide no information on the actual FFP structure. The approach developed in this work uses scanning electron microscopy (SEM) and computerized, quantitative SEM image analysis to obtain component specific fiber and filler properties.

The thesis includes an investigation of the following hypotheses:

1. *Fiber/filler/polymer structures can be designed where the filler material is kept off the fiber material*

2. *Fiber/filler/polymer structures can be designed by using different polymers and different filler/polymer addition processes*

3. *Quantitative data can be obtained from SEM micrographs using objective and statistically sound processes*

4. *By comparing image data and physical testing data, differences in fiber/filler/polymer structures can be detected or inferred*

Chapters two through five contain the bulk of the work done and discuss the majority of the data. The experimental section, chapter two, describes the overall SEM analytical approach and the five designed structures that were created for the development of the SEM analysis. Chapter two describes the first significant contribution made by this work; the SEM method developed to obtain objective images and quantitative data. Chapter three is the application of the SEM method where quantitative physical testing data (macroscopic) was correlated with image analysis data (microscopic) revealing relationships between select physical tests and filler particles that varied from structure to structure. The application of this method and the resulting conclusions regarding the sheet structure are the second significant contribution of this work. Chapters four and five present the results and discussion of the physical testing data, SEM work, including PASS analysis and PCA analysis, respectively. Chapter six is an extension of the SEM work that describes the Transmission Electron Microscopy (TEM) based analytical technique and presents some promising preliminary results. The technique used represents a new method for employing gold colloid to mark polymers in paper structures.

1.1 Background Material

This section will discuss the components used to formulate the designed structures, including fibers, filler and polymers. Fiber properties that affect bonding are discussed as well as fiber properties in general. Aspects of filler characteristics as they relate to the designed structures are examined. Lastly, polymers and retention chemistry are discussed.

1.1.1 Fibers

Paper fibers retain most of their original structure during the papermaking process. As a result, their properties largely determine the properties of the paper sheet. Fiber properties affect the paper in mainly two respects, one being the formation and

consolidation of the paper structure and the other being the properties of the dry paper (Retulainen, 1998). The two basic groups of fibers are those from *softwood* (SWD) (gymnosperm) species, such as pines, firs, and cedars, and *hardwood* (HWD) (angiosperm) species, such as maples, oaks, poplars, and elms. Some of the most common softwoods species used for papermaking are Pines and hardwoods are Birch and Aspen. Recycled fibers are also an important fiber group to consider in papermaking.

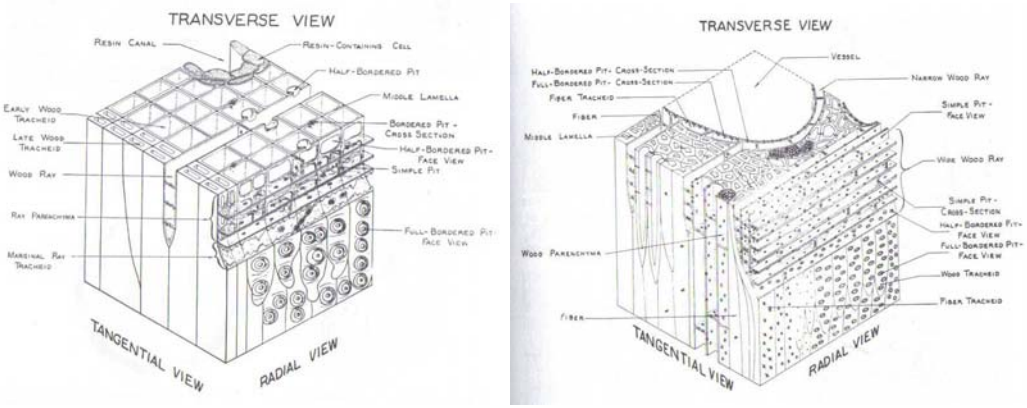

Figure 1-1: Composite wood block illustrating the structural features of a softwood and hardwood (Smook, 1997)

Fiber length is one of the most important characteristics of fibers. A long fiber has the opportunity to bond to a greater number of fibers and thereby be more strongly held in the fiber network than a short fiber. Hardwood fibers on average are shorter than softwood fibers, narrower in width, and typically have a narrower length distribution. Fiber length is the most noticeable difference between SWD and HWD fibers. Paper sheets with a higher SWD content typically have superior strength than paper sheets with a higher HWD content. Sheets with a high HWD content often have superior tactile feel, as in smoothness and softness, compared with SWD sheets. Thus linear board, sack paper and newsprint tend to have high SWD content; where as fine writing paper and tissue often contain a larger percentage of HWD fibers.

Table 1-1: Dimensional properties of plant fibers (Retulainen, 1998).

Species	Fiber length, mm	Fiber width, μm
Acacia (HWD)	0.8	14
Black alder (HWD)	1.2	28
Birch (HWD)	1.3	25
Eucalyptus (HWD)	1.1	20
European beech (HWD)	1.2	21
European aspen (HWD)	0.9	19
Balsam fir (SWD)	3.5	30-40
Parana pine (SWD)	7.2	47
European spruce (SWD)	3.5	27
Radiata pine (SWD)	2.8	37
Scots Pine (SWD)	3.6	39
Sequoia (SWD)	7.0	30-65

HWD and SWD also differ in chemical composition. There are three main components in wood fibers; cellulose, hemicellulose and lignin. Table 1-2 summarizes the different components and there abundance with in the fibers. HWD fibers have less lignin and it is generally thought that HWD fibers are more easily pulped because of the lower lignin content. Different fibers are better suited for various pulping processes because of fiber morphology, such as fiber length and lignin content. Almost all species produces good kraft pulp, where as selected HWD and SWD species are better suited for mechanical and chemimechanical pulps (Biermann, 1996).

Table 1-2: Typical compositions of North American hardwoods and softwoods (Biermann, 1996)

Component	Hardwood, (%)	Softwood, (%)
Cellulose	40-50	45-50
Hemicelluloses		
(Galacto)gulcomannans	2-5	20-25
Xylans	15-30	5-10
Lignin	18-25	25-35
Extractives	1-5	3-8
Ash	0.4-0.8	0.2-0.5

Mechanical pulps are made from a grinding/refining action as opposed to a chemical process in chemical pulping. Mechanical pulp fibers are delaminated, meaning there is internal fibrillation of the fiber wall as well as external fibrillation. TMP (thermo-mechanical pulping) is a pressurized refiner based pulping process and is the

primary process used for the production of newsprint. The chips are brought into the refiner between the two discs. At least one of the discs rotates at high speeds (1500-1800 rpm) and the chips are forced between the plates and are broken up into fibers (see Figure 1-2). In TMP, the pulp is pre-heated before it heads to the first refining stage. There the conditions are typically 300-500 kPa and 143º-158ºC. The combination of the mechanical action and heat produce the desired TMP qualities (see Figure 1-3).

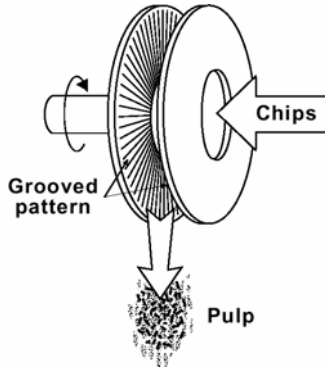

Figure 1-2: Principal of refiner mechanical pulping (Tienvieri, 1998)

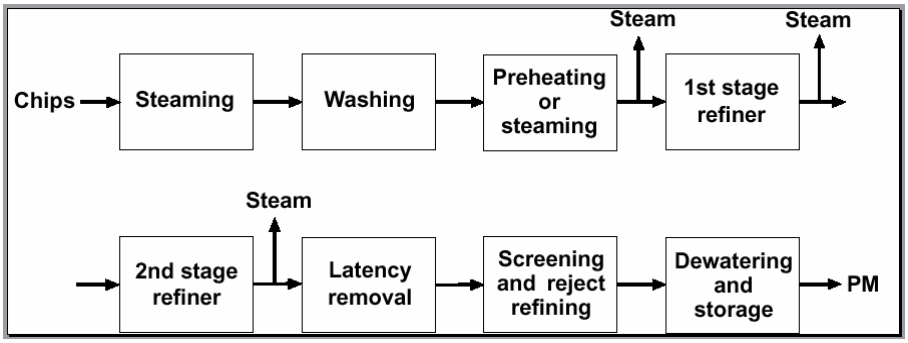

Figure 1-3: Simplified flowsheet of a typical TMP plant (Tienvieri, 1998)

Mechanical pulping produces high yields, typically 97-98% (Lindholm, 1998). It produces a sheet with high opacity, brightness, bulk, smoothness and a suitable pore

structure at low basis weights. Low basis weight with good opacity and bulk is an advantage of mechanical pulp. However, the bonding capacity of mechanical fibers is lower than for chemical pulps. They have a significantly greater amount of lignin on the fiber external surfaces and are much stiffer. Lignin interferes with the fiber to fiber bonding process because lignin does not support hydrogen bonding. The higher stiffness results in less fiber-fiber contact and less bonded area. Mechanical pulps also contain a higher percentage of fines due to the nature of the process (Sundholm, 1998).TMP has the best strength properties but the lowest optical properties. Usually TMP is best for runnability but not as good for printability. Mechanical pulps are used for entertainment and advertising in newspapers, inserts, magazines and catalogues (Hostetter, 1991). Mechanical pulps are used to a lesser extent in other paper grades (Sundholm, 1998).

1.1.2 Filler

A variety of fillers are used in the paper industry today. Fillers are pigments that are added to the sheet to improve opacity and brightness. They can also improve print quality by creating a smoother surface and more uniform ink absorption. The ideal properties of fillers are high brightness, high index of refraction (light scattering), small and uniform particle size, low water solubility, inertness, low cost, low specific gravity and high retention levels (Biermann, 1996). The shape of filler material is also important because it will affect the light scattering properties of the paper.

The white clay most commonly used in the paper industry today is called kaolin clay, which is composed of the mineral kaolinite. Kaolinite is one of the most widely occurring minerals (Drage, 2000). The largest deposits of kaolin are in England, North America (primarily Georgia) and Brazil. Kaolin deposits can be classified as primary and secondary depending on the origination of the deposit. There are some differences between the primary deposits in England and secondary deposits in North America and Brazil. North American kaolin tends to have higher brightness than English and Brazilian kaolin (Drage, 2000). Kaolin has been used in the paper industry for many years with the first recorded use in 1723 (Drage, 2000). One of the paper grades in which

kaolin is used heavily (20%-30% filler content by weight) is magazine paper grade (Eklund, 1991). Various other grades also use kaolin including newsprint.

Kaolinite has the empirical formula $Al_2O_3 \cdot 2SiO_2 \cdot 2H_2O$ (see Figure 1-4) (Biermann, 1996). The surface chemistry of kaolinite effects how the particle interacts with other particles in the papermaking furnish. The mineral has an amphoteric surface character meaning it can be cationic or anionic, depending on whether the hydroxyl (OH^-) groups are protonated or deprotonated, a function of pH. Kaolin can be processed to various grade structures, which differ by brightness level and particle size distribution. The particle shapes also differ slightly. Kaolin clay particles have many thin hexagonal plates that are laminated (stacked) or delaminated (platelets). Average aspect ratios (plate diameter:plate thickness) can vary between 10:1 and 80:1 depending on the process (Drage, 2000). Particle shape can also influence the retention of the clay (Beazley, 1998). Typically, kaolin clay with a particle size of 0.5-10 μm is suitable for filler material. Typically 49-90% of that is less than 2 μm (Biermann, 1996).

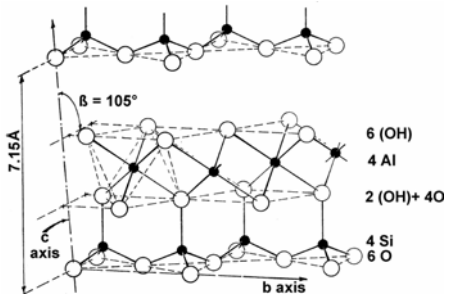

Figure 1-4: Idealized structure for the aluminium-silica layers of kaolinite (Drage, 2000)

1.1.3 Polymers and Retention Systems

Fibers have a negative surface charge in water and filler and fines often have a negative charge in water. Fines and fillers can be attached to fibers, despite negative charges on both through the use of polymers and other retention mechanisms. Some of the properties of polymers that are manipulated to enhance retention include molecular weight (MW), charge (anionic, cationic) and charge density (high, medium, low),

flexibility due to structure or conformations (architecture), and the functional groups present on the polymer chain.

Polymers adsorb on cellulose and filler surfaces in three different ways: trains (flat conformation), loops and tails as shown in Figure 1-5 (Norell, 1999). The adsorption of polymers on cellulose usually decreases as the molecular weight increases (Eklund or Scott). For example a highly charged polymer has more bonding sites and when it is added to a filler or fiber slurry it lays down flat because of its strong attraction, where a low charged polymer would be attached at a limited number of sites, creating loops and tails. The polymer tails and loops interact with the charged surfaces and form bridges in between the particles.

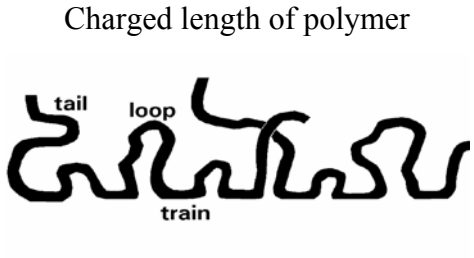

Figure 1-5: Illustration of adsorbed polymer chains on fiber with trains, loops and tails (Norell, 1999)

Flocculation, coagulation and agglomeration are the mechanisms most commonly used to describe polymer applications. Flocculation refers to the bonding of colloidal particles (fines, fillers) with polymer. However, before flocculation occurs adsorption is needed. This is a physical phenomenon governed by Van der Waals verses electrostatic (coulombic) forces. It works quickly and seconds after addition, adsorption on the fibers is achieved. Variables that can affect these mechanisms include chain length, charge distribution, conformation, hydrogen bonding, and polymer concentration.

These three mechanisms also depend on how the polymer interacts with the solvent in solution. Favorable solvent interaction allows the polymer chain to spread out. Unfavorable solvent interaction changes the conformation of the polymer hindering absorption. Unfavorable interaction results in a smaller surface area which reduces the

polymer's ability to promote flocculation. In papermaking the solvent is water. Clean water is a good solvent. In papermaking, the solvent is water. During papermaking, however, the white water can develop a build up of salts, causing undesirable curling of polymer chains.

A polymer's functional groups determine the charge on each polymer. Anionic polymers are pH dependent, consisting mainly of carboxylic acids, and thus can be protonated at higher pHs (see Figure 1-6). Cationic polymers primarily consist of tertiary amines or quaternary amines which are always positive. In a typical anionic polymer, ~30% of units carry charge (-COOH, $-SO_3H$). For cationic polymers, 4-10% of units carry charge (ammonium chlorides, quaternary amines).

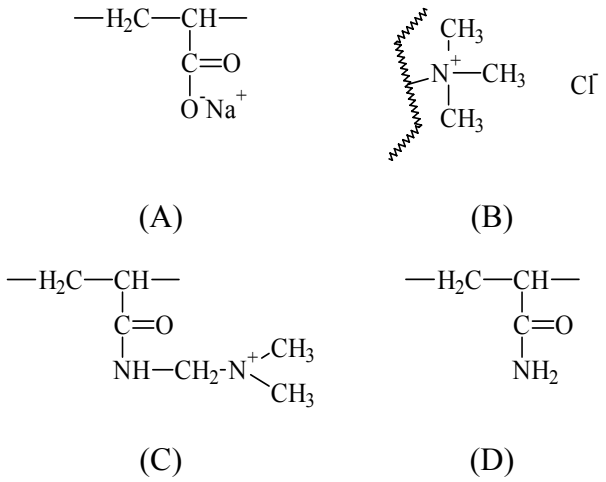

Figure 1-6: (A) A-PAM; (B) Quaternary Amine; (C) C-PAM; (D) PAM (Eklund, 1991).

The physical characteristics of polymers that are important to flocculation include molecular weight, conformation, charge density and size. Chemical properties that are important to flocculation include molecular structure, bond strength and functional groups.

Three types of flocculation mechanisms include charge neutralization, patch and bridge. Charge neutralization occurs when components of the same electrostatic charge repel each other until this charge is neutralized at which point the attractive forces dominate and the components flocculate. This is predicted by the DLVO-theory, which

states that the stability of the components depends on the two particles having enough energy to overcome the energy barrier to be attracted to each other (Eklund, 1991). The electrostatic double layer is compressed to the point where the repulsive energy barrier is reduced, leading to coagulation or flocculation (Eklund, 1991). Once the flocculent is added in excess, beyond the point of charge neutralization, the components are re-dispersed. Retention aids that abide by this mechanism are typically low molecular weight, high cationic charge compounds. They usually do not extend beyond the electrical double layer but decrease the net charge to zero (Norell, 1999). These types of retention aids include polyvalent cations (e.g. polyaluminum species), polyethyleneimine, poly-DADMAC, polyamines and polyamideamine epichlorohydride (PAE) (Norell, 1999).

Patch-flocculation is an electrostatic mechanism that is different from the charge neutralization theory. It based on the formation of cationic sites or "patches" by cationic polyelectrolytes on the anionic fiber or filler surfaces (see Figure 1-7). The polymer is absorbed in cationic patches on the negative surface of the particle. Flocculation will then take place by electrostatic forces between the oppositely charged sites on the particles. The degree of attraction depends on the charge density of the polymer and the surface coverage of the polymer. In order for the patch model to work, these areas of opposite charge must remain localized and not spread over the entire particle. This means that the patches must be thicker than the electrostatic double layer so they can attract the other particles. If the patch does not protrude beyond the electrostatic double layer, the charge associated with it will only serve to neutralize the opposite charge around it (Scott, 1996). As can be seen from the mechanism, the polymers most suited for patching are short-chain, cationic polymers with a high charge density. Polymers with these qualities include modified polyethylene imines (PEI), polyamines and polyamideamine (PAM) epichlorhydrin (PAE) (Scott, 1996).

In bridging flocculation, the polymer acts to form a "bridge" by attaching to various absorption sites on the particle, while the other parts of the polymer remain free in the solution. The polymer forms loops and tails, which then can attach on other particles (see Figure 1-8). In order for bridging to occur, the loops and tails must form. This is dependent on contact time, the properties of the polymer, solution properties and

the surface properties of the particle (see **Error! Reference source not found.**). As in patch flocculation the part of the bridge on the particle must be thicker than the electrostatic double layer to form the loops and allow the loops and tails to attract other particles (Scott, 1996). Charge density is critical for bridging flocculation. It is necessary for the polymer to have a high molecular weight and linear structure for bridging to occur. Polyethylene and polyacrylamide (PAM) are often used for bridging flocculation (Eklund, 1991).

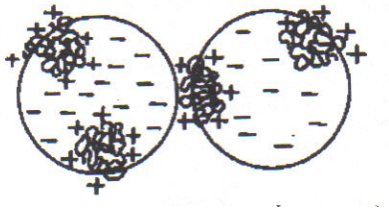

Figure 1-7: Pictorial representation of patch flocculation (Eklund, 1991)

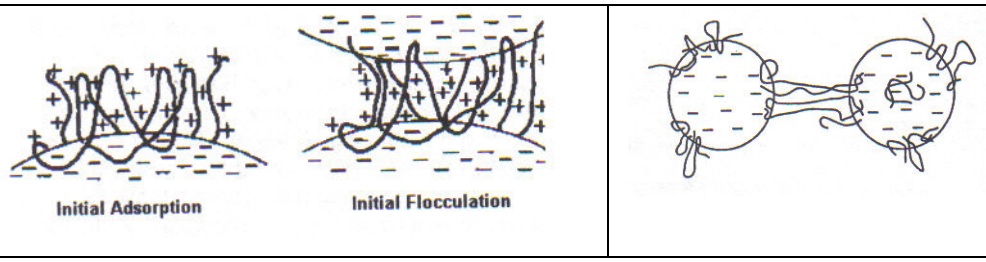

Figure 1-8: Various representations of bridging between particles (Eklund, 1991)

Flocculation systems commonly in use today include dual polymer applications, micro-particulate and network flocculation. Typically, the cationic polymer is added first. This allows it to flocculate the fibers and fillers. The flocs are then re -dispersed by a shear stage after which the anionic polymer is added. It then forms new flocs by bridging between the cationic floc fragments (see Figure 1-9) (Norell, 1999). The dual polymer systems are typically based on a cationic polymer (polyethyleneimine, poly-DADMAC, or cationic starch) and an anionic polymer (anionic polyacrylamide) (Au, 1995).

Microparticulate systems are slightly different. A cationic polymer is introduced first and flocculates the fibers and fillers by bridging. After a shear stage where the flocs are re-dispersed, the anionic nano- or microparticles are added to reflocculate the furnish components into very small, dense, strong flocs. In some cases, the anionic nanoparticle can be supported by an anionic polymer, in which case a combination of the dual polymer and nanoparticle mechanisms occurs (Norell, 1999).

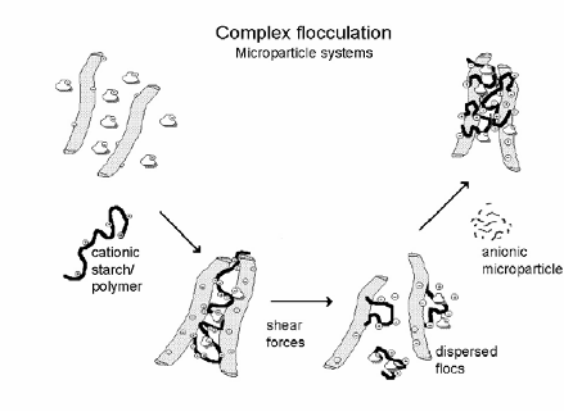

Figure 1-9: Schematic picture showing the initial adsorption of a cationic polymer (high charged, low molecular weight) and after a shearing stage, bridging by flocculation by an anionic polymer (low charged, high molecular weight polymer) (Norell, 1999)

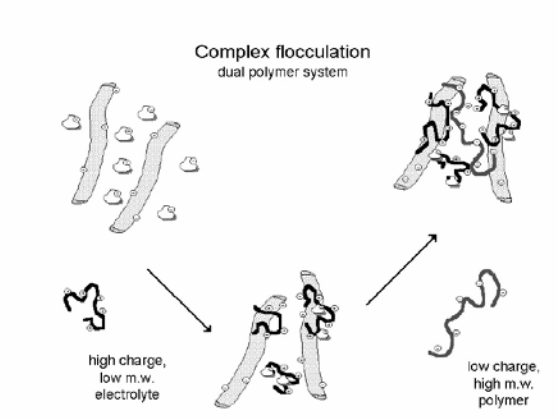

Figure 1-10: Schematic picture showing the initial adsorption and bridging flocculation of a cationic polymer (high molecular weight starch or synthetic polymer) and, after the shearing stage, the reflocculation by an anionic microparticle (Norell, 1999).

The *network* flocculation mechanism is based on hydrogen bonding-electrostatic bridging interactions, and is typical of systems based on phenolic resin and polyethyleneoxide or montmorillonite (bentonite) and anionic polyacrylamide. The hydrogen bonding mechanism is especially prevalent in systems with salts and other charged species in the white water systems where high conductivity suppresses the electrostatic interactions. The term network stems from the model of a network formed between the two components added to the fiber furnish. The transient, unstable networks were believed to trap the fines and fillers by an occlusion process.

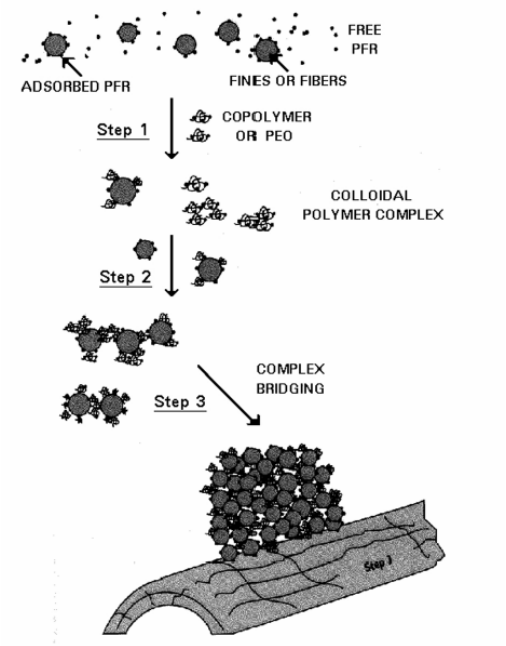

Figure 1-11: Schematic illustration of the complex bridging mechanism (network flocculation) (Xiao, 1996)

Polyamines, or epihalohydrin types, are used throughout the paper industry and are typically used in dual polymer systems (Scott, 1996). PEA is a condensation polymer produced from aliphatic amines and epichlorhydrin. The charged nitrogen is in the chain itself as opposed to the branched portions of the polymer. Polymerization gives a three-dimensional polymer structure that can have a relatively high molecular weight. Since PEA has a high content of quaternary amines, it has a high charge density and is effective over a pH range of 4-8 (Eklund, 1991).

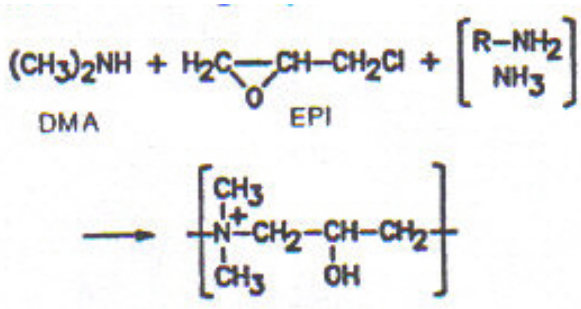

Figure 1-12: PEA condensate reaction (Eklund, 1991)

Polyacrylamide is one of the most used retention polymers in the paper industry (Doiron, 1998). With the aid of suitable catalysts/initiators, acrylamide can be polymerized to polyacrylamide (PAM) (see Figure 1-13). PAM can be produced in a wide range of molecular weights up to 20 million g/mol (Halverson, 1992). PAM is nonionic after polymerization and must be modified to be useful as a retention aid. Cationic PAM (C-PAM) is made by modifying nonionic PAM and incorporating cationic groups into it. This is often done by the Mannich Reaction. C-PAMs used in the paper industry contain between 20 to 70% cationic groups. Anionic PAM (A-PAM) can be modified either by co-polymerization of acrylamide with acrylic acid or by hydrolysis of some of the amide groups (Scott, 1996). One aspect of this formulation is that up until the time of this study anionic PAM had not been reported as retention aid for kaolin clay filler materials.

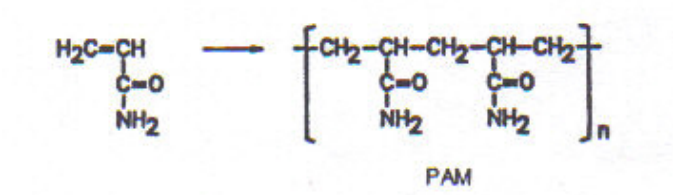

A

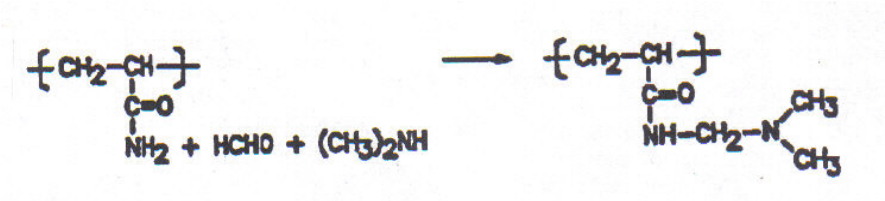

B

Figure 1-13: A→Polymerization of acrylamide, B→ Synthesis of C-PAM by the Mannich reaction (Eklund, 1991), (Scott, 1996)

With the aid of suitable catalysts/initiators, ethylene oxide can be polymerized to polyethylene oxide (PEO) (see Figure 1-14). When PEO is produced for flocculation the molecular weight is higher than for other applications, up to 3 million g/mol (Halverson, 1992). PEO is a linear polymer (Doiron, 1998) and adsorbs strongly onto mechanical

pulp fibers because it has a strong affinity for the phenolic groups in lignin. Hydrogen bonding is the main reaction mechanism for PEO and lignin particles (Doiron, 1998). Because of this, it exhibits good retention with mechanical pulps (Eklund, 1991). This is why PEO is the most common retention aid used in newsprint production (Doiron, 1998).

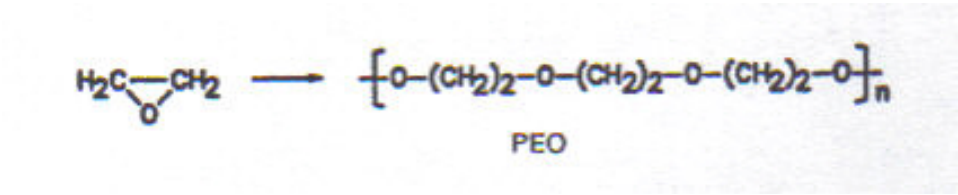

Figure 1-14: Polymerization of ethylene oxide (Eklund, 1991)

Once the starch adsorbs it remains fixed to where it adsorbed. As was mentioned above, cationic starch adsorbs directly on to the fiber, which is anionic. Fines and fillers are also anionic and starch will adsorb onto fines and fillers, often to a greater extent than fibers. Because of this the addition order and addition locations are important for starch efficiency (Ketola, 1999). Currently, cationic starches are starch ethers produced at high pH and high temperature. They are made by etherification using an epoxy reagent containing a quaternary ammonium group (see Figure 1-15). Cationic starches can be manufactured from any native starch. For reasons of stability and molecular weight they are mainly produced from potato and waxy maize starches (Ketola, 1999).

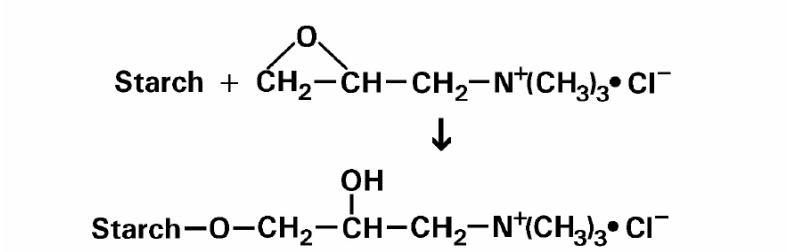

Figure 1-15: Reaction between starch and a cationization agent (Ketola, 1999)

Once starch adsorbs it remains fixed to the fiber or other furnish components. As was mentioned above, cationic starch adsorbs directly on to the fiber, which is anionic.

Fines and fillers are also anionic and starch will adsorb onto fines and fillers, often to a greater extent than fibers. Because of this the addition order and addition locations are important for starch efficiency (Ketola, 1999).

Starch, primarily cationic, is often added as a dry-strength agent to improve the final properties of the sheet such as burst strength, tensile strength, printability, internal bond strength and stiffness (Georgeson, 1995), (Brouwer, 1998). Dry-strength additives are thought to increase bonding by the development of numerous hydrogen bonds between the fibers. Starch has a chemical structure capable of forming hydrogen bonds (Brouwer, 1998). It is also thought that the starch helps to improve formation which will also lead to increased strength properties of the paper sheet (Scott, 1996).

2 EXPERIMENTAL DESIGN AND SAMPLE PREPARATION

2.1 Overall Approach

Five designed structures were created (Cases I through V) each with varying composition of fiber, filler and polymer components. The clay filler component was varied from 0 to 20 % by weight. Twenty replicate handsheets were made for each of the 25 handsheet types (5 cases at 5 filler levels each) giving a total of 500 handsheets made. The handsheets were made according to TAPPI standard methods. The five cases are discussed in detail in Sub-Section 2.2. Representative samples from the handsheets for each case and filler level were subjected to conventional bulk physical analyses and the new SEM procedure (see Figure 2-1). All physical testing was performed according to TAPPI standard methods in a TAPPI conditioned laboratory.

This work developed a method for obtaining statistically significant data from SEM images. The specific application was imaging filler particles in paper, but the method can be applied to similar images. The significant aspect of this method was that it greatly reduced the subjective qualities usually associated with microscopy observation by employing statistical methods to determine the number and type of required SEM images and by utilizing computer based image analysis techniques to quantify the size/shape characteristics of pertinent image features. The data base for developing the method consisted of the five different FFP designed structures. Each structure was assumed, and later shown, to produce different filler distributions. This appears to be the most complete methods to date and it is a significant contribution to the general knowledge.

The SEM method developed for acquiring image was termed a “grid method” and an overview of the method is in Figure 2-2. Using a sub-set of five handsheets out of the twenty made for each case and filler level, five SEM stubs were prepared. Initially each stub was imaged at locations determined by an evenly spaced 5 X 5 grid pattern that was the same for every stub (625 images total per case). The images were then processed and converted to digital information for fiber and filler particle area and perimeter.

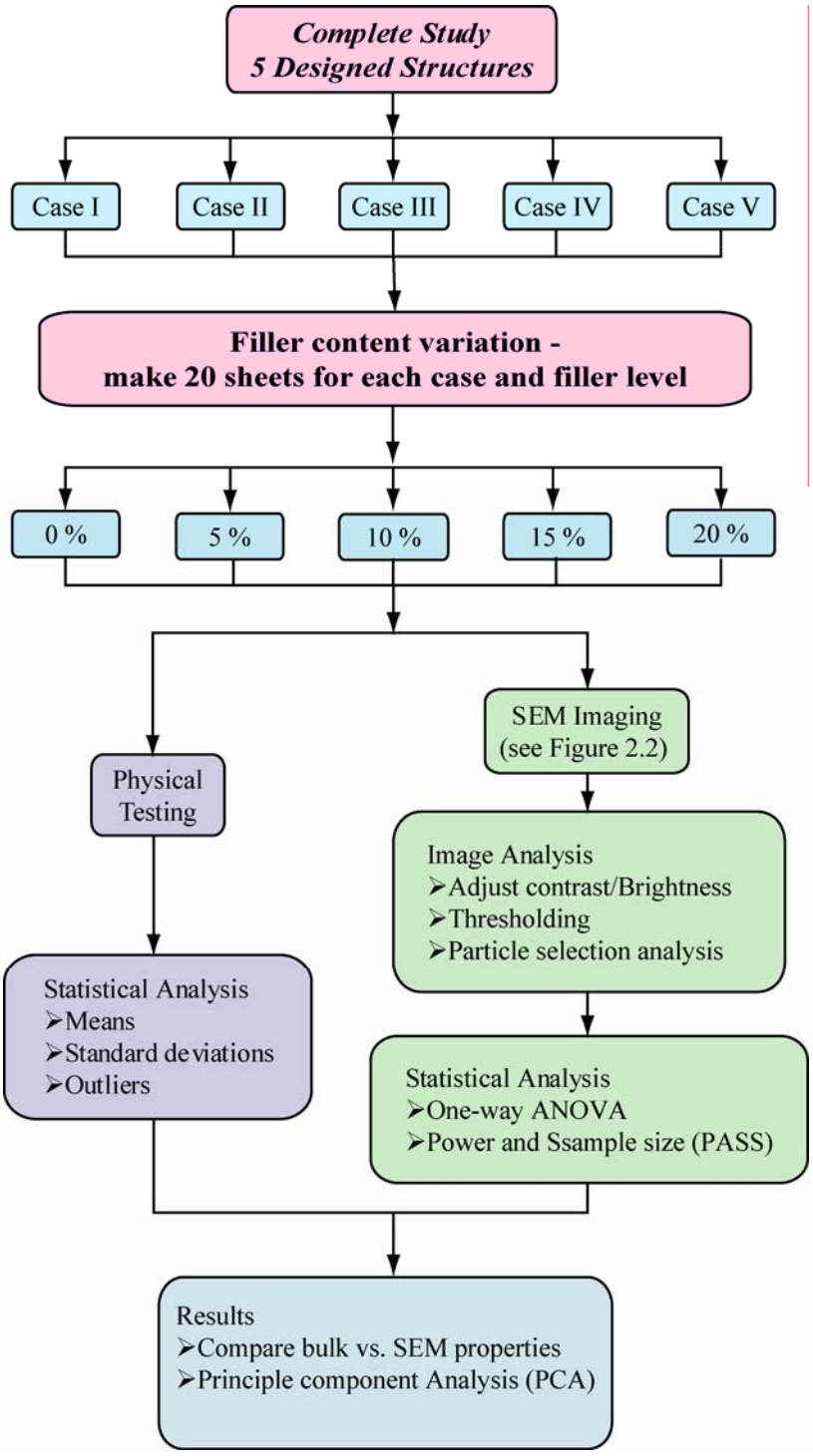

Figure 2-1: Experimental Overview

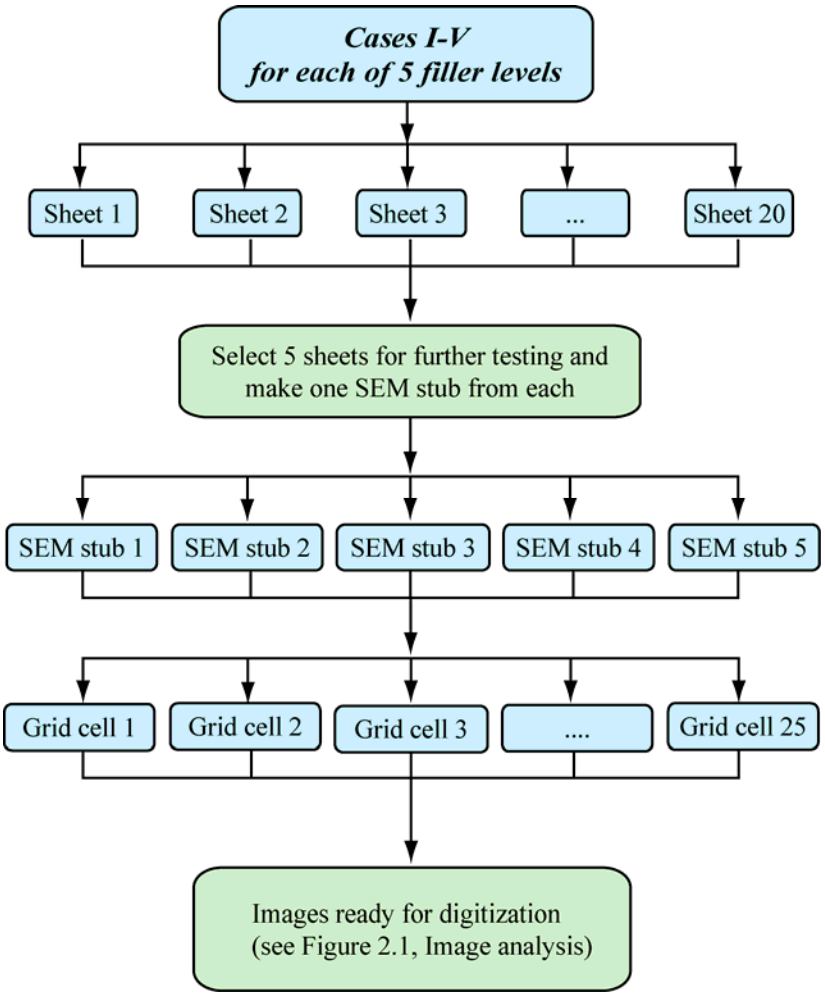

Figure 2-2: SEM Grid Method for Imaging a Sample Overview

2.2 Designed Structures

As mentioned previously the object of the handsheet preparation was to keep the filler particles off the fibers thereby preventing the disruption of fiber-to-fiber bonding; and resulting in increased filler content with limited degradation of strength properties. Designed structures based on paper physics and polymer based chemistry, retention and flocculation mechanisms were developed. The starting point for the designed structures was based on two conceptually structure designs, the *Ball and Chain* and the *Barbell* structures which are shown in Figure 2-3. Both structures form a complex where the filler was in contact with the polymer and bonded to the fiber through the polymer.

In the *Ball and Chain* structure, one end of the long polymer chain attaches to the fiber and the other end attaches to the filler particles. This leaves the filler at the end of the polymer chain free in solution, allowing the filler particles to be in the void areas between the fibers so as not to disrupt fiber-to-fiber bonding. In the *Barbell* structure, the filler particles connect to the ends of the long polymer chain, where the polymer chain is the "bar" and the filler particles are the "bells." The middle of the bar bell is flexible and attaches to the fiber leaving the ends free in solution. This would allow the filler to be in the void areas between fibers so as not to disrupt fiber-to-fiber bonding.

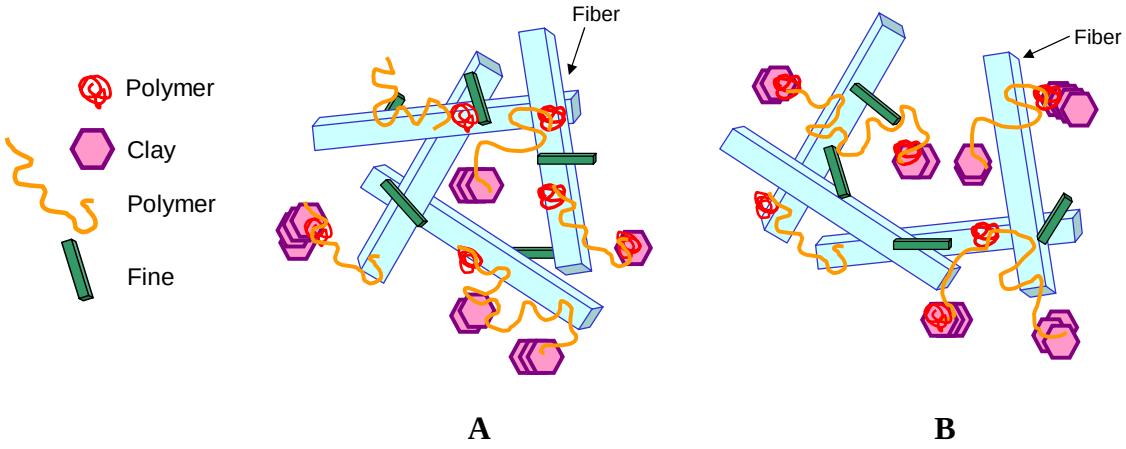

Figure 2-3: Designed structures: A: "Ball and Chain" structure; B: "Barbell" structure

Table 2-1 shows potential methodologies for creating the creation of the *Ball and Chain* and *Barbell* designed structures where, $\mathbf{F}^-$ stand for fiber, **C** stands for clay filler and $\mathbf{P}^+$ and $\mathbf{P}^-$ stand for polymers.

Table 2-1: Descriptive equations for the Ball and Chain and the Barbell structures

Ball and Chain	
1	$\mathbf{F}^- + \mathbf{P}^+$ (high MW, low charge) → **C**
Or	
2	$\mathbf{F}^- + \mathbf{P}^+$ (high MW, low charge) → **C** + $\mathbf{P}^-$
Barbell	
1	**C** + $\mathbf{P}^-$ (low MW, high to med. charge) → $\mathbf{F}^-$ + $\mathbf{P}^+$ (high MW, low charge)
Or	
2	**C** + $\mathbf{P}^+$ (high MW, low to med. charge) → $\mathbf{F}^-$

The *Ball and Chain* and *Barbell* structures are idealized structures. The task for this work was to create a structure which closely resembled one of those two structures and to also create several significantly different structures that could be used as a comparison.. It is believed that pre-flocculation methods could be used to create these idealized structures and two pre-flocculation methods were used one with starch (Case II) and one without starch addition (Case III). In the pre-flocculation methods, polymer was added to the filler prior to furnish addition. In order to evaluate how and if the idealized structures were created, three comparison structures were developed.

The first comparison structure is the control case (Case I) which used only fiber and clay filler, using no polymer. The filler would be mechanically entrapped in the fiber web, and thus could be either on the fibers or between the fibers or both. Filler retention was expected to be poor. The second comparison case employed a conventional polymer retention system. (Case IV) which used a (PEO). In this case it was expected that much of the filler would be retained, but as with the control case the filler could be either on the fibers or in between the fibers. The third comparison structure was the solvent coated method (Case V) where the surface charge of the filler was modified by a solvent to produce. In this case, the filler was likely to be on the fibers with low retention. In summary, the five structures and their components were:

1. Case I: Control → Fiber and filler only, no polymers
2. Case II: Pre-flocculation with starch → Dual polymer system with starch
3. Case III: Pre-flocculation with dual polymer system → Dual polymer system
4. Case IV: Conventional → One of the most common polymers used for NP
5. Case V: Solvent coated → Fiber and solvent coated filler only, no polymers

Table 2-2 is a summary table for the surface charge relationships between the designed components in the handsheets. In this table the expected charge of the clay after treatment, either by polymer or solvent is noted and can then be compared with the polymer treatment, if any. The last column is a description of the filler/fiber (F~F) or filler/fiber/polymer (F~F~P) structure in terms of surface charges. Understanding the

surface charges will help to understand the actual physical structure of the different designed cases.

Table 2-2: Surface Charge Relationships among Handsheet Components

Clay Treatment	Charge	Polymer* Treatment	Charge	Starch Treat.	F~F or F~F~P ionic charge relationship
Case I	Control → Fiber and filler only, no polymers				
None	+/-	None		No	(+/-)~(-)
Case V	Solvent coated → Fiber and solvent coated filler only, no polymers				
EtOH coated	~0	None			(0)~(-)
Case II	Pre-flocculation with dual polymer system → with starch				
T-100 pre-floc	-	MMW T-100 PAM	-	Yes	(+)~(-)~(+)
	-	LMW A159 Polyamine	+	Yes	(+)~(-)~(-)
Case III	Pre-flocculation with dual polymer system → Dual polymer system				
6456I pre-floc	+	LMW 6456I PAM	+	No	(+/-)~(-)~(+)
	+	HMW 5200 Polyamine	+	No	(+/-)~(-)~(+)
Case IV	Conventional → One of the most common polymers used for NP				
None	+/-	HMW PEO	0	No	(+/-)~(-)~(0)

* LMW, MMW and HMW = low, medium and high molecular weight, respectively.

2.2.1 Case I: Control

Case I is the control case. It was a very simple structure where the filler was added to the thin stock and mixed. The furnish was then added to the handsheet mold. There were no polymers added to the sheets. The main retention mechanisms in the control case was expected to be mechanical retention and network flocculation (see Figure 2-4).

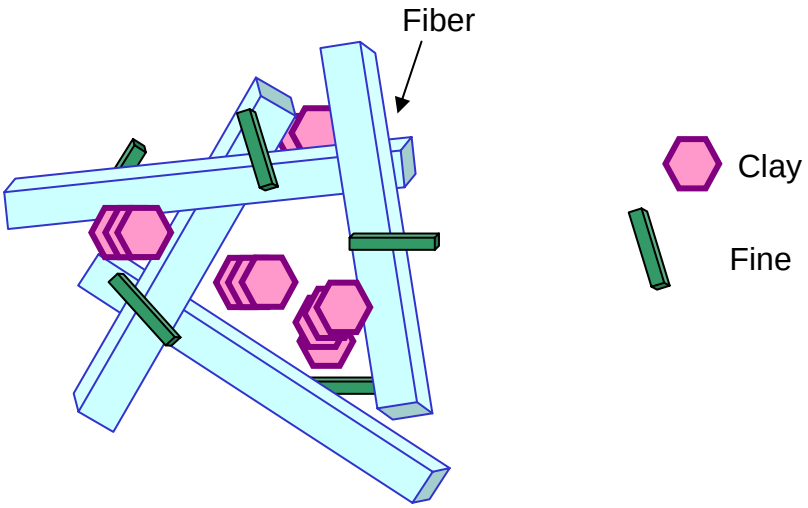

Figure 2-4: Case I-Control

2.2.2 Case II: Pre-flocculation with starch

Case II was the pre-flocculation with starch case (see Figure 2-6). This structure was created by pre-floccing the clay with T-100 flocculant then adding the clay and T-100 to the thick stock, diluting it, adding the starch and then adding A-159 polymer last. This was a unique design, not currently used in newsprint production. Some of the basic properties of the polymers and filler can be found in. The T-100 polymer had a high surface area and was a highly cross linked microparticulate polymer. The A-159 was a short chain polymer. The mixing procedure was as shown in Figure 2-5 and the resulting mixture was put into the handsheet mold.

Step 1	**Step 2**	**Step 3**	**Step 4**	**Step 5**	**Step 6**
Pre-flocc Clay with polymer	Add pre-flocced clay to thick fiber stock	Dilute thick fiber stock to ≈ 0.3% cons.	Add Starch to thin fiber stock	Add polymer to thin fiber stock	Add thin fiber stock to handsheet mold
Clay + T-100→	Fiber (thick)→	Dilute→	Starch→	A-159→	Thin Stock
↓	↓	↓	↓	↓	↓
mix w/ spoon	mix w/ spoon	mix 15 sec	mix 10 sec	mix 5 sec	HS mold

Figure 2-5: Mixing procedure for Case II

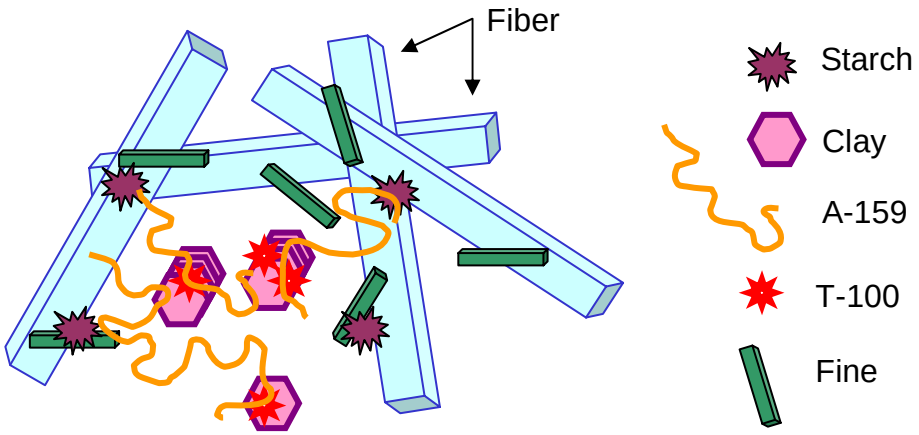

Figure 2-6: Case II- Pre-flocculation with starch

The reasoning behind this structure was that the cationic starch and the cationic polymer (A-159) would be attracted to the fibers. The starch would contribute to the fiber-to-fiber bonding after it was added. The clay pre-flocced with the anionic polymer would then be attracted to the cationic polymer which was already attached to the fibers. The anionic clay particles would not be attracted to the anionic fibers. This should prevent filler from disrupting fiber-to-fiber bonding. The cationic polymers and starch would account for retention.

2.2.3 Case III: Pre-flocculation with dual polymer system

The rational and procedures for this pre-flocced structure was similar to that for Case II, except the starch was omitted from the handsheet (see Figure 2-7). Case III is a dual polymer system, created using the 6456I and 5200 polymers. These polymers were an alternative to A-159 and T100. They were used because they were newer polymers and were thought to be superior to A-159 and T100 (Norton, 2003). The 6456I polymer is commonly used for newsprint (NP) in the southeastern United States. This designed structure is created by first pre-floccing the clay with 6456 I, which was added to the thick stock pulp and diluted. Then the 5200 was added, followed by an additional dose of A-159. A-159 is a low MW cationic flocculant and it was added to retain the anionic trash in the papermaking system, keeping the whitewater clean and improving overall retention. The mixing procedure is described in Figure 2-8 and the resulting mixture was put into the handsheet mold.

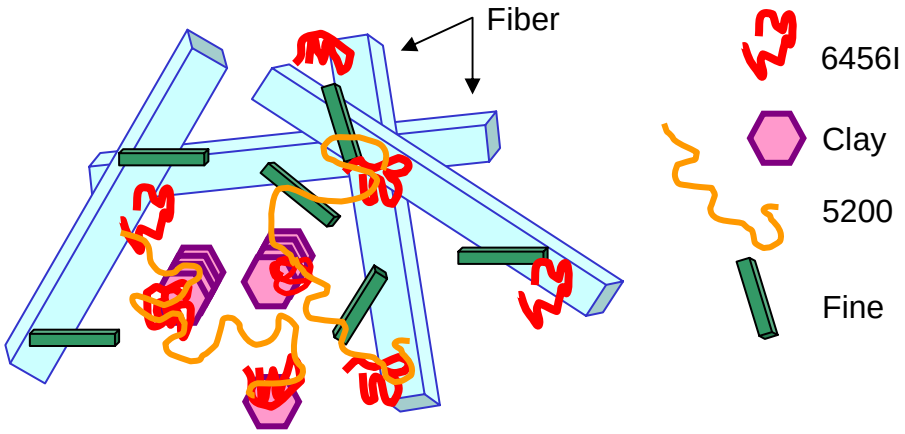

Figure 2-7: Case III-Pre-flocculation with a dual polymer system

Step 1	Step 2	Step 3	Step 4	Step 5	Step 6
Pre-flocc Clay with polymer	Add pre-flocced clay to thick fiber stock	Dilute thick fiber stock to ≈ 0.3% cons.	Add Starch to thin fiber stock	Add polymer to thin fiber stock	Add thin fiber stock to handsheet mold
Clay + 6456I→	Fiber (thick)→	Dilute→	5200→	6456I→	Thin Stock
↓	↓	↓	↓	↓	↓
mix w/ spoon	mix w/ spoon	mix 15 sec	mix 10 sec	mix 20 sec	HS mold

Figure 2-8: Mixing procedure for Case III

2.2.4 Case IV: PEO Case

The PEO case was the conventional case (see Figure 2-9). The reasoning behind this structure is that the PEO would also have an affinity for the clay particles due to the dual surface charges on the clay. The PEO used in this study is *Oxicol*.

It would also be strongly attracted to the fiber and thus would create a connection between the filler and the fiber without them coming in contact, keeping the filler away from in between the fibers. It was expected that patching and bridging would be then primary retention mechanisms.

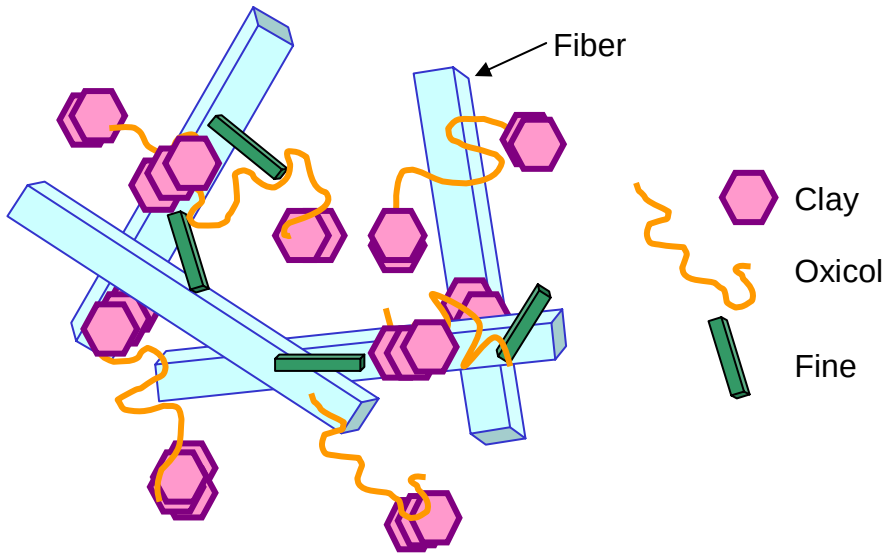

Figure 2-9: Case IV-PEO

2.2.5 Case V: Solvent Case

The final structure employs a different concept, which is depicted in Figure 2-10. Here the filler was modified with ethanol. The filler was prepared in the conventional fashion but instead of water as the solvent, ethanol was used. This should modify the surfaces charges of the filler. It was expected that the filler would attach to the fibers, disrupting the fiber-to-fiber bonding and causing a great deal of strength loss. Because there are no retention polymers in the papermaking furnish, filler retention was expected to be low.

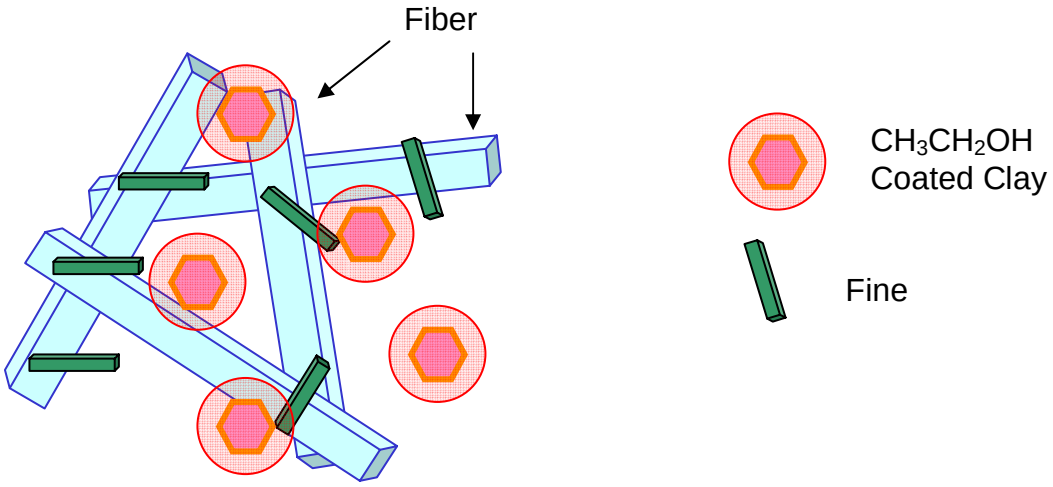

Figure 2-10: Case V-Ethanol coated filler

2.2.6 Designed Structure Materials

2.2.6.1 Fibers

The base fiber material chosen was a southern softwood mix, virgin thermomechanical pulp (TMP) made for newsprint production at the Bowater mill in Calhoun, TN. This fiber was chosen because the original basis of the thesis was developed from the technology of patents donated to the Institute of Paper Science and Technology (IPST). The technology behind the patents was to develop a sheet with higher filler content that was able to maintain bulk, strength and optical properties.

2.2.6.2 Filler Material

The filler material used in this research was a Georgian kaolin clay from IMERYS World Wide Paper Company. Table 2-3 describes the properties of the WP kaolin clay used throughout the thesis work.

Table 2-3: WP kaolin clay properties

WP Clay Sample	PG-0419
Solids	Powder
Brightness (GE)	83.3
L	94.31
a	0.31
b	4.59
pH	7.0
325 mesh residue(%)	0.0026
PSD %<10	95
PSD %<5 microns	84
PSD %< 2 microns	65
PSD %<1	56
PSD %< 0.5	45
PSD %< 0.25	27
PSD %< 0.2	22
PSD %< 0.1	11
D30	0.277
D50	0.639
D70	2.676
Einlehner Abrasion	4.1
Panacea shape factor	20
Steepness	10.4

*PSD = Particle Size Distribution

2.2.6.3 Polymers

Table 2-4 is a summary table of the different polymers used for the designed structures. There were four types of polymers used, PAM, polyamine, PEO and starch. Cases I and V did not use any polymers, cases II, III and IV did use different polymers. The first pre-flocculation (Case II) structure was formed using kaolin clay, a low molecular weight cationic polyamine (A-159), medium weight anionic PAM (T-100) and cationic starch (RediBond). The T-100 polymer was used to pre-flocc the clay. The second pre-flocculation (Case III) was a modification of the first pre-flocculation method using a high molecular weight cationic polyamine (5200) and a low molecular weight cationic PAM (6456I). The 6456I was used in two addition points, the first was to pre-flocc the clay and the second was to re-flocc the fiber furnish after the shear stage. The PEO structure (Case IV) was made with kaolin clay and a high molecular weight, nonionic PEO (Oxicol).

Table 2-4: Polymer characteristics and dosage schedule

Component	A-159	T-100	RediBOND	5200	6465I	Oxicol
Polymer Type	Polyamine	PAM	Starch	Polyamine	PAM	PEO
Molecular Weight	Low	Medium		High	Low	50 (High)
Charge Density	High	High		Medium	Low	N/A
#/ton	**1.5**	**1.5**	**15**	**1.5**	**0.5 (pre-flocc) + 1.5**	**1.0**

2.3 Sample Preparation

2.3.1 Pulp

Six 55 gallon drums of TMP pulp were obtained. Each of the 55 gallon drums was divided into twelve 5 gallon buckets which were then frozen for storage. The drums were labeled 1 thru 6 and the buckets were labeled 1 thru 12 and were also numbered for drum that the pulp was originally in. Drums 1 through 4 contained hydrosulfite bleached TMP and drums 5 and 6 contained peroxide bleached TMP. Initially, selected physical and optical tests were performed on both pulps to determine if bleaching processes

produced different pulp properties. No major differences were detected and the samples for the thesis were made with the hydrosulfite bleached pulp.

Storage of pulp for a long periods can be a challenge. There were concerns that a bio-side would not last long enough and would interfere with surface chemistry. It was decided that freezing the pulp slurry was the best way to preserve the pulp. Any small amount of damage that the fibers might go under during the freezing process would be minor as compared to the mechanical damage the fibers had incurred during the TMP process. Experiments were done on frozen and never-been-frozen pulps and compared for any differences in strength and optical properties. Differences between the two pulps were negligible and all the further experiments were performed using the frozen pulp.

2.3.2 Handsheet Preparation

Handsheets were prepared and tested according to TAPPI Standards. The handsheets were made in a re-circulating handsheet mold to better simulate papermaking conditions. Four or five handsheets were made and discarded each time handsheets were made to establish a "white water" and ensure the fines level would be constant. The different filler levels were made from least to most to reduce any effect a build-up of filler in the white water would cause. The handsheet mold was cleaned between each case to eliminate cross contamination of polymers. The handsheets were 1.2g OD and 60 g/m^2 basis weight. For each structure five filler levels were used, fiber and filler content were adjusted to maintain a constant basis weight, as shown in Table 2-5. Each handsheet was pressed for 5 minutes at 50 psi. The sheets were dried under restraint in a TAPPI conditioned laboratory where they remained for all physical testing.

Table 2-5: Pulp and clay make-up of the handsheets.

Filler Content (%)	0	5	10	15	20
OD Pulp (g)	1.20	1.14	1.08	1.02	0.96
OD Clay (g)*	0.000	0.072	0.144	0.216	0.288

*OD clay was multiplied by a factor of 1.2 to account for lack of complete retention

2.3.3 Clay make-down

The process for making the clay slurry was relatively simple. The WP kaolin clay was supplied as a dry solid. To make the slurry the dry clay was weighed in a chemically resistant plastic bottle and de-ionized (DI) water was added to bring the clay slurry to 20% solids. The slurry was shaken for approximately 30 minutes. Preparing the clay at 20% solids translated to 0.3 ml of slurry for every 5% in desired filler level, making the filler addition consistent throughout. The slurry was shaken continuously during hand sheet preparation to ensure all the solids were thoroughly suspended in the slurry. Fresh slurries were made for each day of handsheet preparation. The procedure was identical for the solvent coated clay with the exception that the de-ionized water was replaced with ethanol. Table 2-6 gives the clay slurry volumes used:

Table 2-6: Clay slurry make down at 20 % solids

Dry clay (g)	Water (g)	Total (g)	% Solids
10	40	50	20
20	80	100	20
30	120	150	20
50	200	250	20

2.3.4 Polymer make-down

The A-159, T-100, 6456I and 5200 polymers were all supplied as neat solutions. The T-100 and 6456I polymers required a two step dilution process to make a 0.1 % solution. The A-159 and 5200 polymers could be diluted directly to a 0.1 % solution. All dilutions used with de-ionized water. The initial dilution of the T-100 and 6456I polymers had a usable life of seven days but the second dilutions of the T-100 and 6456I and the A-159 and 5200 dilutions had usable lives of only one day. Table 2-7 provides a summary of the polymer make-down.

Table 2-7: Polymer make-down

Polymer	Dilution 1	Solution 1 (%)	Dilution 2	Solution 2 (%)
T-100	1.0 ml neat polymer in 99 ml DI water	1.0	10 ml polymer Solution 1 in 90 ml DI water	0.1
A-159	1.0 ml neat polymer in 999 ml DI water	0.1	N/A	N/A
6456I	1.0 ml neat polymer in 99 ml DI water	1.0	10 ml polymer Solution 1 in 90 ml DI water	0.1
5200	1.0 ml neat polymer in 999 ml DI water	0.1	N/A	N/A

The PEO used in this work was supplied as a dry polymer. The make down was as follows:

1. 0.5 g dry polymer
2. Add 3 ml acetone and mix well
3. Add de-ionized water to bring total volume to 100 ml
4. Mix and let sit over night; Solution is at 0.5 %
5. Dilute to 0.1 %; Add 20 ml of 0.5 % to 80 ml of de-ionized water
6. Shake for approximately 15 minutes; Solution is at 0.1 %

2.3.5 Scanning Electron Microscopy Method

Samples were prepared for SEM from handsheets. For each case and filler level, five handsheets were randomly selected from the twenty total handsheets made. A sample (see Figure 2-12) approximately 1 mm by 1mm was attached to a SEM aluminum stub with double sided carbon tape. Each sample was carbon coated with a medium thick layer of carbon (see Figure 2-11). Carbon paint was then applied to each sample corner to prevent excess charging (see Figure 2-12). This method, know as the carbon coated method, is the necessary sample preparation method when using the back scattering electron (BSE) mode on the SEM.

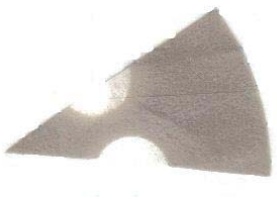

Figure 2-11: Filter paper used to visualize the thickness of the carbon coating, dark area was coated, the white area was protected during the coating process for reference

Figure 2-12: SEM stub prepared and ready for imaging, note carbon paint on each corner of the paper sample

The SEM samples were imaged using BSE mode in order to visualize the difference between filler particles and the other components in the paper samples. Initially, Multiple BSE images were then taken from each SEM stub in a 5 x 5 grid pattern. The SEM used in this research was a JEOL JSM-6400 with a digital camera and image acquisition system. Geller dStep is the computerized controller interface for moving the stage inside the SEM and, is capable of moving the stage inside the SEM by computer interface in one micron increments in either the X or Y direction. Geller dPict32 (**D**igital **P**hoto **I**mage and **C**ollection **T**ool) is the image acquisition software used by the SEM. It is a 32-bit Windows program designed to collect and display electron images from an SEM. The automated stage program on the SEM was used to move each stub to the same coordinates for each sample. This resulted in an automated and objective process for acquiring SEM images of the fiber and filler particles. In theory this process could be automated with a program, such as Geller dStep, and some type of auto-focus device for the beam.

Samples were also prepared with gold colloid in an attempt to visualize the polymers. These samples were selected from the different cases. The gold colloid was prepared in the laboratory. It was stored in amber I L bottles to protect it from light. The gold colloid sheets were made over a short period of time and the colloid solution lasts for a few months. The procedure for making a gold colloid solution can be found in **Error! Reference source not found.**.

2.3.5.1 Image Analysis

The purpose of image processing was to convert the filler particles in a SEM micrograph into digital data that can then be manipulated and analyzed with various statistical methods. There are several steps necessary to process each image: contrast and brightness adjustment, thresholding, particle selection, particle analysis, and anomaly de-selection.

The raw SEM image created by the SEM's Geller Digital Image Acquisition system, is to convert a SEM micrograph into data points. There are several steps necessary to process each image.

1. Contrast/Brightness adjustment
2. Thresholding
3. Particle Selection and Analysis

The raw SEM image created by the SEM's Geller Digital Image Acquisition system, was imported into UTHSCSA ImageTool. The brightness and contrast are then adjusted to make the filler particles easier to select. Due to the nature of SEM micrographs, each image had different initial brightness and contrast levels, making it impossible to apply the same image brightness and contrast levels automatically, thus each image had to be processed by hand. Adjusting the contrast and brightness does not alter the image, it simply stretches the thresholding histogram.

Thresholding makes the color image into a binary; black and white image by assigning each pixel in the image values of either 255 (black), or 0 (white). Due to the nature of BSE electrons, artifacts of fibers could appear light in color in the micrographs. This could interfere with the light color of the clay particles. As the image was thresholded, these fiber artifacts were occasionally incorrectly identified as clay particles. Overcompensating for these artifacts would lead to exclusion of too many clay particles, so a balance in the thresholding process had to be found between including too many fibers and too few clay particles. When identified, fiber artifacts were "de-selected" so they were not included when the particles were analyzed. After the filler particles were selected, the particles were then analyzed for characteristics such as area and perimeter size.

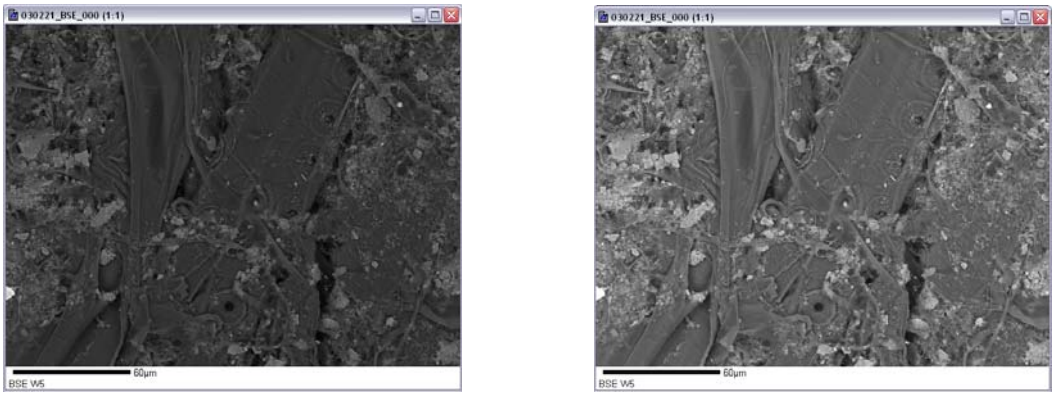

A **B**

Figure 2-13: First image (A) is a raw image from the SEM, second image (B) is the same image after brightness and contrast have been adjusted

In this application, the thresholded images were always compared with the raw image to ensure that all the filler particles were selected and that no non-filler particles were selected. Thus, the primary function of the image analysis software was to identify potential filler particles and then measure the characteristics of confirmed filler particles.

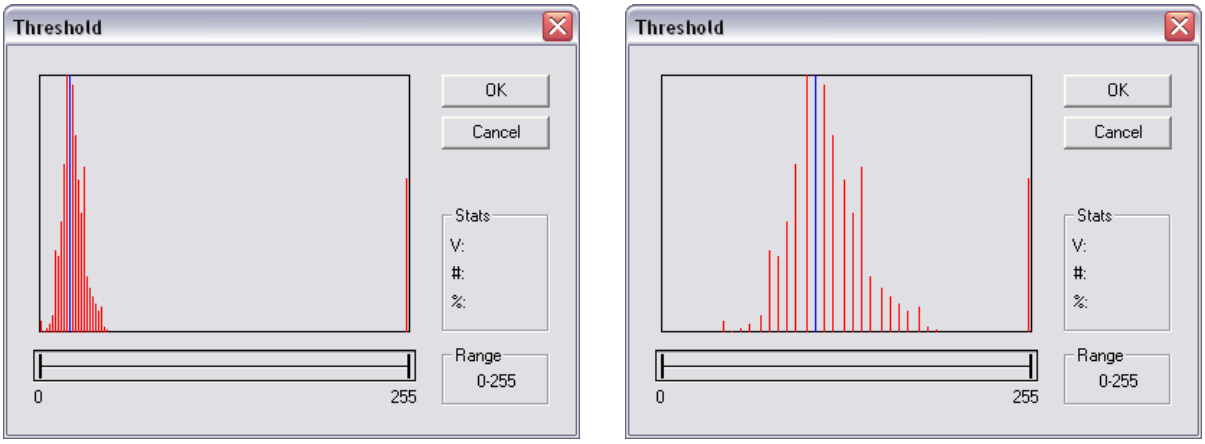

Figure 2-14: These two graphics show the difference between the thresholding ranges. First image is a raw SEM image without brightness and contrast adjustment. Second image is the same image after brightness and contrast have been adjusted

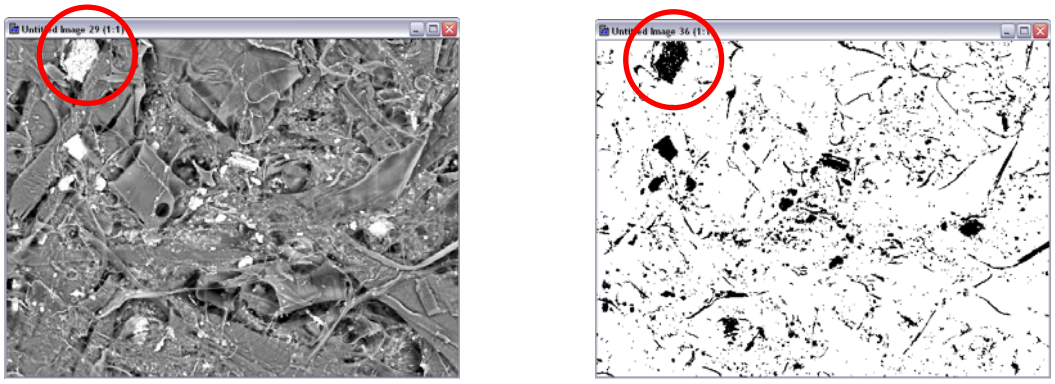

A **B**

Figure 2-15: Image A - SEM micrograph; Image B - Same SEM micrograph after thresholding, black areas now represents filler material and white areas represent fiber and other non-filler materials

3 SAMPLE ANALYSIS - SHEET PROPERTIES AND STATISTICAL METHODOLOGIES

3.1 Physical Properties

Paper is a stochastic network of fibers and other papermaking additives, although orientated sheet formation improves the randomness of paper. The fibers are much longer than the paper is thick giving it a planar network, the in-plane strength properties being significantly greater than the out-of-plane strength properties. When considered from a two-dimensional standpoint, paper is an opaque, bulky and stiff structure while when considered from a three-dimensional standpoint paper is a porous and layered structure (Niskanen, 1998).

The elastic modulus, or Young's modulus, is a measure of the amount of force necessary for a small elongation of a sample. This is represented by the following equation (Niskanen, 1998):

$$E = \frac{d\sigma}{d\varepsilon} \quad at\ \sigma \to 0$$

where

$E = Young's\ modulus$
$\sigma = applied\ stress\ over\ the\ cross\text{-}sectional\ area\ of\ the\ sample$
$\varepsilon = strain\ corresponding\ the\ the\ applied\ stress$

If the stress strain curve or load-elongation curve is linear at small ε, the equation above becomes (Niskanen, 1998):

$$E = \frac{\sigma}{\varepsilon}$$

Paper strength is ultimately controlled by the gradual failure of inter-fiber bonds and in a well-bonded sheet by fiber rupture. In sheets made from mechanical pulps either failure mode is possible. Whether bond or fiber failure is predominant, the bonds serve to distribute the applied loads across a number of fibers. As fibers fail, the load distribution changes. These two failure modes are difficult to control individually since papermaking affects fiber and bond properties and overall sheet structure. However, in a well-bonded sheet, one that is made from conformable fibers and is highly pressed, fiber rupture is the primary failure mode. Prior to the failure of the sheet, there are bond failures which

redistribute the applied loads until individual fiber are forced to carry loads that exceed their tensile strengths.

The physical testing data can be divided into five groups that correlate each test to a fundamental property, as shown in Table 3-1.

Table 3-1: Categorizing of Physical Test into groups based on fundamental physical properties and equations

Fundamental Properties	Fundamental Equations
Surface Characteristics	
Sheffield Roughness Print-Surf	Surface roughness
Static COF Kinetic (dynamic) COF	Surface roughness Surface elements/chemistry Surface element size
Optical	
Brightness	$R_\infty = 1 + \frac{K}{S} - \sqrt{\frac{K^2}{S^2} + 2\frac{K}{S}}$ $\frac{K}{S} = \frac{(1-R_\infty)^2}{2R_\infty}$
Printing Opacity	$Opacity = \frac{R_0}{R_\infty} \cdot 100$
TAPPI Opacity	$TAPPI\ Opacity = \frac{R_0}{R_{0.89}} \cdot 100$
3-D Structure	
Formation Ultra Sonics Thickness	
Stiffness Properties, E **(depends on bond strength, fiber strength)**	
Bending Stiffness (beam bending), S_b	$s_b = \frac{Ed^2}{12}$ $E = \frac{\sigma}{\varepsilon}$
US* Elastic Stiffness US* Specific Stiffness Tear	$G = \frac{\beta\sigma^2 a}{E}$
* = Ultra Sonics	
Tensile Properties **(Bond Strength•RBA)**	
Tensile Index, T (Dry and wet))	$\frac{1}{T} = \frac{9}{8 \cdot Z} + \frac{3 \cdot w_f}{\tau_b \cdot l_f \cdot RBA}$
Zero-Span, Z (Dry and wet)	Z (assuming a well bonded sheet)
Porosity, *p*	$RBA = 1 - \frac{(p-1)(1+v)}{c}$
Z-Directional Tensile	$\frac{1}{P_z} \approx \frac{1}{\tau_b \cdot RBA}$

3.1.1 Physical Testing

As stated previously, the basis for study in this project was to relate macroscopic properties to microscopic properties. Physical testing provided the macroscopic properties. Strength and optical properties were characterized by physical testing using TAPPI Standard Test Methods. Handsheets were prepared and tested according to TAPPI Standards. All imaging and physical testing (where applicable) was performed on the wire side of the handsheets. It was decided that this would b the side of the handsheet used for all surface analysis because filler location/amount would more likely be due to the FFP structure than mechanical entrapment. Table 3-2 is a listing of all the physical tests performed on the handsheets.

Table 3-2: Physical tests performed during this study.

Physical Testing-Non Destructive	Physical Test-Destructive
Brightness	Coefficient of Friction (COF)
Opacity-TAPPI	Tensile-Dry
Opciaty-Printing	Tensile-Wet
Gurley Porosity	Zero Span-Dry
Sheffield Roughness	Zero Span-Wet
Ultrasonic	Tear
Thickness	Bending Stiffness
Parker Print Surf	Z Direction Tensile-Dry
Formation	Basis Weight
	Ash

Appendix 1 contains the summary tables for all the physical testing data for each of the designed structures cases. All averages and standard deviations were normalized to basis weight where applicable. These were the physical testing data that was later correlated with the image analysis data. As all the physical testing data was analyzed, it was noted that the majority of the test results followed a distinct pattern. It appeared that the widest spread in the physical testing data values was at the 15% filler level case. It was believed that if correlations were to be found, they would be easier to discern from data that was more distinct. Although, the same pattern was seen in the 10% filler level, often two or more of the data points were close together. It was decided that in order to understand the data and validate the new SEM method, a full statistical analysis on all of the 15% case data would most likely give the best results. The focus of the rest of the data analysis will be on the 15% filler level data from all five cases.

Table 3-3: Listing of non-destructive and destructive physical testing performed on each case

Physical Testing Non Destructive	Number of Samples	Physical Testing Destructive	Number of Samples
Brightness	20	Ash	N/A
Formation	20	Basis Weight	10
Gurley Porosity	20	Bending Stiffness	10
Opacity-TAPPI	20	Coefficient of Friction (COF)	10
Opacity-Printing	20	Tear	10
Parker Print Surf	20	Tensile-Dry	10
Sheffield Roughness	20	Tensile-Wet	10
Ultrasonic Testing	20	Z-Direction Tensile	10
		Zero Span-Dry	10
		Zero Span-Wet	10

3.1.1.1 Surface Characteristics

Bulk and surface characteristics are important for the physical appearance of paper on the macroscopic level. Surface chemistry seems to be primarily responsible for the friction properties of paper (Kajanto, 1998).

Surface Roughness is important for printing grade papers. Ink absorption is very much dependent on surface roughness. Surface roughness is usually measured indirectly with an air leak method, such as Sheffield Roughness Method. Long fibers tend to give high roughness because of their high mass and are often more coarse than short fibers. Fillers and fines content at the surface of a paper sheet improves surface qualities by filling in voids in the surface. Distribution of fines and fillers in the Z-direction all influence sheet roughness (Kajanto, 1998).

Friction is a property between surfaces and manifests itself as a force that resists the displacement of one surface to another. The surface friction of paper can be very important in converting and printing processes. Forces between the molecules of the paper surfaces causes adhesion bonds only in areas that are in molecular contact. The coefficient of static or kinetic friction is what is typically used to describe the friction of paper. The coefficients of friction (COF) can range from 0.25 to 0.70 depending on the surface properties of the paper. Surface chemistry plays an important role in surface friction because it affects the cohesion bonds. Fillers can either reduce or increase

surface friction, depending on the shape of the filler particles. Plate like particles tend to reduce friction while spherical fillers tend to increase friction (Kajanto, 1998).

3.1.1.2 Optical Properties

Optical properties such as opacity, brightness are important properties for all grades and end use products. Absorption and reflection are caused by refraction or bending of the light as it strikes the solid surfaces in the paper's structure. This is also known as light scattering (Bauch, 1992). Inside the paper sheet, the light scatters in all directions. In paper, the light scattering ability depends on the difference in refractive index between the cellulose (1.53) and air (1.00) (Eklund, 1991). Opacity is the ability of the paper to hide text or pictures on the backside of the sheet. Brightness is the reflectance of paper using light at 457nm, or blue light (Leskela, 1998).

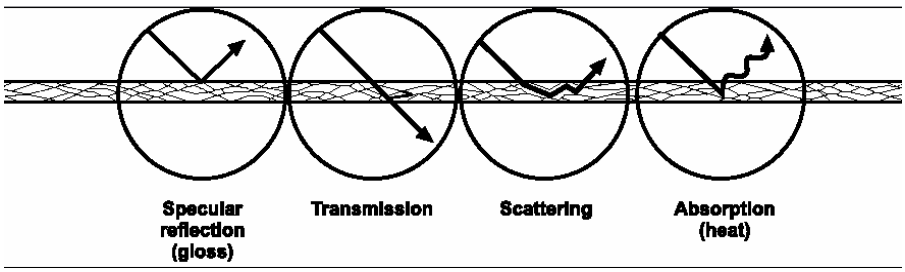

Figure 3-1: Interaction of light with paper (Vaarasalo, 1999)

Opacity is generally determined by the amount of incoming light that is prevented form traveling through the sheet by reflection or absorption (Bauch, 1992). Opacity is the ratio of R_0/R_∞, where R_0 is the reflectance when a single sheet is backed by a black body. R_∞ is the reflectance of an infinitely thick stack of identical paper such that no additional change in reflectance is seen when additional sheets are added to the stack (Scott, 1995). TAPPI opacity differs in that $R_{0.89}$ is the reflectance for a single sheet over a white background with a reflectivity of 89 (Pauler, 2000).

The Kubelka-Munk theory is still the most accepted theory for describing optical properties of paper sheets. Other theories have been less complete or have ended up with

the same results as the Kubelka-Munk theory (Scallan, 1972), (Pauler, 1986). The Kubelka-Munk theory does not explain how the reflectance of a sheet relates to the optical properties. Instead, it describes the scattering coefficient, S, and the absorption coefficient, K. In a sheet of pulp fibers, the scattering coefficient reflects both the scattering coefficient of the single fibers and the bonding between them. The changes in the scattering and absorption coefficients can be interpreted to explain how papermaking variables can control the surface available for light scattering, such as the number of voids in the sheets, the number of small particles or the total number of absorbing particles (Leskela, 1998).

The light scattering coefficient of unbonded fibers comes from the area per unit mass (specific surface area). Mechanical pulp fibers have a higher specific surface area and thus scatter more light (Leskela, 1998). Therefore, the more porous and bulky sheet made from mechanical pulp can often have a high scattering coefficient (see Table 3-4). The absorption coefficient, K, depends primarily on the amount of bleaching as K increases with yellowing (Leskela, 1998).

Table 3-4: Light scattering in different products (Pauler, 2000)

Product	S, m^2/kg
Greaseproof paper	15
Fine paper without filler	30-32
Fine paper with filler	40-60
Coated fine paper	45-60
Newsprint	55-65

Adding fillers to a paper sheet can improve optical properties including opacity and brightness (see Table 3-5). When fillers are added to a sheet, they can create more surfaces so that the amount of light reflected and adsorbed is increased. This translates to an increase in brightness and opacity (Bauch, 1992), (Pauler, 1986). Fillers also have higher specific surface area than fibers and fines. This is due to their smaller size, which is necessary for good opacity. They scatter more light than just fibers (Leskela, 1998).

Table 3-5: Paper property enhancement via filler usage (Gill, 1995).

Property	3.1.1.2.1.1 Fillers to be considered
Brightness	$CaCO_3$, PCC, TiO_2, aluminum trihydrate, amorphous silicas and silicates, calcined clay
Opacity	TiO_2, zinc sulfide, PCC
Smoothness	all fillers
Gloss	delaminated clay, PCC
Printability	$CaCO_3$, PCC, aluminum trihydrate, talc, calcined clay, amorphous silicas and silicates
Ink holdout	amorphous silicas and silicates, PCC, delaminated and calcined clay, talc

Table 3-6: Typical light scattering coefficients and refractive index for fillers and fibers and other paper components(Scott, 1996), (Eklund, 1991)

Material	Scattering Coefficient, cm^2/g	Material	Refractive Index
Filler Clay	1100-1200	Kaolin	1.55
Calcined Clay	2600-3000	$CaCO_3$	1.56
Ground $CaCO_3$	1400-1700	TiO_2 (anatase)	2.55
PCC	2200-2700	TiO_2 (rutiel)	2.70
TiO_2	4500-6000	Talc	1.57
Bleached chemical pulps	220-350	Calcium Sulfate	1.53-1.58
Mechanical pulps	500-750	Air	1.00
		Water	1.33
		Cellulose	1.53
		Starch	1.53
		Paraffin	1.43

3.1.1.3 3-D Structure

Fibers are much longer than paper is thick and the network is planar and almost two-dimensional. Although the two-dimensional structure dictates most of the paper properties, three-dimensional pours properties are also important. Handsheets have no fiber orientation, they are transverse isotropic. However, paper machines gives paper an anisotropic structure where fibers have a preferential orientation in the machine direction (Niskanen, 1998).

Formation describes the uniformity of the fiber, fiber fragments, mineral fillers and other material distribution in a paper sheet (Niskanen, 1998). The formation of a paper sheet is the result of physical interactions during the sheet forming process and can be characterized by the variation in basis weight.

Fibers are bonded together by hydrogen bonds, a special type of chemical bond (see Figure 3-2). In cellulosic material, hydrogen bonds form between hydroxylic

groups, oxygen molecules and carboxylic groups. Covalent and ionic bonds can also form between fibers when using polymer additives (Retulainen, 1998).

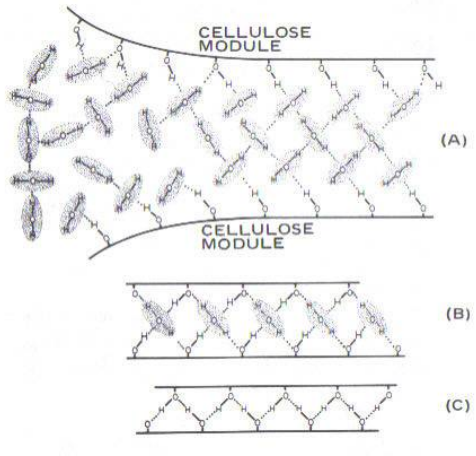

Figure 3-2: Different levels of hydrogen bonding: (A) loosely though water molecules, (B) more tightly through a mono-layer of water, (C) directly (Smook, 1997)

3.1.1.4 Stiffness Properties

Physical properties related to inverse stiffness or the elastic modulus are typically dependent on bond strength and fiber strength. These physical properties include tear index, bending stiffness, and ultrasonic elastic stiffness, specific stiffness, travel time and velocity.

Bending stiffness is an important characteristic for most paper grades, including newsprint. Bending stiffness is necessary for runnability on paper machines and printing presses. Newsprint with high bending stiffness is easier to hold up and read, without it bending over itself. Bending stiffness is controlled by basis weight, which generally translates into increased bulk, and by both fiber stiffness and bond strength, which translate into a combined sheet stiffness modulus.

The bending stiffness, S_b, of paper is derived from the standard expression for a uniform beam and takes into account both the sheet stiffness modulus, E, and the sheet caliper or thickness, d.

$$s_b = \frac{Ed^2}{12}$$

where:

$E = Elastic\ modulus$

$d = Thickness$

Bending stiffness can be measure in two different ways (see Figure 3-3). First the distance between A and B is measured and calculated to give a bending stiffness measurement. Second, the angle α is measure and then calculated to give bending stiffness.

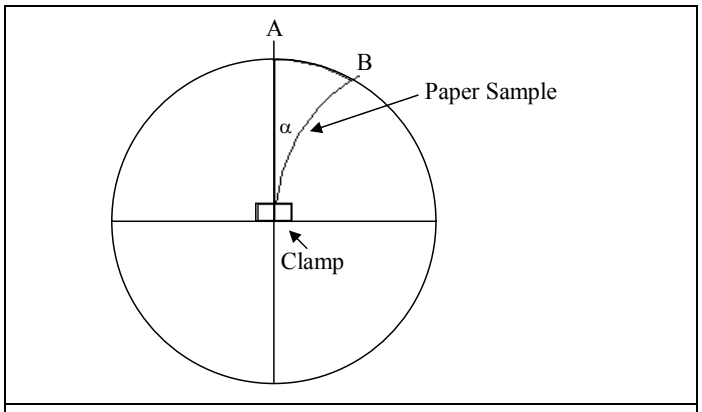

Figure 3-3: Representation of bending stiffness

Each type of pulp has its own bending stiffness potential. Mechanical pulps have a higher bending stiffness potential than chemical pulps. This is due to stiffer fibers, stiffer bonds and bulkier sheets (Kajanto, 1998). Any process which modifies the fiber stiffness, the ability to form strong bonds or the compressibility of the sheet will impact bending stiffness.

Tear strength is the total energy per tear length needed when a sample undergoes tearing. Two types of tests are possible, in-plane and out-of-plane tear measurement (see Figure 3-4). The tearing strength is very dependent on the fiber orientation within the sheet. The tearing strength of a paper sheet is dependent on fiber length, fiber strength, and the degree of bonding between fibers. The bonding degree at which the maximum tearing strength occurs for HWD fibers is much higher than for SWD fibers (Levlin, 1999). Tearing is a fracture process, the energy required to propagate a fracture is the critical fracture toughness which is given by the equation

$$G = \frac{\beta \sigma^2 a}{E}$$

where β is a geometric parameter, *a* is the crack length, σ is the applied stress, and E is Young's modulus. Thus, a primary factor controlling tear strength is Young's modulus.

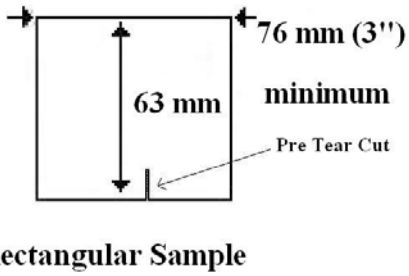

Rectangular Sample

Figure 3-4: Elmendorf tear test, equipment and sample with pre tear cut length (crack length or a)

3.1.1.5 Tensile Properties

Tensile strength of a sheet can be estimated by using the assumption that the fibers alone are responsible for the failure of a paper sheet. This is the simplest estimate and is represented by the following equation (Niskanen, 1998):

$$T = E \cdot \varepsilon_f \qquad \textbf{[Equation 1]}$$

where

T = *tensile strength*
E = *elastic modulus*
ε_f = *elastic breaking strain of the fiber*

Several other theories have been proposed for a more complete model. One model of the process is the Page equation, which was originally formulated for chemical pulps. It is based on the assumption that the tensile strength is proportional to the

fraction of broken fibers along the rupture line. The Page equation is defined as the force per unit cross-sectional area as follows (Page, 1969):

$$\frac{1}{T} = \frac{9}{8 \cdot Z} + \frac{3 \cdot w_f}{\tau_b \cdot l_f \cdot RBA}$$

where

T = *tensile strength*
Z = *zero span strength*
w_f = *fiber width*
τ_b = *breaking force of bond over bond area*
l_f = *fiber length*
RBA = *relative bonded area*

Tensile index relates strength to the amount of material being loaded. Tensile index is primary use to describe the strength of pulps. Tensile index can be calculated as follows (Levlin, 2000):

$$Tensile\ Index = \frac{Tensile\ Strength}{Basis\ Weight}$$

A special form of tensile strength is zero-span tensile strength. This test is performed with a span length as close to zero as possible (see Figure 3-5). This test gives the strength of the individual fibers as opposed to the strength of the paper sheet. It is a useful test for the effect of the pulping process, beating, etc. on the fiber strength. Both wet and dry zero-span tests are valid. Re-wetting the sheet is thought to eliminate the effect of fiber bonding on the test (Levlin, 1999).

The relative bonded area (RBA) of fibers is often used when strength properties, especially tensile, are discussed. RBA is the bonded surface area of the fibers divided by their total surface area. RBA is used to characterize the bonding degree of the paper. When considering a two-dimensional network RBA increased with basis weight. This does not quite hold true for a three-dimensional network, due to the pore structure (Niskanen, 1998). Porosity and thickness have direct correlations with many end uses of paper.

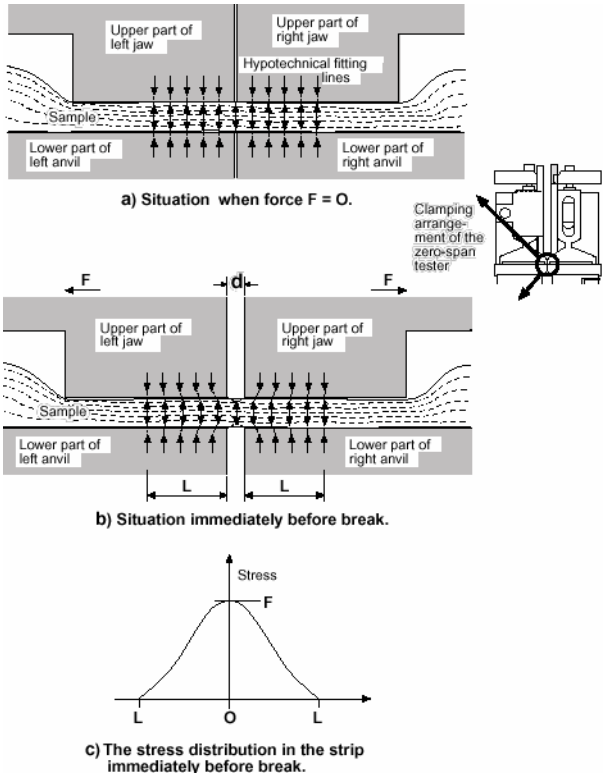

Figure 3-5: Principal of zero-span testing (Levlin, 1999)

Porosity is an important yet complex aspect of paper structure. The three-dimensional pore structure control many paper properties including density, optical properties and mechanical properties. When the basis weight of a paper sheet is very low, the paper in almost two-dimensional because all fibers can bend enough to make contact with the fibers around them. Depending on the fiber, there may be very few pores in the sheet or the fibers may cover the sheet completely and leave no pores in the sheet. As the basis weight increases it is inevitable that pores will form in the fiber structure. Measurement of porosity is often accomplished with liquid or gas flow through a paper sample. Additionally RBA can be measured by the pore structure:

$$RBA = 1 - \frac{(p-1)(1+v)}{c}$$

where:

$p = number\ of\ \ pores$
$c = coverage\ of\ \ fibers$
$v = exp(-c)$

Since mineral fillers do not actually bond with fibers or other fillers, strength properties tend to decrease as filler content increases (Bauch, 1992). Particle size and shape determine the severity of this effect for a given filler. In general, the smaller the filler particle, the more strength is reduced (see Figure 3-6). Clay is particularly detrimental because of its plate like structure (Scott, 1996).

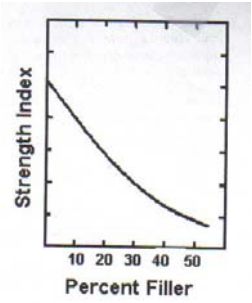

Figure 3-6: General adverse effect of filler on paper strength (Scott, 1996).

3.2 SEM Analytical Procedure

3.2.1 SEM Procedure – Grid Method

Scanning electron microscopy (SEM) has become a popular tool for pulp and paper research. However, most commonly it is used subjectively; observations are made with the intent of finding an example that supports the research. There is little mentioned use of SEM as an objective tool found in the literature. Thus, developing an objective SEM observation method was the first task in this work. Along with the SEM method, a procedure for finding, selecting and measuring all the clay particles in the SEM images was developed using an image analysis program. The image analysis program was able to measure various characteristics of the clay particles, including particle area and perimeter.

The SEM procedure is described pictorially in Figure 3-7. A samples is cut from a handsheet (A), it is then placed on a SEM stub (B), SEM micrographs are taken at pre-

determined coordinates (C), so there is no bias in where the image is taken and what is contained within the image, then the image is processed with the image analysis program, UTHSCSA ImageTool, where the image is thresholded (D), the imaged is processed and all the particles in the image are analyzed and data can then be statistically compared with other physical testing data (E).

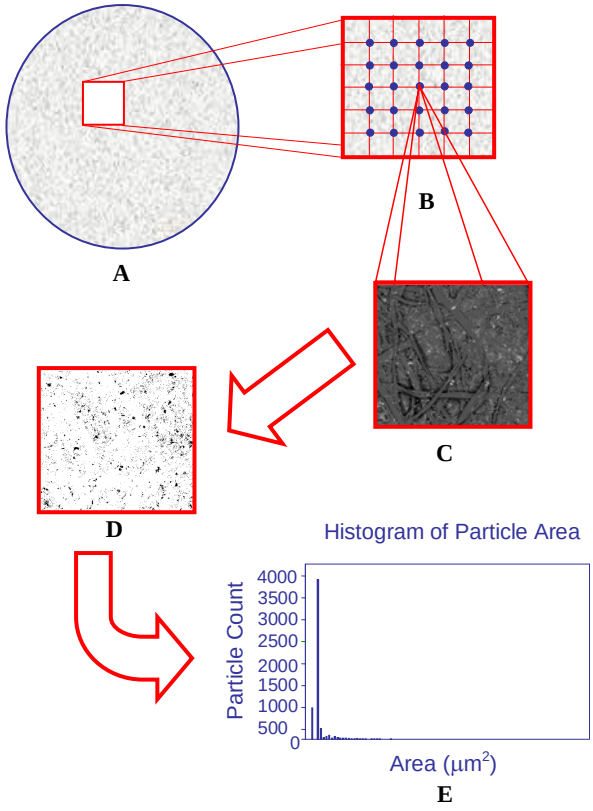

Figure 3-7: Overview of SEM Grid Method

It was critical to obtain the SEM images in a random or objective process in order to perform statistical calculations on the data. The SEM samples were imaged using back scattered electrons (BSE) in order to visualize the difference between filler particles and the other components in the paper samples. Two magnification levels were chosen, 500X and 1000X. It was originally believed that both magnification levels were necessary for studying the designed structures. While both magnification levels gave valuable

information, it became apparent that one or the other should be chosen as the primarily magnification level of study.

The 500X level image contained approximately 10-15 fibers and a wide range of filler particles, giving a wide field of view while still allowing for a significant level of detail. The 1000X level image contained about 2-5 fibers and while it provided greater detail of the filler particles, there were a limited number of filler particles in any given image. When the particle data was summarized and then analyzed, the total area value and the total perimeter value was not the same between the 500X and 1000X images. That result was not unexpected and meant that there was some fundamental difference in the amount of filler being imaged between the 500X and 1000X images. The magnification levels could not be compared directly. Therefore, 500X was chosen as the default magnification level. Also, 500X appears to be a common magnification level used in the literature (Retulainen, 1998).

3.2.2 Statistical Treatment of SEM Data

The SEM image analysis method needed to answer two critical questions:

1. Are the number of samples and the sample sizes adequate to produce valid data?
2. Are the five designed FFP structures different?

Power analysis and sample size, or *PASS*, was used to answer the first question by calculating the required sample size, given the sample means and standard deviation. The one-way analysis of variance, or *ANOVA*, tests for significant differences in the means of the samples and was used to determine if the five structures had different filler area and perimeter characteristics. Development of the SEM methodology was more difficult than anticipated because the filler data proved to be non-normal data with an unknown distribution.

3.2.2.1 Non-Normal Data

One of the major obstacles in understanding the image analysis data was that the data did not follow a normal distribution (see Figure 3-8 and Figure 3-9). Not only was it

difficult to determine what the distribution of the data was, it was even more difficult to find statistical procedures to compare the data. Sometimes it is possible to transform non-normal data to fit a normal distribution. This is accomplished with transformation functions including the Weibull model, the Fisher and Inverse Fisher transformation, the Exponential distribution, the Gamma distribution (γ), the Step-wise function, and the Chi-squared (χ^2) distribution (McDonough, 2003). None of these transformation functions were able to transform the data to fit the normal distribution. Therefore, statistical methods that relied on the data following the normal distribution, or parametric statistics, could not be used.

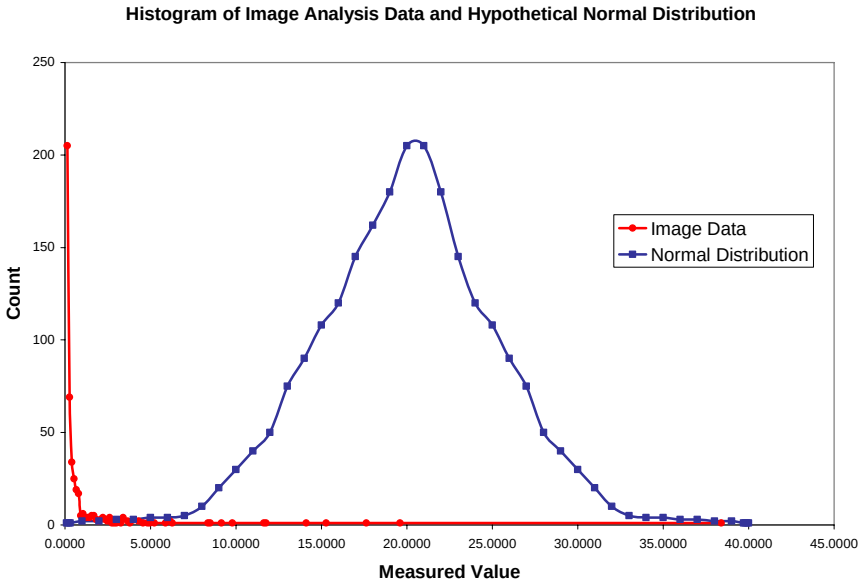

Figure 3-8: Example of actual image analysis data and a hypothetical normal distribution

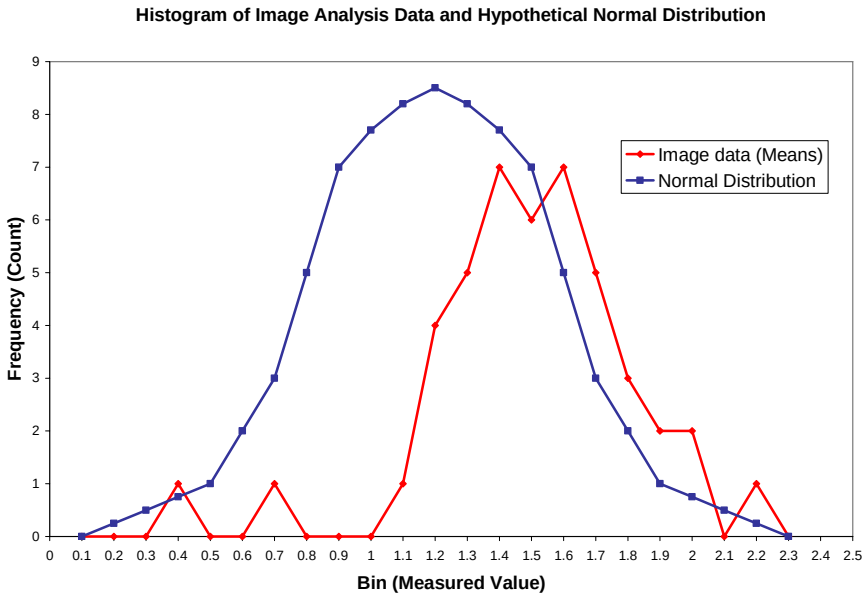

Figure 3-9: Example of actual image analysis data (means) and a hypothetical normal distribution

The failure to identify a suitable transformation method lead to another branch of statistics; non-parametric statistics. Non-normal data requires more complicated statistical methods because there are fewer assumptions required about the data. The most notable assumption is that these methods do not require the underlying populations to fit the normal distribution. With fewer assumptions, the form of the equations cannot be simplified and are difficult to solve without the use of computer methods. The Kruskal-Wallis test is a nonparametric substitute for the one-way ANOVA when the assumption of normality is invalid. Therefore, by using nonparametric statistics it was possible to compare the image analysis data from the different possible FFP structures.

3.2.2.2 Power Analysis and Sample Size

In the initial effort, BSE images were taken from each SEM stub in a 5 X 5 grid giving twenty five micrographs per SEM stub, for a total of one hundred twenty five images per sample (25 image per 5 SEM stubs) and a total of 625 images per designed structures case. This represented a considerable time and resource investment. For the

SEM method to be useful to other studies, it was necessary to determine the minimum appropriate number of samples for SEM imaging and image analysis.

Power Analysis and Sample Size (PASS) calculates the statistical power and determines sample sizes necessary to produce valid results. There are many different PASS analyses and selection of the appropriate method is dependent on the statistical method being used. Some of the PASS analyses include the study of means, variances, correlations, analysis of variance (ANOVA), log rank tests, and multiple regression (Hintze, 2000). A statistical test's *power* is the probability that the test will result in statistical significance. Since statistical significance was the desired outcome of this study, it was necessary to determine if the power was high enough to verify that the data did produce statistical significance.

The *effect size* is the size of the difference in the variable of interest that can be detected by an experimental method. Therefore, the main goal of PASS analysis is to find the useful effect size. The power analysis performed during the design phase of a study to determine the sample size is the type most often used. This type of study would determine the value of N (total sample size) for set values of alpha (α, type I error) and beta (β, type II error) (Hintze, 2000). This was the method used in this study.

A power calculation requires means (or hypothesized means) and the standard deviation (or variance) of those means (Hintze, 2000). Since there was no prior work to take means from, it was decided that one complete set of data was needed in order to use those means to calculate the minimum sample size. It was assumed that five samples combined with the 5 X 5 grid method would be representative of the whole population. The 125 images, analyzed by the image analysis process to obtain particle area and perimeter data. The means from the particle area and perimeter data from each image were used to calculate the means of the data (5 groups of 25 means each). Case II was used. It was the first case studied because it was based on the P&G methodology. Power calculations to determine the minimum needed sample size were performed. The results showed that five samples with 25 images each was 5 times above the minimum sample size required to detect the differences in variation. This was a critical step that affected all the data collection on the remaining four cases.

The PASS method used was for the one-way analysis of variance (ANOVA). Suppose the goal is to determine the sample size needed for *k* groups (SEM stubs). Then:

$$n_1 = n_2 = \ldots = n_k$$

are the number of subjects in each group (number of images per SEM stub) and let *N* be the total sample size of all groups combined (number of SEM stubs times number of images per SEM stub). Also let $\bar{\mu}_w$ be the weighted mean of all groups, therefore (Hintze, 2000):

$$\bar{\mu}_w = \sum_{i=1}^{k} \left(\frac{n_i}{N} \right) \mu_i$$

Next the means of Case II were used to run the power calculation. These means represent the group under the alternative hypothesis, all means are not equal (the null hypothesis (H_0)is that they are equal). The standard deviation of these means (σ_m) is used in the power calculations to calculate the average size of the differences among the means. The standard deviation of the means is calculated using the formula (Hintze, 2000):

$$\sigma_m = \sqrt{\sum_{i=1}^{k} \frac{(\mu_i - \bar{\mu})^2}{k}}$$

This quantity gives the magnitude of the differences among the group means specified above. Note that when all means are equal, σ_m is zero. Therefore one can enter a group of means that are known and be able to calculate n_i. The value of n_i (number of images per SEM stub) calculated in the power analysis can be used as the number of images per SEM stub in the subsequent designed structures cases.

3.2.2.3 One-way Analysis of Variance

If the means of each data set are unique, they can be used to show differences between the data sets from which they originated, in this case differences in the designed structures. The *analysis of variance* is the statistical procedure used to test whether the difference between the means for two or more data sets are significant. While the one way ANOVA for normal data can be calculated by hand (due to assumptions simplifying the equations) it is not so easily done with non-normal data. It was not until the advent of computer programs that non-parametric statistics were widely used (Gibbons, 1976). The

non-parametric version of the one-way ANOVA is the *Kruskal-Wallis one-way Analysis of Variance on Ranks*. The Kruskal-Wallis test is a non-parametric substitute for the one-way ANOVA when the assumption of normality is not valid.

The one-way analysis of variance compares the means of two or more groups and it will determine if at least one group mean is different from the others. In the *one-way analysis of variance*, the null hypothesis, H_0, is that the means of two or more independent samples were equal and the samples could be regarded as coming from the same population, i.e. there was no difference between the samples. The F-ratio, similar to the t-test is used to determine statistical significance. The tests are non-directional in that the null hypothesis (H_0) specifies that all means are equal and the alternative hypothesis states that at least one mean is different, but does not state which one(s) are different (Hintze, 2000). The Kruskal-Wallis ANOVA uses a test called the *Multiple-Comparisons Z-Value Test* which shows what means are different.

There are two possible types of errors in hypothesis testing, *Type I* and *Type II*. Type I error is when a true null hypothesis is rejected and this is specified by the level of alpha, α, here $\alpha = 0.05$ was used throughout the study. A Type II error is when a false null hypothesis is thought to be true and the possibility of committing a Type II error is noted by beta, β (see Table 3-7). Therefore, the *power* of statistical test is the likelihood of rejecting a false null hypothesis, or $(1-\beta)$.

Table 3-7: Error types in hypothesis testing (Gibbons, 1976)

		Actual Situation **H_0 True**	**H_0 False**
Researcher's Decision	**Accept H_0**	Correct Acceptance	*Error (Type II)*
	Reject H_0	*Error (Type I)*	Correction Rejection

The assumptions for the one-way ANOVA and the Kruskal-Wallis ANOVA are as follows (Hintze, 2000):

a. The data are continuous (not discrete).

b. The data follow the normal probability distribution. Each group is normally distributed about the group mean.
c. The variances of the populations are equal.
d. The groups are independent. There is no relationship among the individuals in one group as compared to another.
e. Each group is a simple random sample from its population. Each individual in the population has an equal probability of being selected in the sample.

The Kruskal-Wallis Test Assumptions (Hintze, 2000) are:

a. The variable of interest is continuous (not discrete). The measurement scale is at least ordinal.
b. The probability distributions of the populations are identical, except for location. Hence, we still require that the population variances are equal.
c. The groups are independent.
d. All groups are simple random samples from their respective populations. Each individual in the population has an equal probability of being selected in the sample.

The only different between the normal one-way ANOVA and the Kruskal-Wallis one-way ANOVA is the assumption of normality. Two key assumptions in the Kruskal-Wallis one-way ANOVA are that the distributions are at least ordinal in nature and that they are identical, except for location. This means that ties (repeated values) are not acceptable and when ties are present in the data, the corrected version of this test should be used. Therefore, the data presented here meets all the assumptions for the Kruskal-Wallis ANOVA. It was used as the ANOVA method for all data analysis.

Chi-Squared (χ^2), or H, is the Kruskal-Wallis test statistic. If the ANOVA test returns a value higher than the test statistic, H, then the null hypothesis is accepted. If the value of H is high, then it is most likely that the null hypothesis will be rejected. Therefore in the data analysis the larger the value of H, the greater chance of rejecting the null hypothesis and the greater then chance that the means being compared are significantly different. The formula for H, where H is uncorrected for ties is (Hintze, 2000):

$$H = \frac{12}{N(N+1)} \sum_{i=1}^{k} \frac{R_i^2}{n_i} - 3(N+1)$$

The Kruskal-Wallis test statistic corrected for ties is calculated by dividing H by a correction factor and is given by (Hintze, 2000):

$$H_C = \frac{H}{1 - \frac{\sum t\left(t^2 - 1\right)}{N\left(N^2 - 1\right)}}$$

In both of the above formulas, N is the total sample size, n_i is the sample size of the i^{th} group, k is the number of groups, R_i is the sum of the ranks of the i^{th} group, and t is the count of a particular tie (Hintze, 2000).

3.3 Principal Components Analysis

Relationships between the physical test data and the SEM image analysis results were evaluated using a statistical method referred to as *principal components analysis* or *PCA*. PCA has been useful for other data analysis including statistical process control (Wise, 1991), capillary electrophoresis spectra of wood extracts (Bronze, 1998), fiber properties and corss-sectional characteristics of mechanical pulp handsheets (Nesbakk, 2001), recycling effects on pulp fiber properties (Khantayanuwong, 2003) and modeling sulfur K-XANES spectra of humic acid (Beauchemin, 2002). When research is performed and data can be collected for many different variables, the goal is to find relationships or *correlations* between the different data. Often there will be some redundancy in the information provided by the variables. PCA is a data analysis tool that is used to take a large data set and break it down into smaller *principal components* of the data which contain a minimum amount of redundancy. It is an effective technique to reduce the dimensionality (number of variables) of a large set of interrelated variables, yet at the same time retaining as much of the information (variation) as possible.

The principal components derived from the data are called *factors*, which are linearly related to each other and should be minimal in number (Sheskin, 2000). PCA is a computational procedure that uses eigenvalues and eigenvectors to derive the factors. PCA can use either a *correlation matrix* (standardized) or a *covariance matrix* (non-standardized). The data is standardized by subtracting the mean and dividing by the standard deviation. When dealing with variables measured in different units, the correlation matrix must be used (Palmer, 2004). Because many different physical testing data and image analysis data was compared, the correlation matrix was used.

The data set consisted of 21 physical paper tests and 2 image analysis parameters for a total of 23 variables. The aim of using PCA was to relate the data to a smaller number of variables. It can be explained in a graphical fashion. Here is an example for finding the eigenvalues for a 2 X 2 matrices. Consider the following matrix in which the rows are the coordinates of a pair of points in 2-D space:

$$\begin{bmatrix} 4 & 8 \\ 8 & 4 \end{bmatrix}$$

Using the (0,0) coordinate as the centre it is possible to construct an ellipse, such that the two points fall on its perimeter. The ellipse is two dimensional because there are two sets of data, or two variables. Points on the ellipse represent all the different possible combinations of the two variables. If there were three variables, the plot would be an ellipsoid similar to a rugby ball.

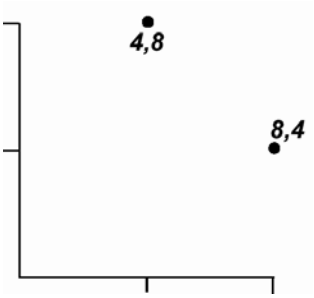

Figure 3-10: Graphical representation of a 2 X 2 matrix (Fielding, 2004)

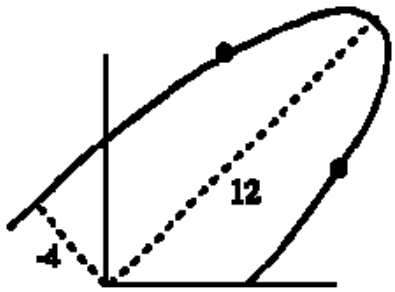

Figure 3-11: Ellipse though the two points of the 2 X 2 matrix, with the two eigenvalues shown (Fielding, 2004)

A 2 X 2 matrix has two eigenvalues (λ_1, λ_2) an in the above example they are 12 and -4, (the lengths of the major and minor axes of the ellipse that encloses the points). There are two eigenvectors (unit vectors) associated with each of the two eigenvalues. In order to draw an ellipse, not only are the lengths (eigenvalues) needed, so are information about their orientation, i.e. their coordinates. The eigenvectors are the coordinates that specify the orientation of the axes and the eigenvalues are the length of the axes. (Fielding, 2004).

In this study the relationships between all 23 variables (dimensions) must be determined to find out which data is redundant and which is unique. There will be 23

linear equations, where the first equation will relate the first variable to all the other variables, the second equation will relate the second variable to all the other variables, etcetera. These 23 equations need to be solved simultaneously. PCA solves these equations and calculates the corresponding eigenvalues and eigenvectors for each of the linear equations.

Eigenvectors are unit vectors. The magnitude is given by the eigenvalue. Eigenvector components have positive and negative directions within each eigenvector. The eigenvector components are a portion of the total eigenvector in a particular "direction." The eigenvalue is the "amount" in the direction of the eigenvector "direction." The mathematical explanation of PCA is as follows:

PCA assumes that the observed physical and particle data can be expressed as a linear combination of components, where each component is weighted. Let **D** be an *s* by *v* data matrix (of *s* rows by *v* columns), where the rows are samples (Case I, Case II, Case III, Case IV, Case V) and the columns are the variables (bright, bend, COFK, COFS, Form, etcetera). Then **D** is mean-centered such that all its columns, *v*, have zero means. In PCA, **D** is decomposed into the sum of the product of *v* pairs of vectors (Jackson, 1981). Each pair of vectors is composed of a *v* by *1* vector call the factor loading, $\mathbf{f}_i$, and a *s* by *1* vector call the factor score, $\mathbf{c}_i$. Then **D** can be re-written as:

$$\mathbf{D} = \mathbf{c}_1\mathbf{f}_1^{\mathrm{T}} + \mathbf{c}_2\mathbf{f}_2^{\mathrm{T}} + \cdots + \mathbf{c}_v\mathbf{f}_v^{\mathrm{T}}$$

The matrix of loads vectors $\mathbf{f_i}$ form a new orthogonal basis for the vector space spanned by **D** and the individual $\mathbf{f}_i$, are then the eigenvectors of the covariance matrix of the data matrix **D**, such that:

$$\text{covariance}(\mathbf{D}) = \frac{1}{s-1}\mathbf{D}^{\mathrm{T}}\mathbf{D}$$

Therefore,

$$\text{covariance}(\mathbf{D})\mathbf{f}_i = \lambda_i\mathbf{f}_i$$

where λ_i is the eigenvalue associated with eh eigenvector $\mathbf{f}_i$. If **D** has been transformed so that each column has been scaled to a variance of 1, then the covariance matrix becomes the correlation matrix. The factor loadings, $\mathbf{f}_i$, are referred to as the principal components because they are linear combination of the original variables and together they account

for the majority of the variance (information) from the original data matrix **D**. Then, each of the factor score vectors, $\mathbf{c}_i$, is a projection of **D** onto the factor vector $\mathbf{f}_i$:

$$\mathbf{c}i = \mathbf{D}\mathbf{f}_i$$

PCA finds a set of dimensions (eigenvectors) in a subspace of the space defined by the set of variables (eigenvalues). These coordinates are represented as axes. They are orthogonal (perpendicular) to one another. For example, suppose you analyze three variables that are represented in three-dimensional space. Each variable becomes one axis. Now suppose that the data lie near a two-dimensional plane within the three dimensions. A PCA of this data should uncover two factors (eigenvalues) that would account for the two dimensions (eigenvectors), so that now the data can be explained by two dimensions instead of three. Therefore, relating this back to the analysis of the 23 variables, there would be 23 eigenvalues with 23 eigenvectors. This plot gets very complicated as we are now in a 23 dimensional space (23-D space)!

By imputing all 23 variables PCA takes in all 23 variables and reduces all the variables into 23 or fewer *factors*. A factor is a correlation equal to an eigenvalue multiplied by an eigenvector which consist of eigenvector components. The eigenvalues are important because they are used to determine which factors to keep. PCA on 23 variables or dimension can return as many as 23 factors or unique correlations of the 23 variables. Each factor has an eigenvalue and the sum of the eigenvalues of all the factors is equal to the number of variables. However, not all the factors are going to retain enough of the original data (from the original variables) to be of significant value. When the PCA is run on the variables, one rule-of-thumb is to retain those factors whose eigenvalues are greater than one.

4 RESULTS

This chapter presents the pertinent results related to the physical properties, the SEM method, image analysis including PASS and ANOVA and the PCA analysis. Interesting aspects of the results will be pointed out but any significant discussions and conclusions are presented in chapter 5. Both the results chapter and discussion chapter are organized in a similar fashion.

4.1 Bulk Physical Properties

Recall from Table 3-1 that the physical tests are grouped based on fundamental properties:

- *Surface Characteristics*: Sheffield Roughness; Print-Surf; and Static and Kinetic Coefficient of Friction
- *Optical*: Brightness; and Printing and TAPPI Opacity
- *3-D Structure*: Formation; Basis Weight; and Ultra Sonics Thickness
- *Inverse Stiffness*: Tear Index; Bending Stiffness; and Ultra Sonics Elastic and Specific Stiffness, Travel Time and Velocity
- *Inverse Tensile*: Tensile Index; Z-Directional Tensile; Zero-Span Tensile; and Porosity

The results are presented in keeping with these groups. Before presenting the physical testing results, the image analysis results of the particles from SEM micrographs are first presented.

4.1.1 Filler Characteristic from SEM Images

Table 4-1 is a summary of the particle data as determined by the image analysis program for all the SEM micrographs. For every SEM micrograph, the area of the image is 40,000 μm^2. There are two unusual results in the data that can be explained. First, the area and perimeter data for the 0% filler levels appears to be inconsistent with the area and perimeter data for the remaining filler levels. This is due to the 0% filler levels having very few particles per image. This skews the data because the 0% filler level samples are dominated by a few large particles, without the hundreds or thousands of small particles figured into the average particle area and perimeter of the remaining filler

levels. Second, there were 125 SEM micrographs taken for each filler level in Case II, but only 45 SEM micrographs were taken for the rest of the cases. The sample size difference is apparent in the total filler column of Case II verses Cases I, III, IV and V, but it has already been factored into the rest of the table (i.e. normalized to number of samples, 125 or 45).

Table 4-1: Particle Data from Image Analysis of the SEM Micrographs for all Cases and all Filler Levels (Target Filler Levels) *See footnotes for column definitions*

Case Identification	Ash Content (%)	Average Area (μm^2)	Average Perimeter (μm)	Total Filler (area, μm^2)	Average Filler (area, μm^2)	Number of Particles per Image	Average Coverage (area, μm^2)	Average % Filler (area, μm^2)
Case I 0%	0.00%	5.19	7.83	685.62	15.24	2.02	0.00	0.04%
Case I 5%	2.04%	2.10	3.39	16,113.21	358.07	350.69	0.01	0.90%
Case I 10%	5.27%	1.25	2.86	28,288.52	628.63	502.98	0.02	1.57%
Case I 15%	6.86%	1.55	3.03	30,625.26	680.56	439.82	0.02	1.70%
Case I 20%	10.52%	2.05	3.36	40,187.56	893.06	434.76	0.02	2.23%
Case II 0%	0.00%	5.12	5.54	1,599.60	12.60	1.13	0.00	0.03%
Case II 5%	5.42%	1.48	3.14	155,609.78	1,244.88	843.63	0.03	3.11%
Case II 10%	10.03%	1.50	3.31	374,380.49	2,995.04	1,991.94	0.07	7.49%
Case II 15%	14.58%	1.63	3.63	517,897.65	4,143.18	2,537.66	0.10	10.36%
Case II 20%	16.88%	1.83	3.91	632,668.00	5,061.34	2,770.53	0.13	12.65%
Case III 0%	90.00%	0.20	0.66	619.75	13.77	68.15	0.00	0.03%
Case III 5%	5.58%	1.01	2.75	39,671.04	881.58	874.19	0.02	2.20%
Case III 10%	9.72%	1.12	3.03	75,473.66	1,677.19	1,499.00	0.04	4.19%
Case III 15%	14.55%	1.44	3.50	123,403.61	2,742.30	1,899.74	0.07	6.86%
Case III 20%	19.50%	1.33	3.40	131,166.68	2,914.82	2,187.37	0.07	7.29%
Case IV 0%	1.09%	0.45	1.48	900.37	20.01	44.78	0.00	0.05%
Case IV 5%	5.40%	0.69	2.29	32,012.66	711.39	1,032.41	0.02	1.78%
Case IV 10%	8.60%	0.64	2.27	88,111.03	1,958.02	3,039.83	0.05	4.90%
Case IV 15%	12.89%	0.90	2.70	171,270.59	3,806.01	4,244.89	0.10	9.52%
Case IV 20%	16.88%	0.78	2.60	218,223.03	4,849.40	6,231.85	0.12	12.12%
Case V 0%	0.00%	5.19	7.83	685.62	15.24	2.02	0.00	0.04%
Case V 5%	3.08%	1.51	2.77	5,177.07	115.05	76.16	0.00	0.29%
Case V 10%	5.69%	3.23	4.40	17,221.92	382.71	118.65	0.01	0.96%
Case V 15%	8.59%	0.36	0.17	4,344.31	96.54	267.42	0.00	0.24%
Case V 20%	12.98%	1.95	3.67	47,959.45	1,065.77	546.64	0.03	2.66%

Area (μm^2) refers to the average area of all the particles found by the image analysis.

Perimeter (mm) refers to the average perimeter of all the particles found by the image analysis program.

Total Filler (area, μm^2) refers to the total filler area of all particles in all the SEM micrographs.

Average Filler (area, μm^2) refers to the average total filler area of all the particle in all the SEM micrographs.

Number of Particles per Image refers to the average number of particles per SEM micrograph.

Average Coverage (area, μm^2) refers to the average coverage area in the all SEM micrographs by of all the particles.

Average % Filler (area, μm^2) refers to the average percent coverage area in the all SEM micrographs by of all the particles.

The image analysis data reveals several telling facts about the different FFP cases. The total filler area increases rapidly from the 0% filler levels, especially in Case II, Case III and Case IV where the magnitude is a factor of 10 higher than Case I and Case V. This is due to the higher actual filler content of the handsheets. The number of particles per image all increase rapidly from the 0% filler level. Again, Cases II, III and IV are a factor of 10 greater than Cases I and V.

The last column in Table 4-1 is particularly interesting because it gives the percentage of filler coverage on the wire side of the handsheets. The wire side is a surface view of the paper sample and is one layer of the paper structure. If the z-direction filler distribution was constant then percent filler coverage would be equal to the actual filler content of the sheet (see Figure 4-1). Cases II, III and IV had higher percentages than Cases I and V. This was expected because Cases II, III IV all had higher overall filler retention. Cases II and IV have the highest filler retention. Case III had lower percentages, which is interesting because it was expected that Cases II and III would be similar to each other since they are the two pre-flocculation cases.

There is a deviation in Case V (Ethanol) at the 15% filler level. The actual filler content for the 15% level is in between 10% and 20% actual fillers levels as expected. However, this is not evident from the SEM micrograph data. Without further study, there is not a logical explanation fir the clay content of the 15% filler level in Case V.

Figure 4-1 shows how the particle area and perimeter vary with actual filler content (ash). The filler area and perimeter size was most consistent with Case II (excluding 0%), Case III and Case IV. The particle area and perimeter size appears to increase slightly for Case II and Case III. However, the data shows that the pre-flocculation of the clay does not appear to greatly increase or decrease the area and perimeter of the filler particles relative to filler that was not pre-flocced i.e., Case IV. The average area and perimeter is slightly smaller for Case IV than Cases II and III. Cases I and V have variation in the area and perimeter size, even if the 0% filler level is eliminated. It appears that not only do polymers increase filler retention, they also stabilize the size of the filler particles.

4.1.2 Ash content of designed structures

Percent ash approximates the filler content of paper. Figure 4-2 below show the measured ash content versus the initial percentage of clay added to each sheet. Percent ash increased as added clay content increased for all cases. The slope of all the series plotted (Cases I, II, III, IV, and V) was less than 1 which suggests less than 100% filler retention. As can be seen from Figure 4-2, the cases which include polymer addition (Cases II, III and IV) have significantly higher ash content than the two cases without polymer addition. This is expected since the polymers used in Cases II, III and IV are designed to improved filler retention. Cases II and III are identical through the 15% filler level, at 20% filler level, Case III approaches 20% actual filler content and Case II approaches 17% actual filler content. Case IV does not have the same ash content as Case II and Case III after the 5% filler level

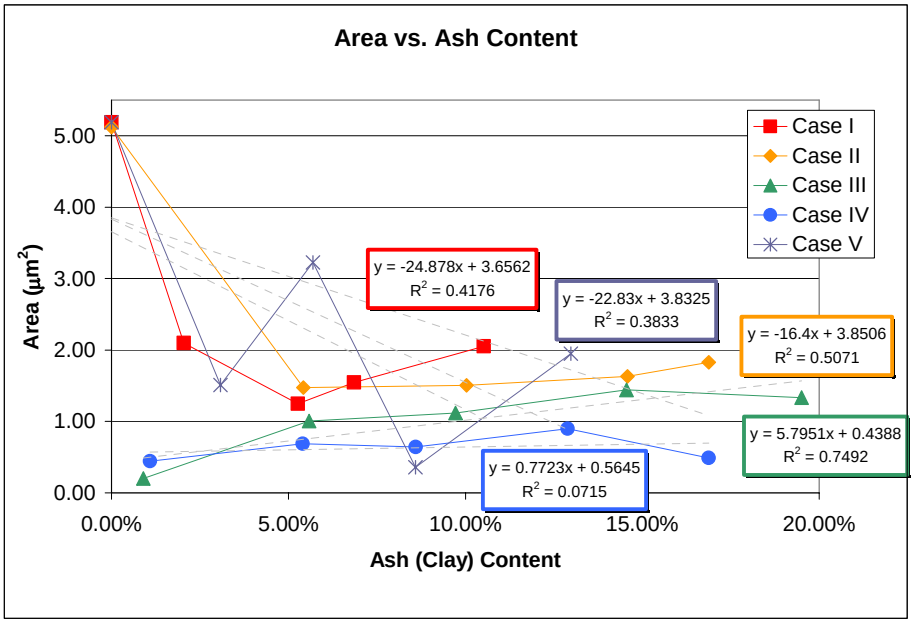

A

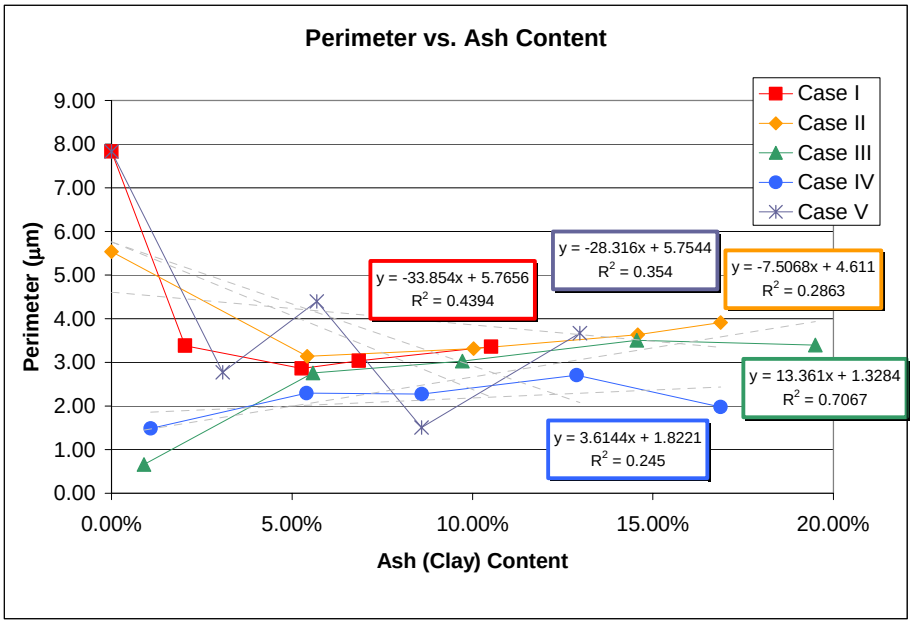

B

Figure 4-1: (A) Average Area (µm^2) and (B) Perimeter (µm) measured by Image Analysis for the Actual Filler Content (Ash) of the Five Different FFP structures.

The data falls into two groups: Cases I and V; and Cases II, III, and IV. The slopes for Case I and Case V are 0.51 and 0.62 respectively, indicating much less than complete retention. The slopes for Case II, Case III and Case IV are 0.85, 0.92, 0.78 respectively indicating a much higher retention but still not complete retention. The overall retention is calculated by:

$$Overall\ retention\ (\%) = \frac{amount\ retained\ in\ sheet}{amount\ added\ with\ stock}$$

Recall that initial filler addition was multiplied by a factor of 1.2 to account for lack of complete retention. If the actual filler addition accounts for that over compensation then the table is as follows:

Table 4-2: Overall Retention of Kaolin Filler after Accounting for Addition Factor of 1.2

Overall Retention (%)	0%	5%	10%	15%	20%
Case I	N/A	34.00%	43.88%	38.08%	43.83%
Case II	N/A	90.33%	83.58%	81.00%	70.33%
Case III	N/A	78.00%	81.00%	80.83%	81.25%
Case IV	N/A	71.83%	71.67%	71.61%	70.33%
Case V	N/A	51.33%	47.42%	47.72%	54.08%

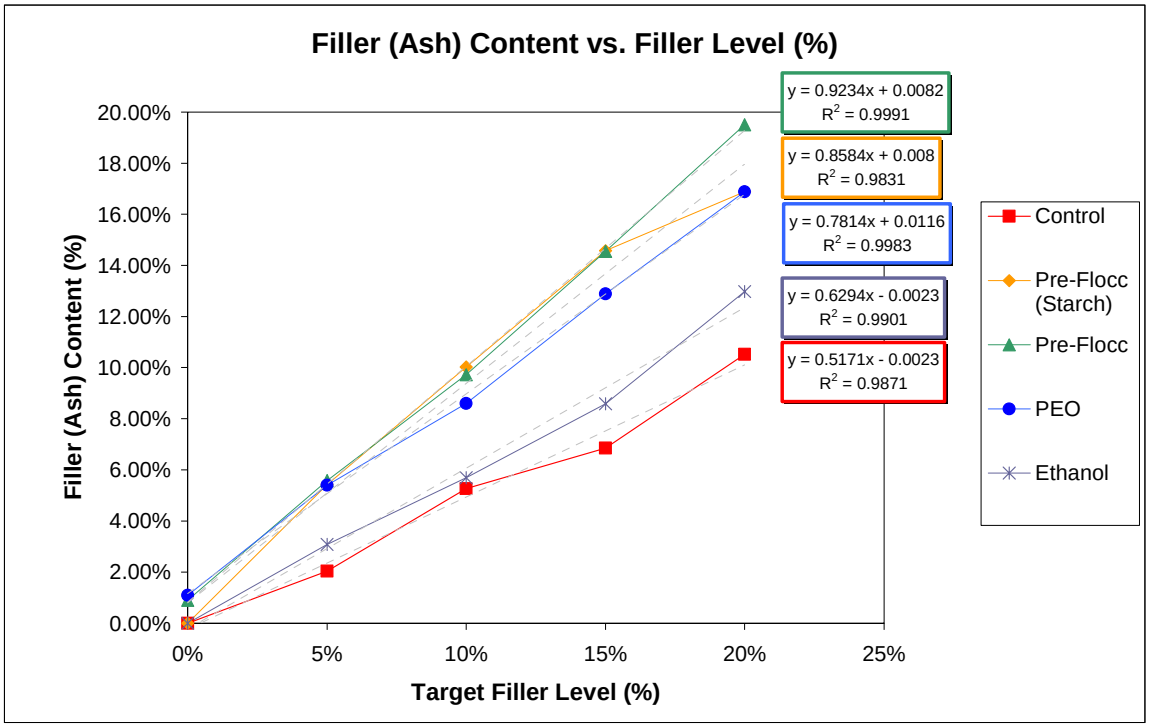

Ash	0%	5%	10%	15%	20%
Case I	0.000%	2.040%	5.265%	6.855%	10.520%
Case II	0.000%	5.420%	10.030%	14.580%	16.880%
Case III	0.900%	5.580%	9.720%	14.550%	19.500%
Case IV	1.090%	5.400%	8.600%	12.890%	16.880%
Case V	0.00%	3.08%	5.69%	8.59%	12.98%

Figure 4-2: Target Filler Content vs. Actual Ash Content

The lowest filler retention occurs in Case I, with Case V being only slightly higher. The solvent (ethanol) coated filler is the only difference between Case I and Case V. It appears that it has some effect on retention. It was anticipated that Case V would have lower retention than Case I, which is the opposite of what the data showed. The retention of Cases III and IV is roughly constant across all filler addition levels. The

retention of Case III is 10% higher than Case IV, average ≈80% vs. ≈71%. Case II is very interesting because retention drops from ≈90% down to ≈70%. This is the only case to have such a large drop in filler retention.

4.1.3 Surface Characteristics

The *surface characteristics* studied were static and kinetic coefficient of friction (COF), parker-pint surf and Sheffield roughness. Figure 4-3 includes both static and kinetic COF plotted against ash content. COF is a measure of the friction on the surface of the sample and may increase or decrease with filler addition, depending on the surface chemistry. Overall, the static and kinetic coefficient of friction (COF) appear to have a positive correlation with filler content (see Figure 4-3). The one exception is the static COF for Case IV. Both static and kinetic COF are highest for Case V, which was the only case to use ethanol. Case I contained only filler and fiber and is the second highest static COF. Also, Cases II and III have identical static COF which makes sense because the surface chemistry is likely to be similar. However, it is possible that the starch in Case II causes the difference in kinetic COF between Cases II and III. Case IV follows a different trend which could be due to the addition of PEO.

The data from the Print-Surf measurements is inconclusive (see Figure 4-4). As Print-surf decreases, the surface of the paper should be smoother. There does not appear to be explainable correlations. The data suggest a weak negative correlation with filler content, but each case follows a different pattern. It would be expected that Print-surf would decrease due to increased filler content. However, Print-surf is most commonly used in coated papers and thus there may not be any useful results. The Print-surf results will not be included in the PCA analysis for this reason.

The Sheffield roughness has a negative correlation with increased filler content (see Figure 4-5). This is what was expected because the higher the Sheffield units, the rougher the surface is. However, it is interesting that Case III has a higher surface roughness because it had equal or higher actual filler content than Cases II or IV. It was expected that the surface of Cases I and V be high, but Case V surface roughness is lower than Case III and after 0% filler level, roughly equal to Case II.

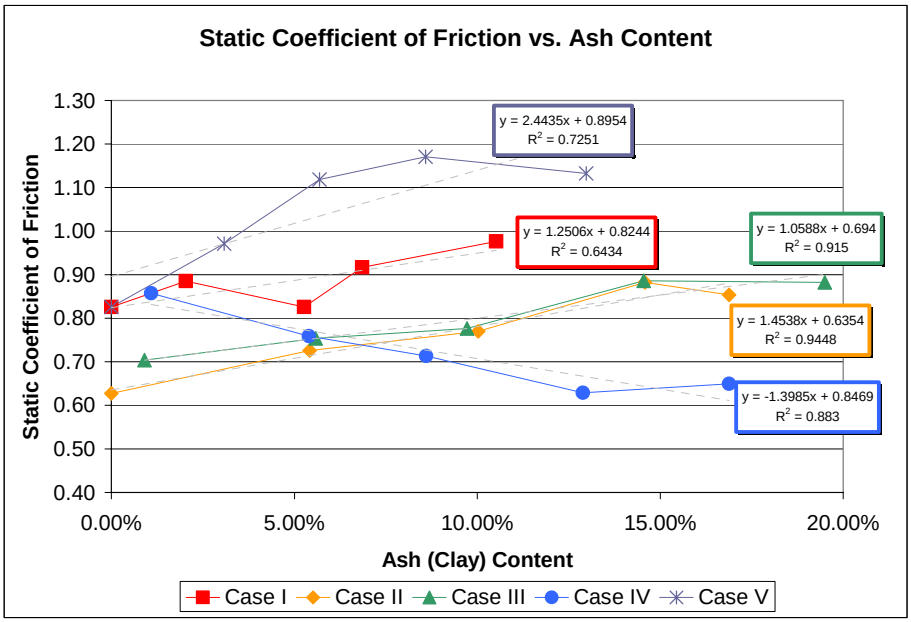

A

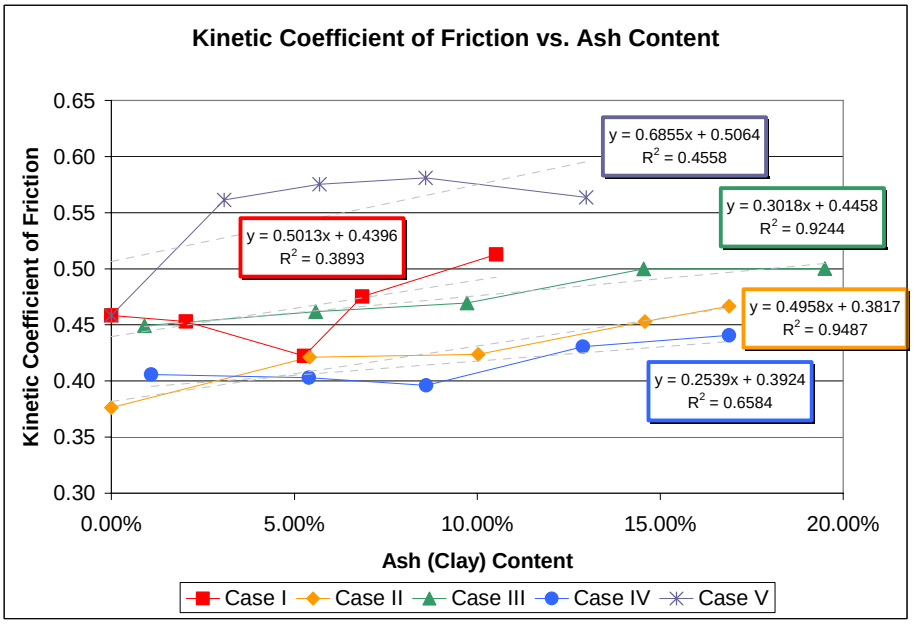

B

Figure 4-3: Static and Kinetic COF vs. Ash Content

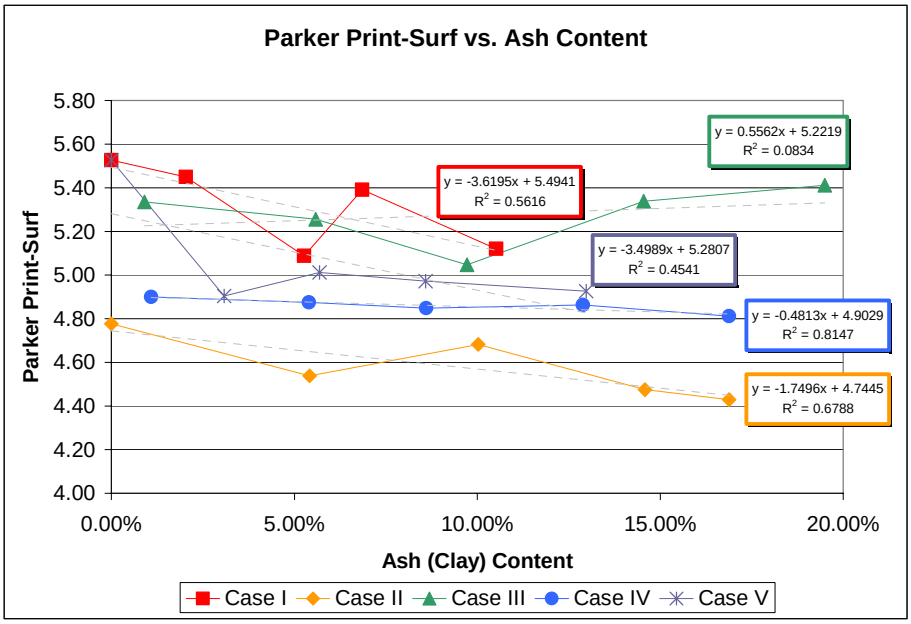

Figure 4-4: Parker Print-Surf vs. Ash Content

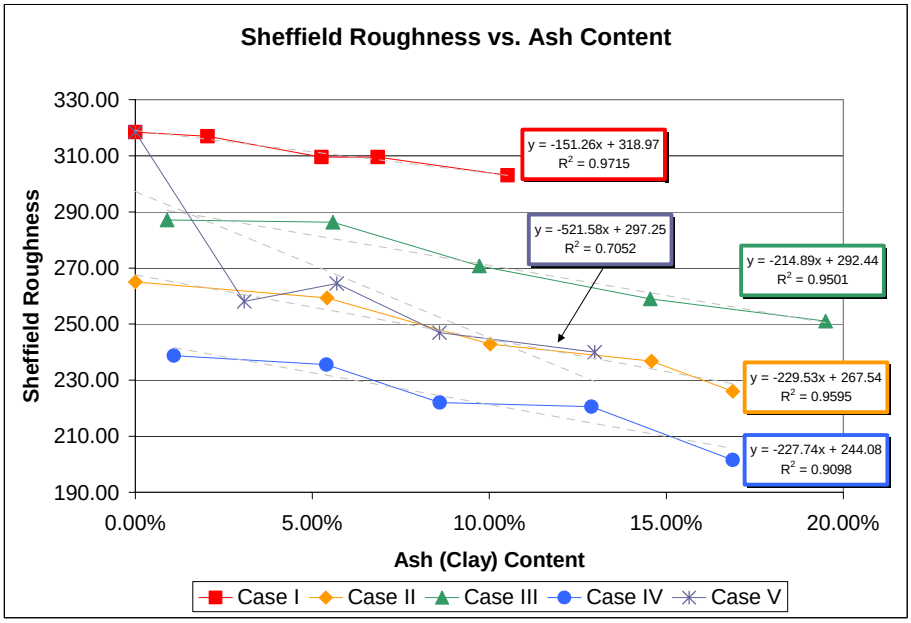

Figure 4-5: Sheffield Roughness vs. Ash Content

4.1.4 Optical Properties

The *optical properties* examined were brightness, printing opacity and TAPPI opacity. The only other physical characteristic that displays a strong positive correlation

with ash content is brightness (see Figure 4-6). This was expected since it is widely recognized that filler content generally increases brightness and scattering coefficient. At low ash content both Cases I and V (no polymers) are constant at ≈60-61 % and rise only slightly with further increases in ash content. This too is expected because the filler retention for Cases I and V was less than 50%.

Cases with polymer show a strong positive linear correlation with no leveling off at low or high ash values. From this plot, brightness could be extrapolated to increase with even higher filler content. It is possible that brightness would only level off with failure of the polymers to gain higher retention. At the highest ash contents, Case IV had the highest brightness while Case III had the highest ash content suggesting other factors of secondary importance may be affecting sheet brightness.

Opacity did not appear to have the strong positive correlation with increased filler content that was expected (see Figure 4-7). Cases I, IV, and V have a negative correlation with ash content, albeit very small. Case II is the only case to have a strong positive correlation with ash content. with the starting opacity lower and the final opacity higher than the other cases.

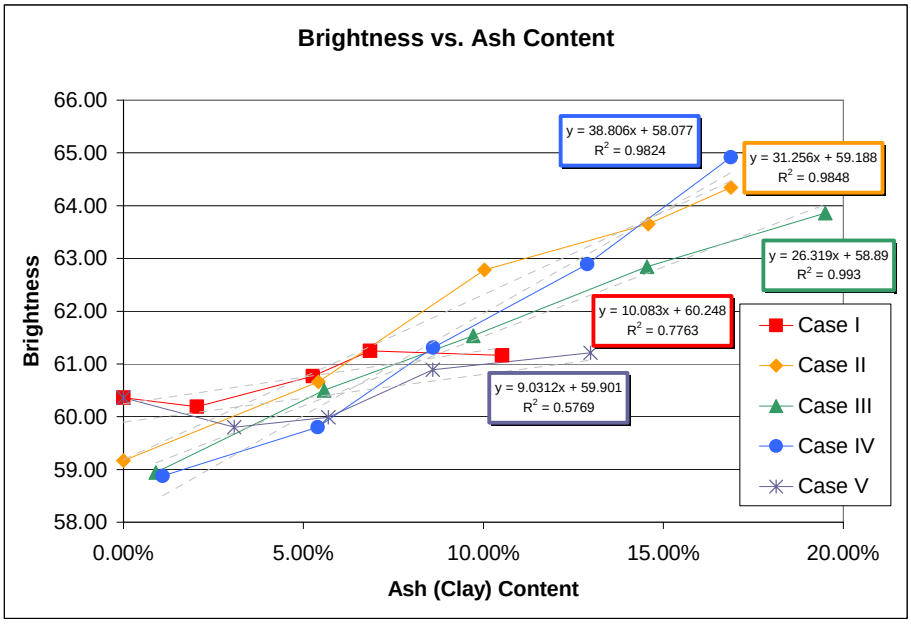

Figure 4-6: Brightness vs. Ash Content

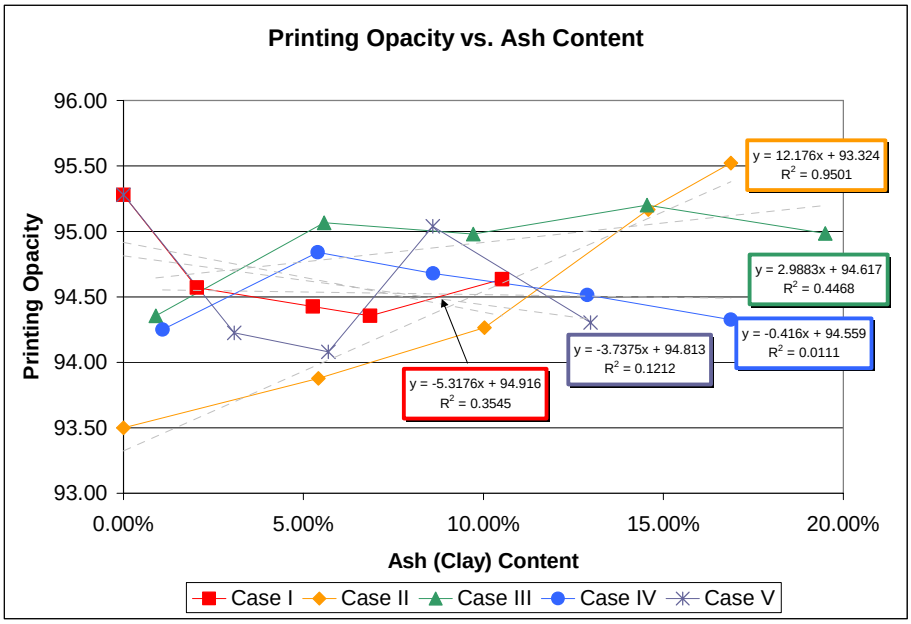

A

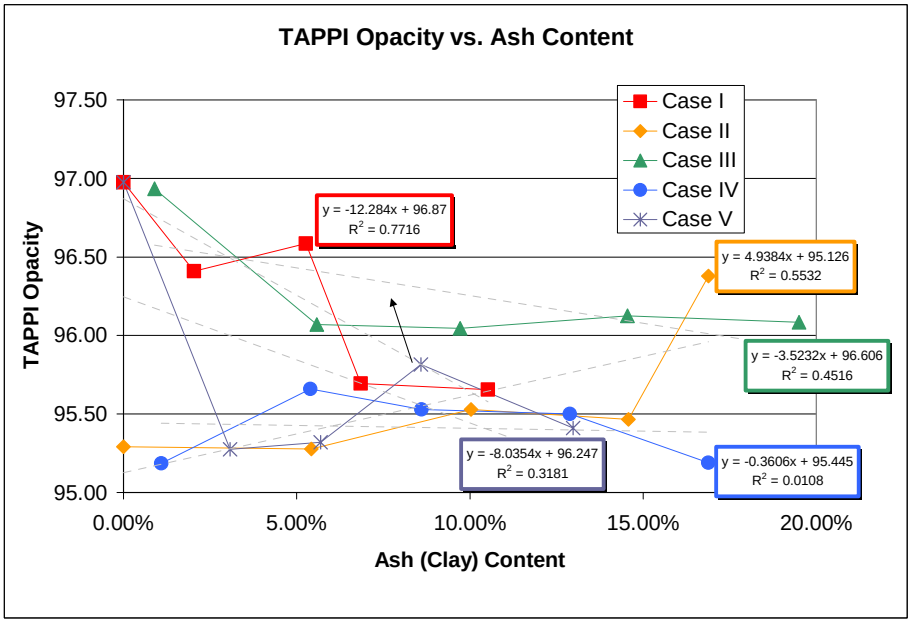

B

Figure 4-7: Printing (A) and TAPPI (B) Opacity vs. Ash Content

4.1.5 3-D Structure

Three properties were studied as they related to *3-D structure*; formation, basis weight and ultrasonic thickness. Basis weight was expected to decrease because filler

addition was by weight hence as filler was added fiber weight decreased. Therefore, an overall negative correlation was expected even more so for in Cases I and V. Basis weight for Case I decreases steadily as filler addition increases, where as it is remains relatively constant for Cases II, III and IV. The discrepancies in starting basis weight for each case could be from each case being made from different buckets of thick stock. For Case V basis weight decreased rapidly with filler content with the exception of the second highest filler level, which may be simply a bad data point. It appears that the ethanol adversely affected the handsheet formation.

High formation index values equates to good formation. It was expected that formation would worsen as filler content increased, which was the general result. Cases I and V have significant drops in formation, which was anticipated. Case IV had the best formation, which maybe one reason that PEO is used so frequently with mechanical pulp. Formation is highly correlated with basis weight. If one compares the basis weight and formation charts, the plots for each are similar. It is unclear why Case II had the worst formation, but it may have been caused by over flocculation of the furnish or starch addition.

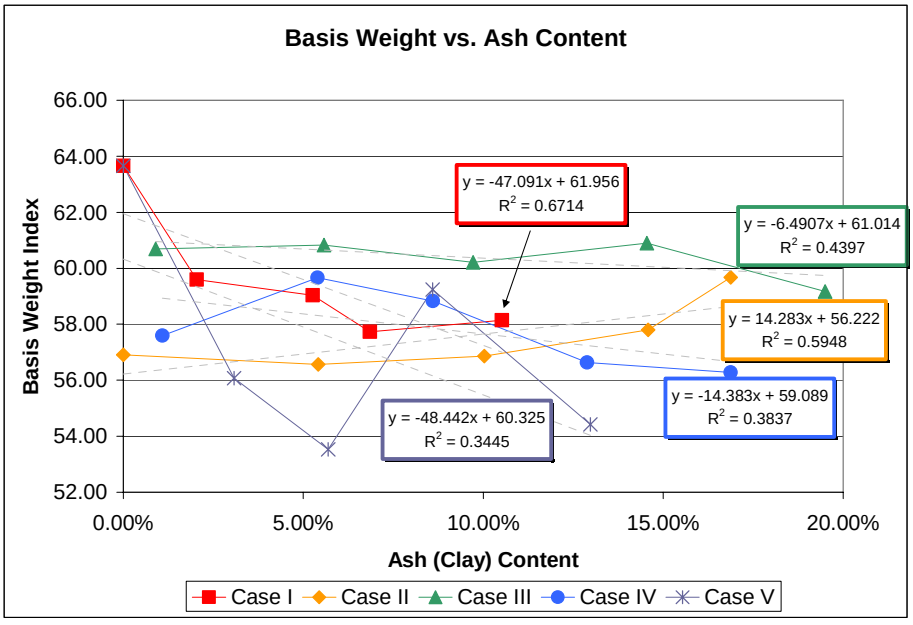

Figure 4-8: Basis Weight vs. Ash Content

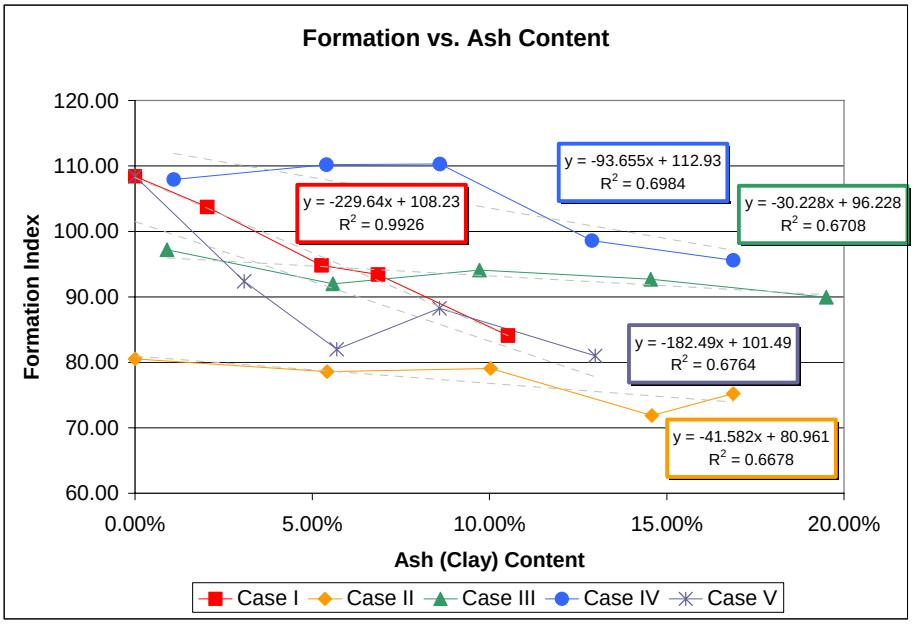

Figure 4-9: Formation Index vs. Ash Content

The ultrasonic results are interesting (see Figure 4-10). Ultrasonic measurements are closely tied to the elastic modulus, E. Bonded area, bond strength, sheet consolidation (caliper) and fiber elastic modulus all have an impact on sheet elastic modulus. It was not expected that any of the cases would have such different results as Cases I and II had with Cases III, IV and V. This pattern is repeated with all but one of the other ultrasonic results (see Figure 4-13). The reason for this is error in ultrasonic thickness for Cases I and II. This error propagated through to the velocity and elasticity (which is proportional to velocity squared). The error does not effect travel time because measured caliper is not a factor. Therefore, ultrasonic thickness, velocity, elastic stiffness and specific stiffness will not be analyzes with PCA.

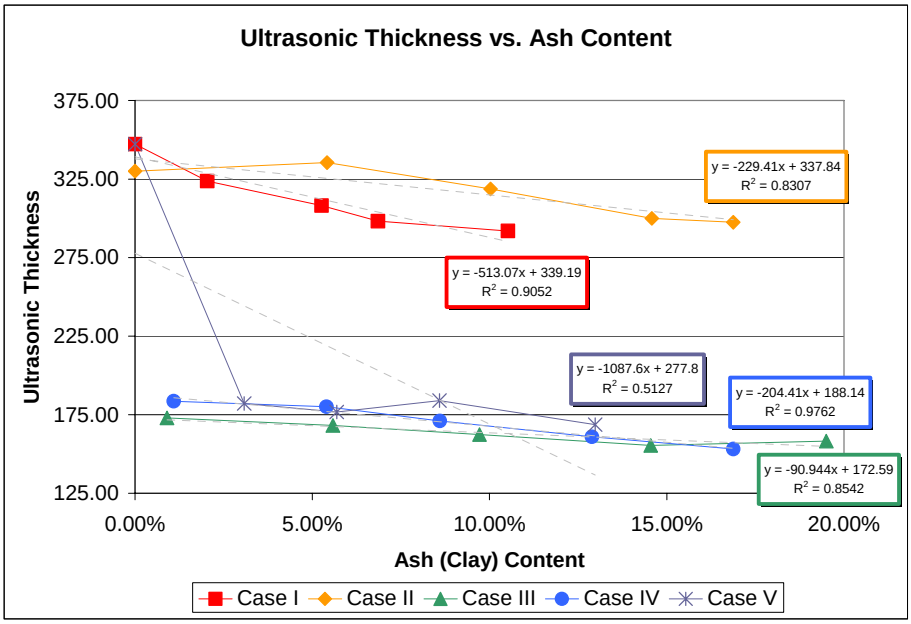

Figure 4-10: Ultra Sonics Thickness vs. Ash Content

4.1.6 Stiffness, E

Several paper properties were studied related to stiffness including tear index; bending stiffness; and ultrasonic elastic stiffness, specific stiffness, travel time and velocity. The variation of tear index with ash content is presented in Figure 4-11. Tear index shows a negative correlation with ash content. This makes sense because strength generally decreases with increased filler content. Case IV (PEO) has the lowest tear index, but it also has a higher ash content. Case II has high tear index and high filler retention, could be due to the starch addition. Case III had the least drop in tear and had the highest tear compared to all the other cases at the last (20% target) filler level.

Bending stiffness is analogous to beam bending in mechanical engineering (see Figure 4-12). Filler content usually causes a decrease in bending stiffness, which is supported by the data. Bending stiffness is typically governed by the elastic modulus, E as well as sheet caliper. Bending stiffness typically decreases with decreasing basis weight, which could explain Case II since it had low basis weight.

The ultrasonic results in Figure 4-13 are similar to those in Figure 4-10. Since the same fiber was used for all cases, the elastic modulus should be similar from case to case. Elastic modulus can increase with density, so perhaps the sheets are becoming more

dense. Elastic stiffness remains fairly constant across the cases, as does velocity. Travel time is the exception to the odd pattern. It has a very strong negative correlation with filler content. Something about the sheet structure changes allowing for shorter travel time through the sheet.

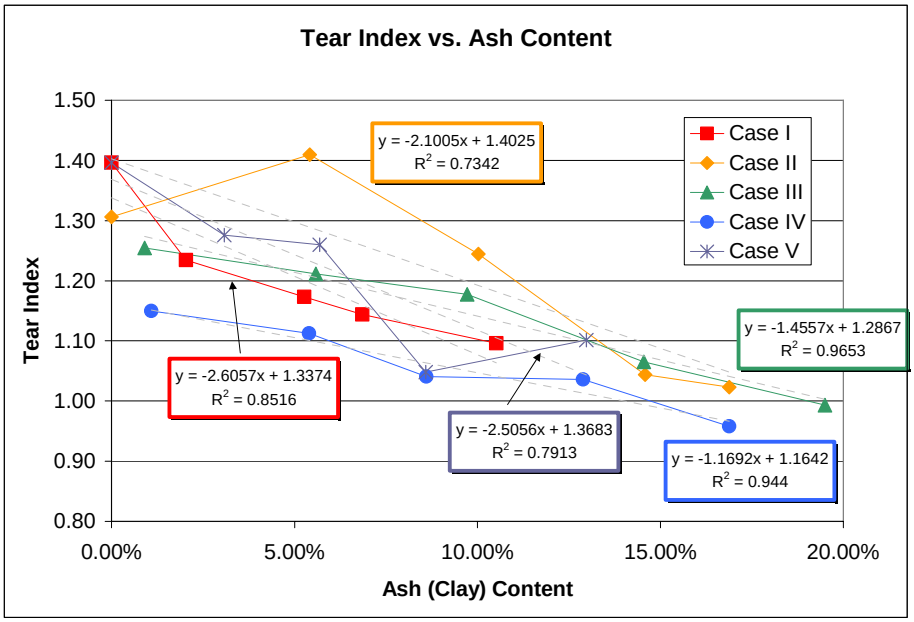

Figure 4-11: Tear Index vs. Ash Content

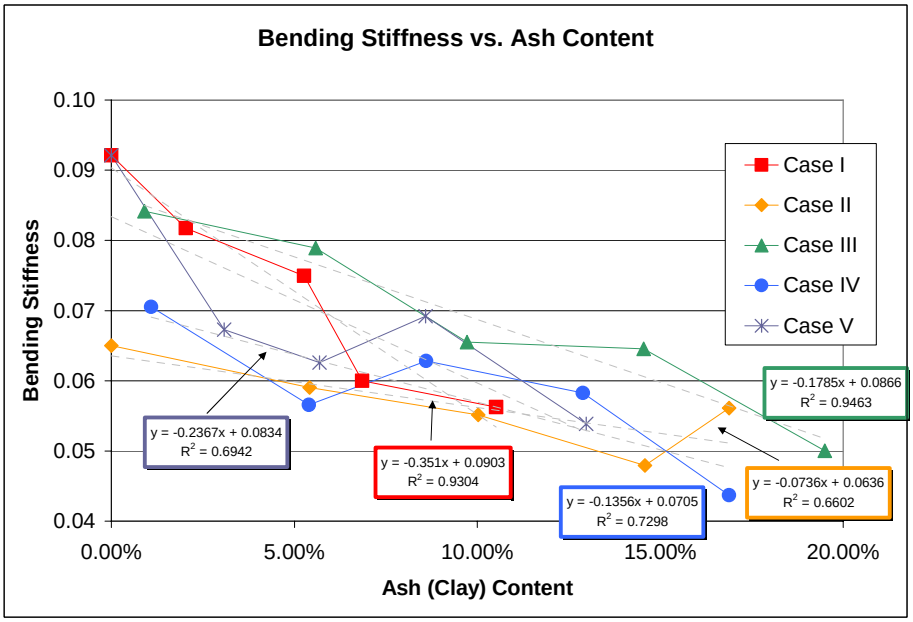

Figure 4-12: Bending Stiffness vs. Ash Content

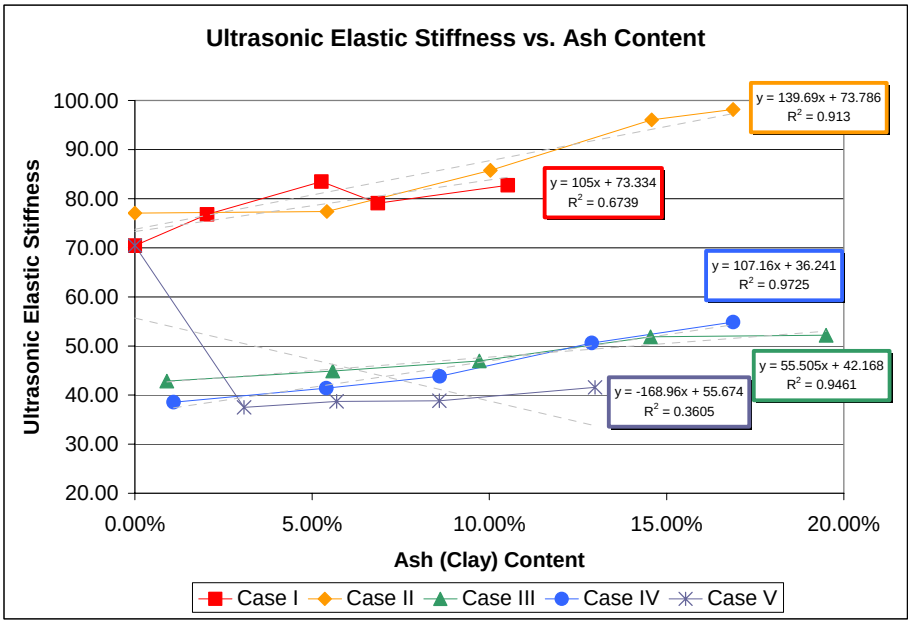
Ultrasonic Elastic Stiffness vs. Ash Content
Ultrasonic Elastic Stiffness
100.00
90.00
80.00
70.00
60.00
50.00
40.00
30.00
20.00
0.00%
5.00%
10.00%
15.00%
20.00%
Ash (Clay) Content
y = 139.69x + 73.786
R2 = 0.913
y = 105x + 73.334
R2 = 0.6739
y = 107.16x + 36.241
R2 = 0.9725
y = 55.505x + 42.168
R2 = 0.9461
y = -168.96x + 55.674
R2 = 0.3605
Case I
Case II
Case III
Case IV
Case V

A

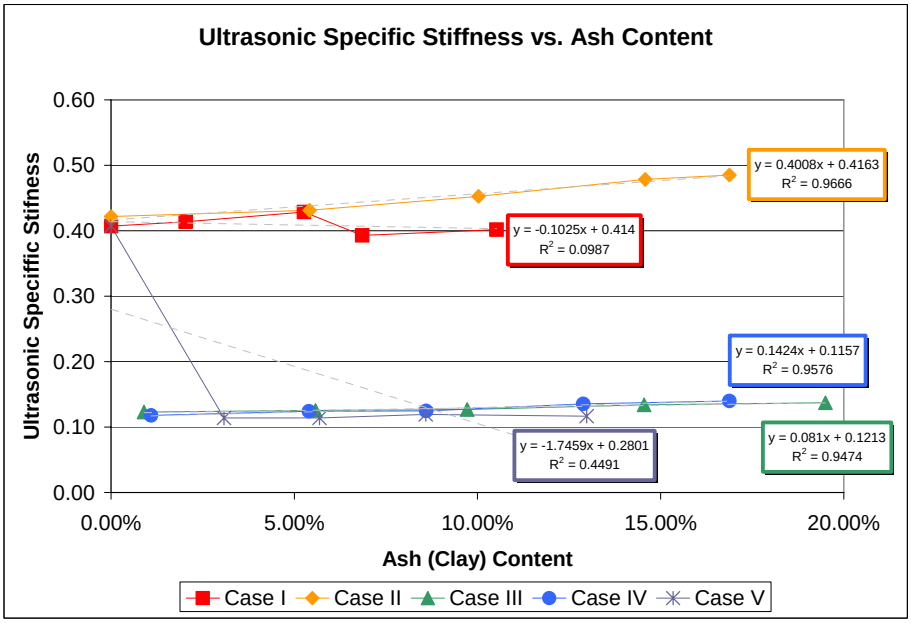
Ultrasonic Specific Stiffness vs. Ash Content
Ultrasonic Specific Stifness
0.60
0.50
0.40
0.30
0.20
0.10
0.00
0.00%
5.00%
10.00%
15.00%
20.00%
Ash (Clay) Content
y = 0.4008x + 0.4163
R2 = 0.9666
y = -0.1025x + 0.414
R2 = 0.0987
y = 0.1424x + 0.1157
R2 = 0.9576
y = 0.081x + 0.1213
R2 = 0.9474
y = -1.7459x + 0.2801
R2 = 0.4491
Case I
Case II
Case III
Case IV
Case V

B

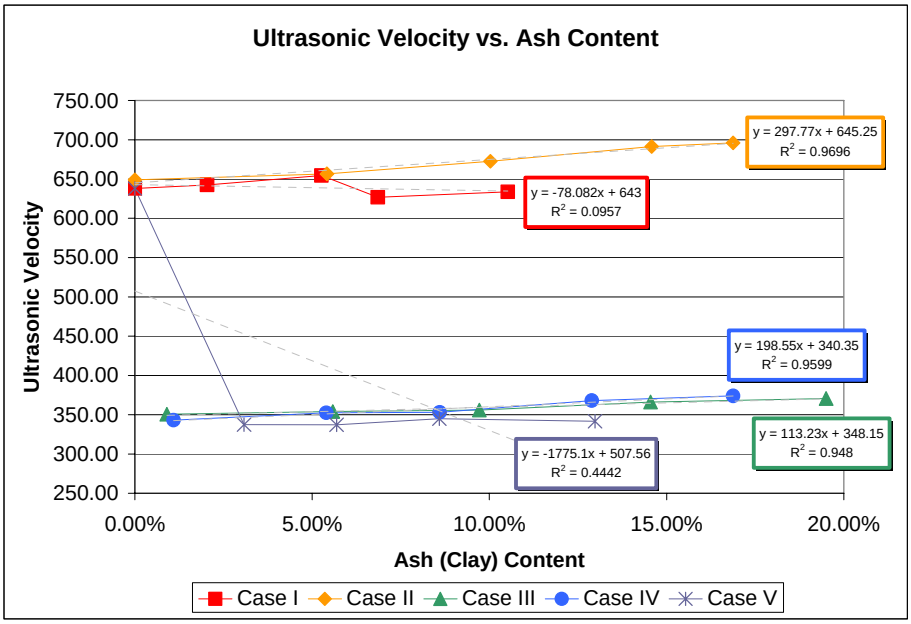

C

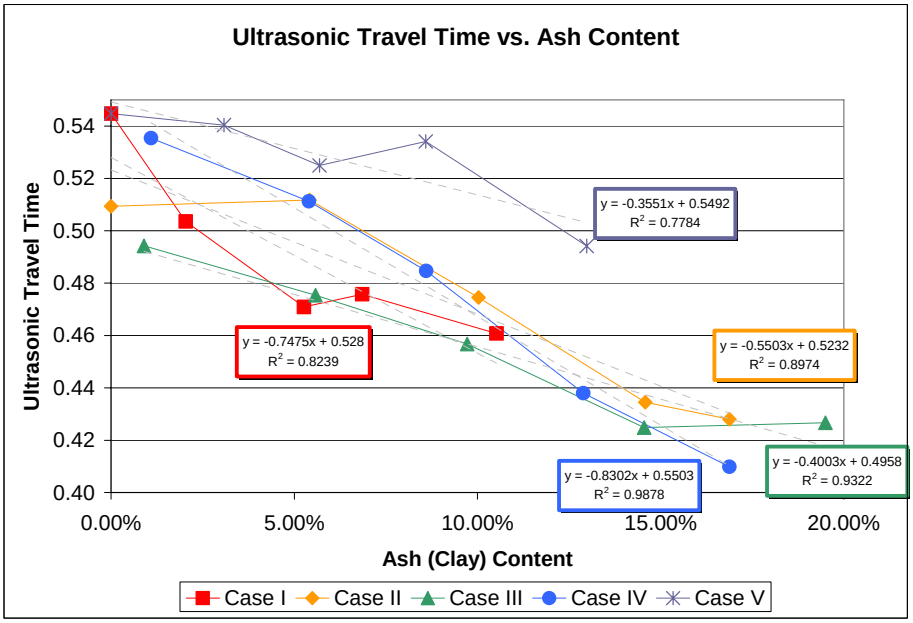

D

Figure 4-13: Ultra Sonics (A) Elastic and (B) Specific Stiffness, (C) Velocity and (D) Travel Time vs. Ash Content

4.1.7 Tensile

The paper properties examined by *tensile properties* included wet and dry tensile index; z-directional tensile; wet and dry zero-span and porosity.

Dry and wet tensile index verses ash content can be found in Figure 4-14. Dry tensile index decreased linearly (except for Case III at 10%) in every case with increased filler content. This was expected as it is generally accepted that strength decreases with filler addition. Case II actually had the lowest tensile even though it had starch added to the furnish. Cases I and V have roughly the same tensile strength as Cases III and IV, however Cases I and V contained less filler. Wet tensile index is very similar to dry tensile. All cases have a strong negative correlation with filler content, even more so than with dry tensile. Again, Case II has the lowest wet tensile index.

Z-direction tensile (ZDT) measurement differs considerable from case to case and had a negative correlation in all cases (see Figure 4-15). This is what was expected because filler interrupts fiber-to-fiber bonding. Fines and filler distribution in the thickness direction of the sheet influences the physical properties of paper. Here Case II has the highest ZDT perhaps due to the added starch. Case V had the lowest ZDT, despite the ash content. It is possible that the ethanol may have some effect on the z-directional distribution of the filler. The high ZDT for Cases II and III could be from the pre-flocculation of the fillers, creating a more even distribution in the z-direction.

The dry and wet zero-span results are interesting (Figure 4-16). Zero-span should be primarily dependent on fiber strength. It is expected that zero-span decreases with filler addition, because there are fewer fibers supporting the sheet. Case II had lower zero-span results than the other cases. This is possible due to the retention behavior of Case II. Cases I, III and IV and all followed the same trend and had similar linear slopes. Case V had a steeper slope but was close to the values of Cases I, III and IV. It could be that the ethanol affects the fibers, fines and fillers, causing the trend in the data.

The porosity results are interesting because porosity decreases in case with polymers and increase in cases with out polymers. Porosity is dependent on basis weight and thickness of the paper. Fillers typically decrease porosity because they can fill in void spaces and thus reducing the pores volume. The data make sense because the sheets with the higher filler levels, Cases II, III and IV, decrease porosity. Where as Cases I and

V increase in porosity indicating that the pore structure is increasing. This could be from fillers getting on the fibers and thus decreasing bonding, which creates a more porous structure.

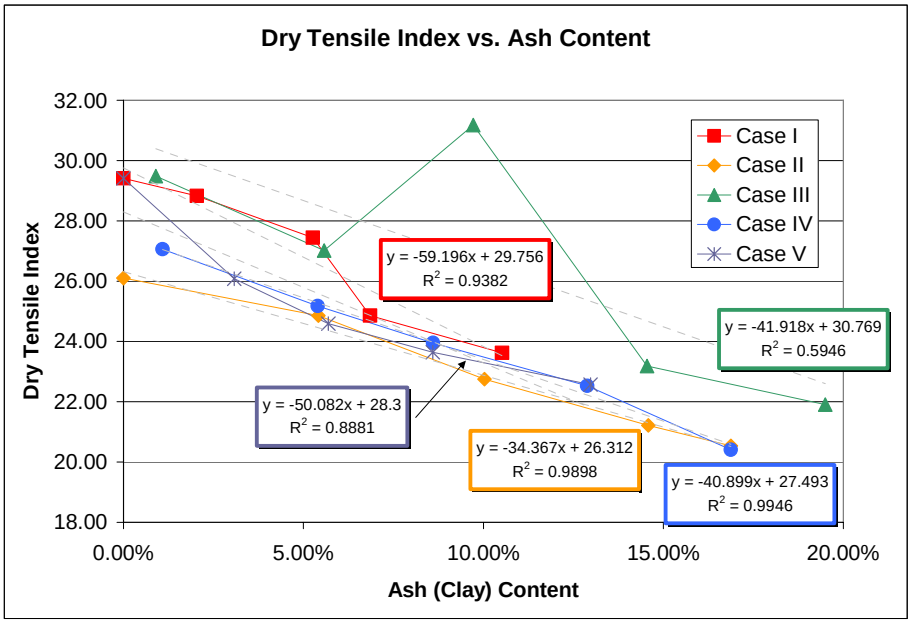

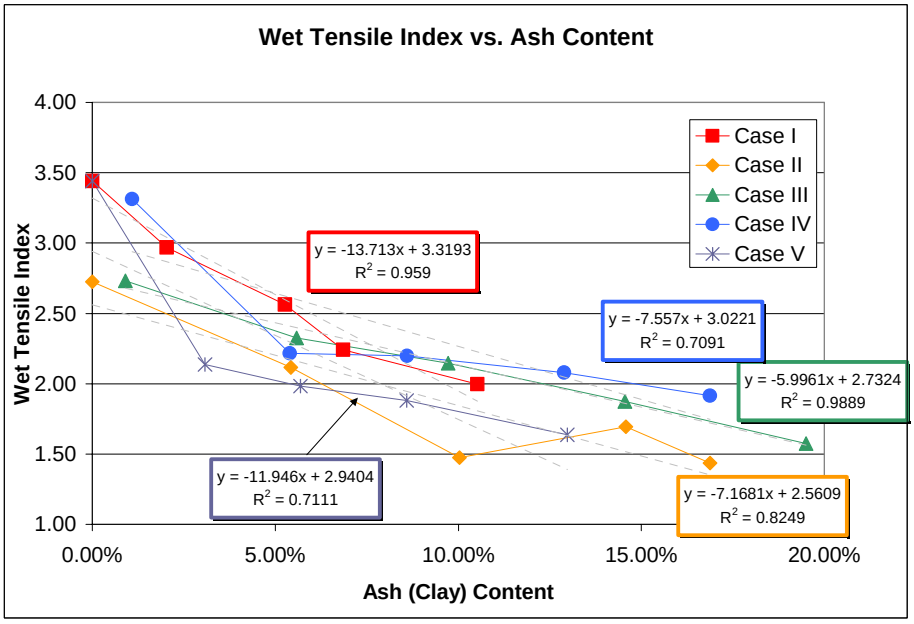

Figure 4-14: Dry and Wet Tensile Index vs. Ash Content

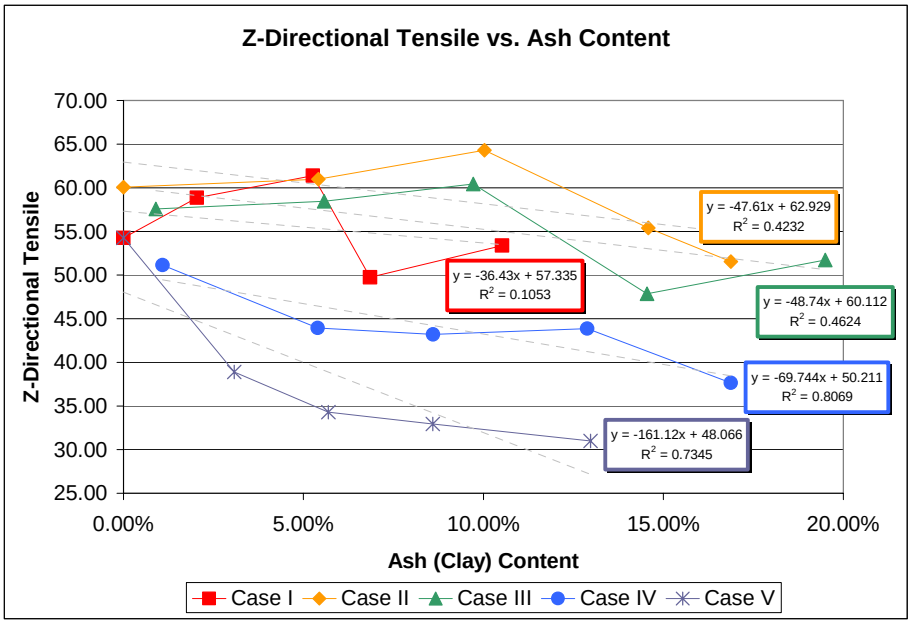

Figure 4-15: Z-Directional Tensile vs. Ash Content

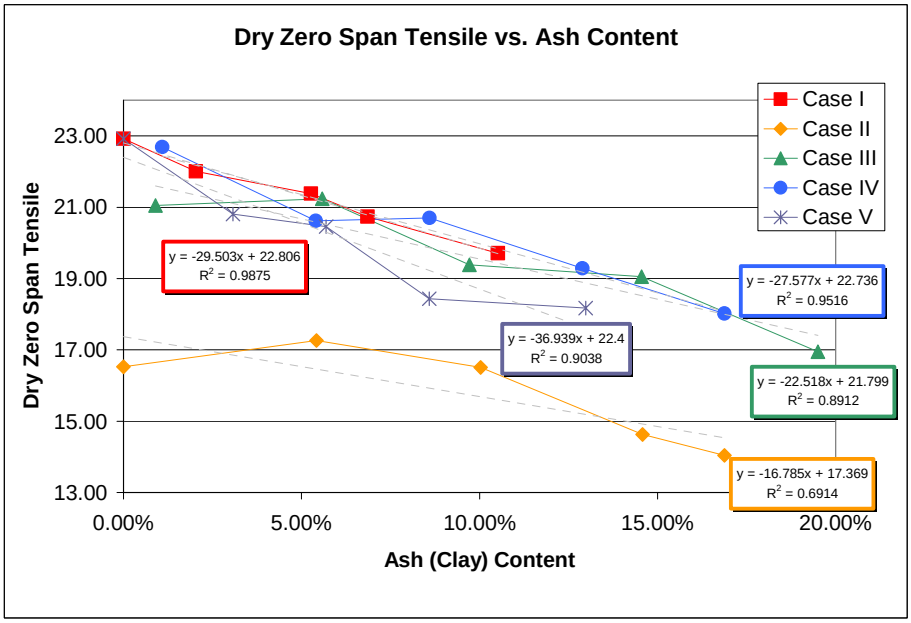

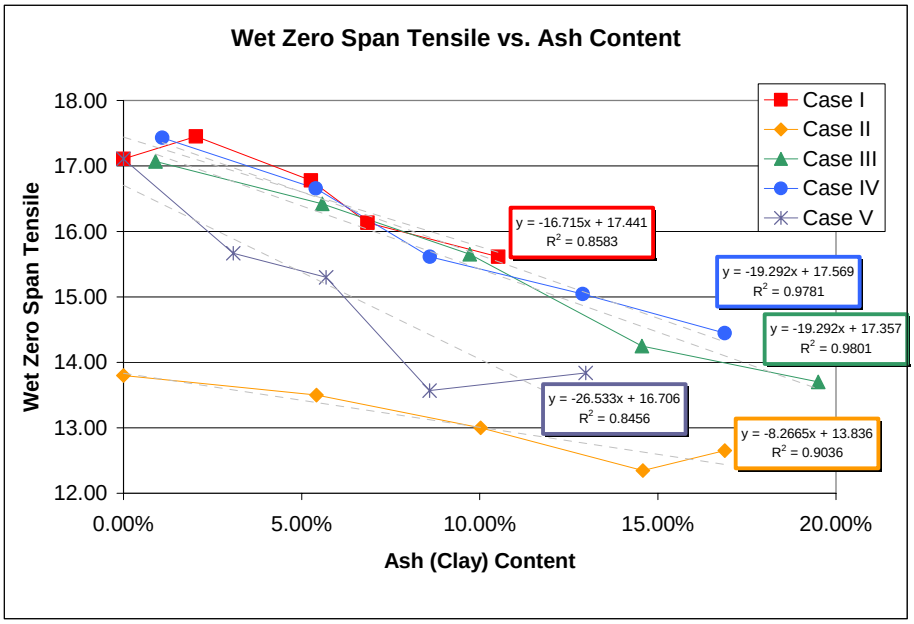

Figure 4-16: Dry and Wet Zero-Span Tensile vs. Ash Content

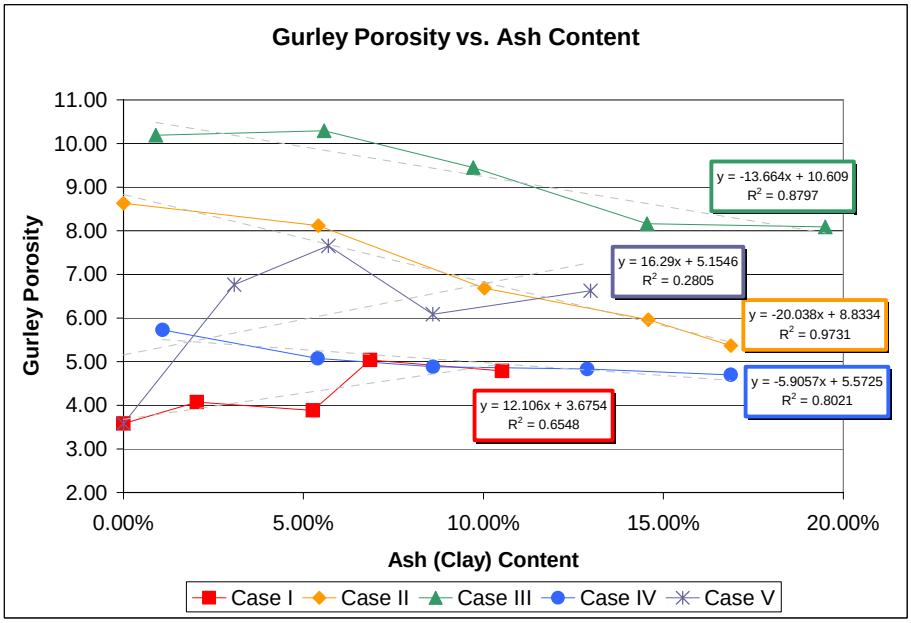

Figure 4-17: Gurley Porosity vs. Ash Content

Table 4-3 is a summary of positive or negative correlations and if they are strong or weak correlations. For the majority of the physical test, all five cases followed the same correlation trend. In some of the other physical tests, Cases I and V followed the same trend and Cases II, III and IV followed a different trend.

Table 4-3: Summary of Correlations between the Physical Test and Actual Filler Content (ash)

Physical Test	Case I	Case II	Case III	Case IV	Case V
COF-Static, μ_s	+	+	+	-	++
COF-Kinetic, μ_k	++	++	+	+	++
Parker Print-Surf	--	--	+	-	--
Sheffield Roughness	-	-	-	-	--
Brightness	+	++	++	++	+
Printing Opacity	--	++	+	-	--
TAPPI Opacity	--	+	-	-	--
Basis Weight (g/m^2)	--	+	-	-	--
Formation Index	--	-	-	-	--
Bending Stiffness	--	-	--	--	--
Tear Index	--	--	-	-	--
Zero-Span (wet)	--	-	--	--	--
Zero-Span (dry)	--	-	--	--	--
Ultra Sonics-Elastic Stiffness	++	++	+	++	--
Ultra Sonics-Specific Stiffness	-	-	+	+	--
Ultra Sonics-Velocity	-	++	++	++	--
Ultra Sonics-Travel Time	--	-	-	--	-
Tensile Index-dry	--	--	--	--	--
Tensile Index-wet	--	-	-	-	--
ZDT	--	--	--	--	--
Ultra Sonics-Thickness	--	-	-	--	--
Air Permeance (Porosity)	++	--	--	-	++

4.2 Power Analysis and Sample Size

One of the significant pieces in the SEM methodology was being able to use the image data collected form the SEM images to determine how many images were needed to obtain statistical significance. Recall that it became readily apparent that the number of pictures per sample was too large to be a practical method. If the SEM grid method is to be useful to other applications, there must be a way to determine the minimum number of samples required for detectable statistical differences. This was accomplished by

using *power analysis and sample size* (PASS) to reduce the number of images taken for each of the five samples.

Determining the variation between samples was important because it was necessary to justify that the five paper samples taken randomly from the whole paper samples represented the total population. It was also time intensive to take one hundred twenty five SEM micrographs and to process them with the image analysis program (see Table 4-4). The first part of the table calculates the total SEM images taken and the second table calculates the number of hours to take the SEM images and perform the image analysis on each image.

Table 4-4: Time difference between acquiring and processing the 5 X 5 grid technique verses the 3 X 3 grid technique

# of samples	# of filler levels	# of cases	Total	# X-dir	# Y-dir	# of mag.	Total	SEMs/ Case	SEMs/ filler level	Total SEMs
5	5	5	125	5	5	2	50	1250	250	6250
5	5	5	125	3	3	2	18	450	90	2250

Grid Size	# of Image Analysis/hr.	# of SEMs/hr.	Total SEMs	Total SEM hrs.	Total Image hrs.	hrs./day	# of days	# of weeks
5 X 5	10	20	6250	312.5	625	10	93.75	15.625
3 X 3	10	20	2250	113	225	10	33.75	6

The first sample studied was the pre-flocculation with starch sample. Case II was the first case created in the laboratory because it was based on the P&G technology. This sample was used for the power calculations to determine the minimum necessary sample size. As stated previously, the images from Case II were taken on a 5 X 5 grid. It was presumed that five samples with a grid size of 5 X 5 images each would provide more than enough data. However, without any previous work of this type of image analysis there was no procedure to follow. Therefore all 25 images (5 X 5 grid), from each of the five SEM stubs (125 images), from each of the five filler levels (625 images total) had to be taken.

In order to process the data for the PASS analysis, the data were grouped by filler level (five levels) and SEM stud (five studs pre filler level). To calculate the minimum necessary sample size, the averages and standard deviations for particle area or perimeter for each of the five SEM studs was needed. The data input to the PASS analysis program

required the five averages, or means, and the standard deviation of those five means. The SEM stubs were labeled as follows and the average of the particle area and perimeter were calculated. These are given in Table 4-5.

Table 4-5: Summary of data for the PASS analysis

0% Filler Level	Stub (K)	Z1	Z2	Z3	Z4	Z5
	Area Average	9.73	4.61	6.54	3.14	1.59
	Standard Deviation	3.16				
	Perimeter Average	9.57	4.62	7.13	3.66	2.73
	Standard Deviation	2.78				
5% Filler Level	Stub (K)	Y1	Y2	Y3	Y4	Y5
	Area Average	1.55	1.46	1.34	1.45	1.59
	Standard Deviation	0.10				
	Perimeter Average	3.21	3.17	3.02	3.06	3.21
	Standard Deviation	0.09				
10% Filler Level	Stub (K)	X1	X2	X3	X4	X5
	Area Average	1.31	1.58	1.52	1.57	1.54
	Standard Deviation	0.11				
	Perimeter Average	3.20	3.38	3.33	3.34	3.31
	Standard Deviation	0.07				
15% Filler Level	Stub (K)	W1	W2	W3	W4	W5
	Area Average	1.62	1.85	1.58	1.55	1.56
	Standard Deviation	0.12				
	Perimeter Average	3.67	3.86	3.52	3.54	3.56
	Standard Deviation	0.14				
20% Filler Level	Stub (K)	V1	V2	V3	V4	V5
	Area Average	2.02	2.08	1.62	1.87	1.54
	Standard Deviation	0.24				
	Perimeter Average	4.18	3.96	3.73	4.05	3.64
	Standard Deviation	0.22				

An example of the report generated from PASS 2002 and the results of the power calculations for each of the filler levels is shown in Figure 4-18. Table 4-6 shows that sample size (n) is between 4 and 6. This is much less than the 25 that was the original sample size chosen. The number of groups (k) is still 5 since there are five filler levels. The total sample size (N) is 25, which is much less than the 125 total sample size used originally. The means of the 5 groups (k) used to calculate the sample size (n) are in the lower portion of the report. Since the PASS report calculated that the samples size (n) was between 4 and 6, it was decided that 25 samples per group was too large. **A new sample size (n) of 9 was chosen because it was well above the 5 required statistically by PASS and 9 samples works out to a *3 X 3* grid on the SEM stubs.** For the four remaining cases a grid size of 3 X 3 was chosen, still using five SEM samples as with the

5 X 5 grid. This gave nine images per SEM stub for a total of 45 images per sample per filler level. Nine images were well above the five images calculated by the power calculation.

One Way ANOVA Power Analysis

Numeric Results

Power	Average n	k	Total N	Alpha	Beta	Std Dev of Means (Sm)	Standard Deviation (S)	Effect Size
0.90743	5.00	5	25	0.05000	0.09257	2.83	3.16	0.8944

Report Definitions
Power is the probability of rejecting a false null hypothesis. It should be close to one.
n is the average group sample size.
k is the number of groups.
Total N is the total sample size of all groups.
Alpha is the probability of rejecting a true null hypothesis. It should be small.
Beta is the probability of accepting a false null hypothesis. It should be small.
Sm is the standard deviation of the group means under the alternative hypothesis.
Standard deviation is the within group standard deviation.
The Effect Size is the ratio of Sm to standard deviation.

Summary Statements
In a one-way ANOVA study, sample sizes of 5, 5, 5, 5, and 5 are obtained from the 5 groups means are to be compared. The total sample of 25 subjects achieves 91% power to detect diffe among the means versus the alternative of equal means using an F test with a 0.05000 significanc The size of the variation in the means is represented by their standard deviation which is 2.83 common standard deviation within a group is assumed to be3.16.

Details when Alpha = 0.05000, Power = 0.90743, SM = 2.83, S = 3.16

Group	Ni	Percent Ni of Total Ni	Mean	Deviation From Mean	Ni Times Deviation
1	5	20.00	9.73	4.61	23.03
2	5	20.00	4.61	0.51	2.55
3	5	20.00	6.54	1.42	7.09
4	5	20.00	3.14	1.98	9.90
5	5	20.00	1.59	3.54	17.68
ALL	25	100.00	5.12		

Figure 4-18: Sample report of a power sample size from PASS 2002. This is from Case II, 0 % filler level

Table 4-6: Results from power calculation for Case II

Filler Level	0% Filler	5% Filler	10% Filler	15% Filler	20% FIller
Minimum Sample Size based on Area	5	5	5	5	5
Minimum Sample Size based on Perimeter	5	5	4	5	6

4.3 One-Way Analysis of Variance

The one-way analysis of variance (ANOVA) was performed on the designed structure cases to determine if differences between the mean of the area and perimeter data existed. If the means of the area and perimeter data are different, then it is hypothesized that structural differences are responsible for the difference in particle data.

The null hypothesis (H_0) of the Kruskal-Wallis one-way ANOVA is that at least one of the means is different. Chi-Squared (χ^2), or *H*, is the Kruskal-Wallis test statistic. If the results of the ANOVA test is higher than the test statistic, *H*, then the null hypothesis is accepted. The null hypothesis, H_0, was rejected at all filler levels. All the cases at every filler level had at least one mean different from each other. This was one of the first tools to gage if the designed structures had differences. All *ANOVA F-ratio* values were above 1.0 indicating there was statistical significance in the data. *Normality* is rejected in every case, which makes sense because the image data is non-normal (see Figure 3-8 and Figure 3-9). Results from the one-way ANOVA are summarized below in Table 4-7. In the first part of the table are the results for particle area and in the second part of the table are the results for particle perimeter data.

Not only does the one-way ANOVA show that at least one mean is different, the *Multiple-Comparison Z-Value Test* can tell which means are different from the others. In other words, it is possible to know which designed structure case is different from the rest. Table 4-8 is a sample of the Z-value test for area and perimeter for the 0% filler case (see Appendix 5 for complete results). As the designed structures are compared, if the value of the comparison is greater the z-value, then the means are significantly different. Therefore, for area at 0% the mean of Case I is different from the means of Cases II, III and IV, but it is not different from Case V. The complete table can be found in Appendix 5 and a summary of the results can be found in Table 4-9 and Table 4-10.

Table 4-7: One-Way Analysis of Variance of Area and Perimeter on all Cases at each Filler Level.

Area Results for all 5 Cases					
ANOVA Result	**0%**	**5%**	**10%**	**15%**	**20%**
Normality	Reject	Reject	Reject	Reject	Reject
ANOVA-F-Ratio	**4.83**	**3.11**	**49.51**	**101.74**	**24.01**
ANOVA-Prob Level	0.000864*	0.015700*	0.000000*	0.000000*	0.000000*
ANOVA-Power	0.954884	0.811528	1.000000	1.000000	1.000000
Kruskal-Wallis, H_0	**Reject**	**Reject**	**Reject**	**Reject**	**Reject**
KW-Chi-Square (*H*)	**33.50241**	**82.71564**	**157.8082**	**178.4046**	**140.8491**
-corrected for ties	37.87537	82.71948	157.8082	178.4048	140.8491
KW-Prob Level	0.000001	0.000000	0.000000	0.000000	0.000000
-corrected for ties	0.000000	0.000000	0.00000	0.000000	0.000000

Perimeter Results for all 5 Cases					
ANOVA Result	**0%**	**5%**	**10%**	**15%**	**20%**
Normality	Reject	Reject	Reject	Reject	Reject
ANOVA-F-Ratio	**10.60**	**2.87**	**77.74**	**275.34**	**70.98**
ANOVA-Prob Level	0.00000*	0.023394*	0.000000	0.000000*	0.000000*
ANOVA-Power	0.99989	0.774759	1.000000	1.000000	1.000000
Kruskal-Wallis, H_0	**Reject**	**Reject**	**Reject**	**Reject**	**Reject**
KW-Chi-Square (*H*)	**35.31405**	**84.93455**	**167.0117**	**201.1012**	**158.3656**
-corrected for ties	39.92336	84.93854	167.0117	201.1013	158.3656
KW-Prob Level	0.000000	0.000000	0.000000	0.000000	0.000000
-corrected for ties	0.000000	0.000000	0.000000	0.000000	0.000000

Table 4-8: Kruskal-Wallis Multiple-Comparison Z-Value Test

Area 0% Filler Level					
Area	Case I	Case II	Case III	Case IV	Case V
Case I	0.0000	**3.2154**	**5.0156**	**3.1028**	0.0000
Case II	**3.2154**	0.0000	**2.8733**	0.5513	**3.2154**
Case III	**5.0156**	**2.8733**	0.0000	1.9127	**5.0156**
Case IV	**3.1028**	0.5513	1.9127	0.0000	**3.1028**
Case V	0.0000	**3.2154**	**5.0156**	**3.1028**	0.0000
Perimeter 0% Filler Level					
Perimeter	Case I	Case II	Case III	Case IV	Case V
Case I	0.0000	**3.3656**	**5.1372**	**3.1560**	0.0000
Case II	**3.3656**	0.0000	**2.8707**	0.4657	**3.3656**
Case III	**5.1372**	**2.8707**	0.0000	**1.9811**	**5.1372**
Case IV	**3.1560**	0.4657	**1.9811**	0.0000	**3.1560**
Case V	0.0000	**3.3656**	**5.1372**	**3.1560**	0.0000
Regular Test: Medians significantly different if z-value > 1.9600					

From Table 4-9, at 0% filler level, Cases I and V have equal means, and Cases II, III and IV all have similar means. This supports the trend of Cases I and V being similar.

At 5% filler level Cases I and III and Cases II and V have similar means while Case IV is different from all other cases. At 10% filler level Cases I and III again have similar means, while the rest are all different. There is some loose correlation between Cases I and III from the data, but it is not clear how they are related. Cases IV and V are not similar to any of the cases at 15% filler level. Cases I, II and III all have similar means, possibly indicating some correlation between those cases. At 20% filler level, Cases III and IV are not similar to any other cases, while Cases I, II and V all have similar means. There is not a clear pattern between cases and filler level overall. Each filler level gives a different picture of the relationship between the means of the particle area.

Table 4-9: Kruskal-Wallis Multiple-Comparision Z-Value Test Results for Particle Area of all five Designed Structure Cases

0%	**Case I**	**Case II**	**Case III**	**Case IV**	**Case V**
Different	II, III, IV	I, II, IV	I, II, V	I, V	II, III, IV
Same	V	IV	IV	II, III	I
5%	**Case I**	**Case II**	**Case III**	**Case IV**	**Case V**
Different	II, IV, V	I, III, IV	II, IV, V	I, II, III, V	I, III, IV
Same	III	V	I		II
10%	**Case I**	**Case II**	**Case III**	**Case IV**	**Case V**
Different	II, IV, V	I, III, IV, V	II, IV, V	I, II, III, V	I, II, III, IV
Same	III		I		
15%	**Case I**	**Case II**	**Case III**	**Case IV**	**Case V**
Different	IV, V	IV, V	II, IV, V	I, II, III, V	I, II, III, IV
Same	II, III	I, III	I		
20%	**Case I**	**Case II**	**Case III**	**Case IV**	**Case V**
Different	III, IV	III, IV	I, II, IV, V	I, II, III, V	II, IV
Same	II, V	I, V			I, II

The particle perimeter data is similar to the area data, but there are a few differences. From Table 4-10 at 0% filler level, Cases I and V again have similar means, while Cases II and IV also have similar means and Case III is unrelated to every other case. From 5% filler level Cases I and III have similar means and Cases II and V have similar means. Here Case IV is dissimilar to the other four cases. At the 10% filler level, Cases I and III have similar means while the remaining three cases are different from all the cases. The 15% filler level is similar to 10% filler level where Cases I, II and III all have similar means, while Cases IV and V have different means from any other cases. The 20% filler level shows that Cases I, II and V have similar means, while Cases III and IV do not have similar means to any of the cases. What is curious here is that at 5 %,

10% and 15% filler levels, Cases I and III had similar means, which may imply something about the filler particles. Cases II and V had similar means at 5% and 20% filler levels. The only filler level where Case IV had a similar mean to an other case was 0%, this was in the comparison with Case I.

Table 4-10: Kruskal-Wallis Multiple-Comparison Z-Value Test Results for Particle Perimeter of all five Designed Structure Cases

0%	**Case I**	**Case II**	**Case III**	**Case IV**	**Case V**
Different	II, III, IV	I, III, V	I, II, IV, V	I, III, V	II, III, IV
Same	V	IV		II	I
5%	**Case I**	**Case II**	**Case III**	**Case IV**	**Case V**
Different	II, IV, V	I, III, IV	II, IV	I, II, III, V	I, IV
Same	III	V	I, V		II, III
10%	**Case I**	**Case II**	**Case III**	**Case IV**	**Case V**
Different	II, IV, V	I, III, IV, V	II, IV, V	I, II, III, V	I, II, III, IV
Same	III		I		
15%	**Case I**	**Case II**	**Case III**	**Case IV**	**Case V**
Different	II, III, IV, V	I, IV, V	I, IV, V	I, II, III, V	I, II, III, IV
Same		III	II		
20%	**Case I**	**Case II**	**Case III**	**Case IV**	**Case V**
Different	II, IV, V	III, IV	II, II, IV, V	I, II, III	III, IV
Same	III	I, V		V	I, II

Overall, Cases I and V often had similar means, and Cases II and III often had similar means. Case IV was often not similar to any other case. These results were encouraging because it was showing both differences and similarities between specific cases, which could lead to information about the differences in the FFP structures.

4.4 Principal Components Analysis

As stated previously, the principal components analysis was performed on the 15% filler level of every designed structure case. Most of the physical testing data and particle area and perimeter data was entered into the PCA matrix. The following physical testing data was not included in the PCA analysis because there were errors in the data, noted previously: Parker Print-Surf (for coated paper only), Ultrasonic Thickness, Velocity, Elastic Stiffness and Specific Stiffness (errors in Cases I and II). For ease of computation, the names of the data were shortened to the variable names below in Table 4-11. All further discussion of the PCA results will refer to the PCA IDs.

Table 4-11: PCA variable identification

Physical Test	PCA ID	Physical Test	PCA ID
Bending	Bend	ZDT	ZDT
Brightness	Bright	~~Ultra Sonics-Thickness~~	~~UST~~
COF-Static, μ_s	COFS	Ultra Sonics-Travel Time	USTT
COF-Kinetic, μ_k	COFK	~~Ultra Sonics-Velocity~~	~~USV~~
TAPPI Opacity	OT	~~Ultra Sonics-Specific Stiffness~~	~~USSS~~
Printing Opcaity	OP	~~Ultra Sonics-Elastic Stiffness~~	~~USES~~
Air Permeance (Porosity)	Por	Zero-Span (dry)	ZSD
~~Print-Surf~~	~~PS~~	Zero-Span (wet)	ZSW
Sheffield	Sheff	Formation	Form
Tear	Tear	Image Area-Average	Area
Tensile Index-dry	TenD	Image Perimeter-Average	Perimeter
Tensile Index-wet	TenW		

As noted previously, PCA breaks the large amount of data down into smaller components or *factors* that still retain a significant amount of information. Factor 1 retains the most variation followed by factor 2 then factor 3 and so on. By plotting one factor against another, relationships in the data can be discerned. Although any of the factors can be plotted, the most meaningful relationships come from plotting the greatest amount of data, the greatest concentration of significant data is contained in factor 1, factor 2, and factor 3.

Figure 4-19 is a plot of factor 1 verses factor 2 for all the data within all five cases. Figure 4-19 graphically shows the relationship between all five designed structure cases by combining all of the data for all five cases. The closer the variables are to origin the less data they contribute to the factor. This plot is for comparing cases as a whole. The individual cases will be examined in this section as well.

The x-axis is factor 1 which contains 43.56% of the information in the data and the y-axis is factor 2 which contains 25.64% of the data. Here Cases II, III and IV are represented by factor 1 because they fall closest to the x-axis. Cases I and V are represented by factor 2 since they somewhat closer to the y-axis however, Case V is almost equidistant from both the x-axis and y-axis and is represented by both factors. This shows that Cases II, III and IV are correlated with each other. Case II is the most representative of factor 2 because it is furthest from the origin. Cases I and V are also

correlated with each other, but not with Cases II, III and IV. The PCA results for the five difference cases together is in support of the physical testing results.

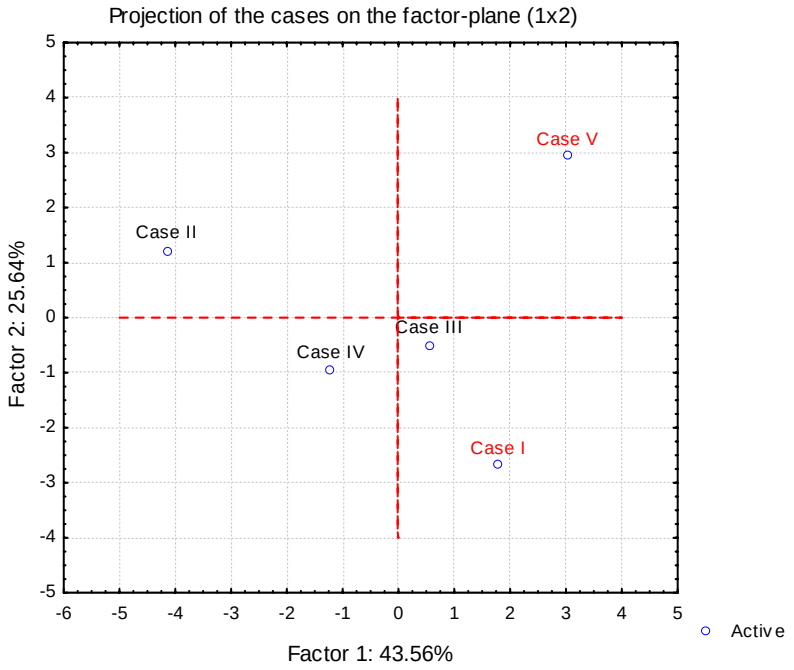

Figure 4-19: Projection of all Cases on Factor planes 1 and 2

4.4.1 Case I

Case I has six significant eigenvalues, which means the data can be reduced to six factors, which account for a total of 84.23% of the total variation of the original data (see Table 4-12). The first, second and third factors contain 29.96%, 22.07% and 10.37% of the total variation respectively. Factors 1, 2 and 3 account for a total of 62.40% of the total variation of the original data. Since factors 1 and 2 only accounted for 52.03% of the data, factor 3 should also be plotted to account for mare of the data.

Figure 4-20 and Figure 4-21 are the factor plots for Case I variables. The interpretation is the same as for the plot of all the cases together (see Figure 4-19). The unit circle and the variable vectors (pointing back to the origin) in Figure 4-20 are added to better accentuate the relationships between the variables. The unit circle is from the correlation matrix that was formed during the PCA analysis where all the variables were

scaled to a variance of one. This allows all the different variables to be compared because the correlation matrix is unit-less. For clarity, the variables Area and Perim are marked in red on all the following plots. However, Figure 4-20 is only a 2-D plot and does not contain as much information and a plot with all three factors. Figure 4-21 is the 3-D plot with all three factors. Plotting three factors is beneficial because it allows for a greater amount of variation to be included in the interpretation of the results. Table 4-13 lists the factor loadings for the first three factors. These coefficients are used to create the factor plots and to aid in the interpretation of relationship between the variables and the factors. Relationships between the variables for Case I can be determined with the eigenvalues, factor plots and factor loadings.

Particle Area and Perim are correlated with both factor 1 (x-axis) and 3 (z-axis). Area and Perim are highly correlated with the variables that also lay closest to both factors 1 and 3. These variables include Bright, COFK, Sheff and ZDT. Area and Perim are less correlated with variable associated with either factors 1 or 3 including, TenD, TenW, USTT and ZSW. In Case I Area and Perim are not highly correlated with any variables that lay closest to factor 2 such as Bend, COFS, OT, OP, Por, Tear, ZSD and Form.

Another graphical representation of the data is the Tree Diagram (see Figure 4-22). The tree diagram shows the relationships between the variable by grouping variables that are most correlated with each other; variable A with it next closest variable B and then variable A and B are next closet to variable C etcetera. The diagram is very similar to a family tree up-side-down. Here the tree diagram shows that Area and Perim are closely related, which make sense. Next Bright and Por are closely related and both are closely related to Area and Perim form both the facto plane plot (see Figure 4-21) and the factor loadings data (see Table 4-13). Looking at the right side of Figure 4-22 shows that OP and OT are highly correlated and that COFS and COFK are highly correlated. Going up to the next level shows that, OP, OT and COFK, COFS are highly correlated. Going up one more level shows that OP, OT, COFS, COFK and Bend are correlated and make a “branch” in the tree of related variables. Note that none of these variable are correlated with Area and Perim (except for COFK) and they are the opposite end of the tree. The tree diagram takes into account all factors and thus offers a more complete

picture than the factor plots. These results are very similar to the factor plane plot, as expected.

Table 4-12: Case I Eigenvalues

Eigenvalues of correlation matrix, and related statistics (PCA All in PCA All) Active variables only

	Eigenvalue	% Total Variance	Cumulative Eigenvalue	Cumulative %
1	5.39	29.96	5.39	29.96
2	3.97	22.07	9.37	52.03
3	1.87	10.37	11.23	62.40
4	1.58	8.76	12.81	71.16
5	1.24	6.88	14.05	78.04
6	1.11	6.19	15.16	84.23
7	0.81	4.52	15.97	88.75
8	0.52	2.87	16.49	91.62
9	0.48	2.66	16.97	94.28
10	0.31	1.74	17.28	96.02
11	0.20	1.10	17.48	97.12
12	0.17	0.94	17.65	98.06
13	0.13	0.74	17.78	98.79
14	0.09	0.47	17.87	99.27
15	0.06	0.34	17.93	99.61
16	0.04	0.23	17.97	99.84
17	0.03	0.15	18.00	99.99
18	0.00	0.01	18.00	100.00

Table 4-13: Case I: Factors 1, 2 and 3

Factor Loadings
Extraction: Principal components
(Marked loadings are >.30)

Variable	Factor 1	Factor 2	Factor 3
Bend	0.38	-0.49	-0.18
Bright	0.64	0.09	0.40
COFS	0.06	-0.58	-0.45
COFK	0.34	-0.67	-0.52
OT	0.47	-0.69	0.05
OP	0.16	-0.88	0.16
Por	0.21	0.68	0.35
Sheff	-0.78	0.10	-0.32
Tear	-0.64	-0.53	0.05
TenD	-0.72	-0.11	0.20
TenW	-0.83	-0.26	0.29
ZDT	-0.42	-0.02	0.31
USTT	-0.61	-0.01	0.12
ZSD	-0.72	-0.44	0.13
ZSW	-0.81	-0.28	0.23
Form	-0.21	0.67	-0.37
Area	-0.46	0.27	-0.48
Perim	-0.47	0.27	-0.52

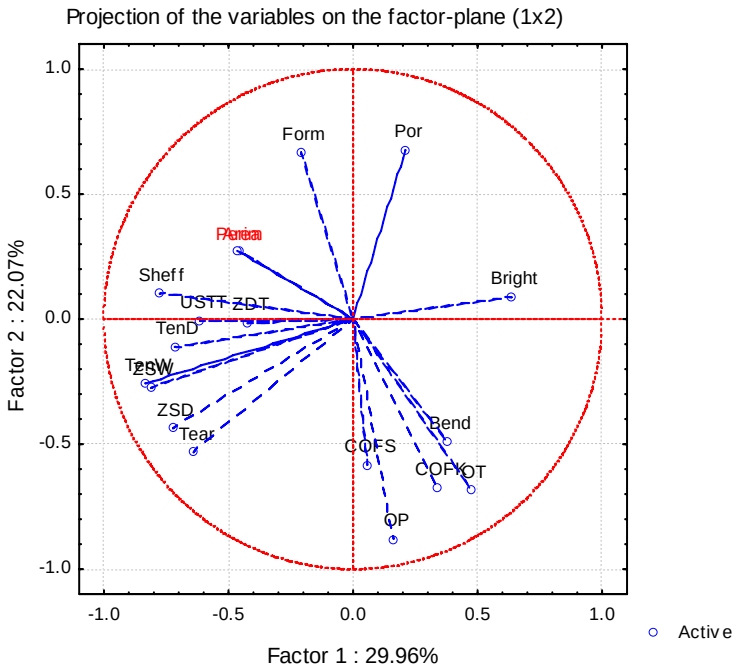

Figure 4-20: Case I PCA Projection on Factor Plane 1 and 2

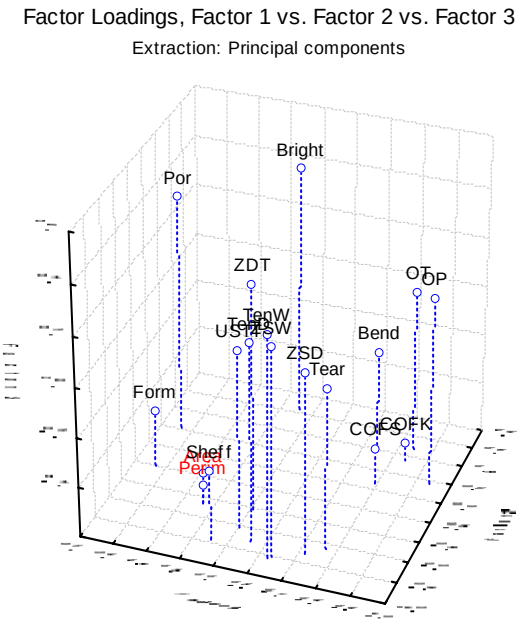

Figure 4-21: Case I 3-D Plot of the first Three Factors

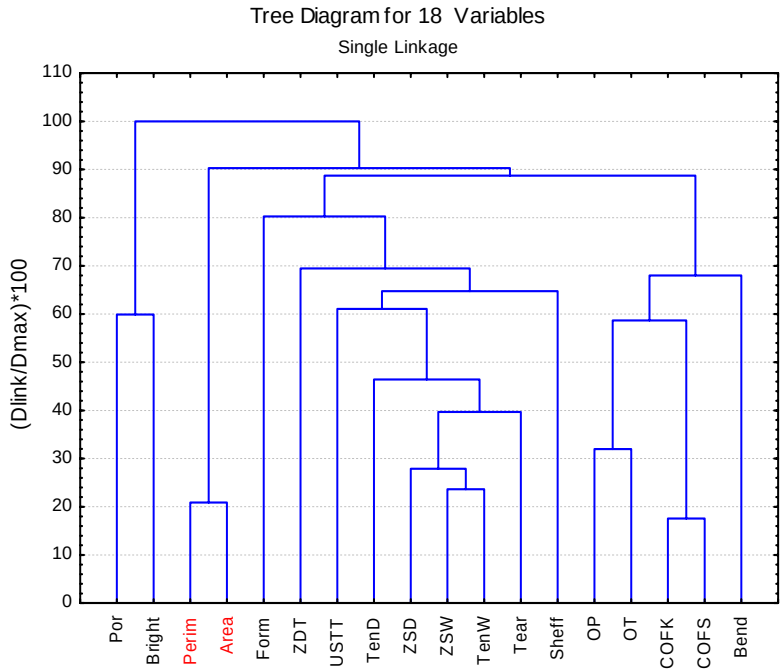

Figure 4-22: Case I Tree Diagram

4.4.2 Case II

Case II has five significant eigenvalues, so that the data can be reduced to 5 factors and still retain the majority of the data. The five eigenvalues would account for 84.73% of the variation in the data. Factors 1, 2 and 3 account for 48.16%, 13.03% and 10.34% respectively, which accounts for 71.53% of the total variation combined. However, the results for Case II are unusual, as Area and Perim do not seem to be correlated to Factor 1 or 2. Area and Perim are correlated with factor 3 but factor 3 is not correlated with any variables (see Table 4-15). Therefore it seems that Area and Perim are not correlated with any of the varivables. When results are that close to the origin then it is difficult to obtain any valuable information because any variables close to the origin become insignificant. From the tree diagram results it would appear that Area and Perim were somewhat correlated with OT, ZDT, Bright.

Table 4-14: Case II Eigenvalues

Eigenvalues of correlation matrix, and related statistics (PCA All in PCA All) Active variables only				
	Eigenvalue	% Total Variance	Cumulative Eigenvalue	Cumulative %
1	8.67	48.16	8.67	48.16
2	2.35	13.03	11.01	61.19
3	1.86	10.34	12.88	71.53
4	1.30	7.23	14.18	78.75
5	1.07	5.97	15.25	84.73
6	0.83	4.63	16.08	89.36
7	0.60	3.34	16.69	92.70
8	0.47	2.59	17.15	95.29
9	0.29	1.60	17.44	96.89
10	0.19	1.07	17.63	97.97
11	0.15	0.84	17.78	98.80
12	0.14	0.78	17.93	99.59
13	0.04	0.23	17.97	99.82
14	0.02	0.13	17.99	99.95
15	0.01	0.05	18.00	100.00
16	0.00	0.00	18.00	100.00
17	0.00	0.00	18.00	100.00
18	0.00	0.00	18.00	100.00

Table 4-15: Case II: Factors 1, 2 and 3

Factor Loadings Extraction: Principal components (Marked loadings are >.30)			
Variable	Factor 1	Factor 2	Factor 3
Bend	-0.84	-0.31	0.03
Bright	0.98	-0.04	0.01
COFS	-0.38	0.81	-0.12
COFK	-0.57	0.64	-0.04
OT	0.50	0.21	-0.17
OP	-0.68	-0.28	0.22
Por	-0.26	-0.61	0.22
Sheff	-0.91	-0.22	0.00
Tear	-0.64	-0.49	-0.04
TenD	-0.82	0.24	-0.14
TenW	-0.74	0.02	-0.05
ZDT	0.79	-0.39	0.13
USTT	-0.57	-0.17	0.15
ZSD	-0.89	-0.05	-0.01
ZSW	-0.86	0.14	-0.12
Form	-0.90	0.02	0.03
Area	-0.02	-0.25	-0.90
Perim	0.05	-0.27	-0.91

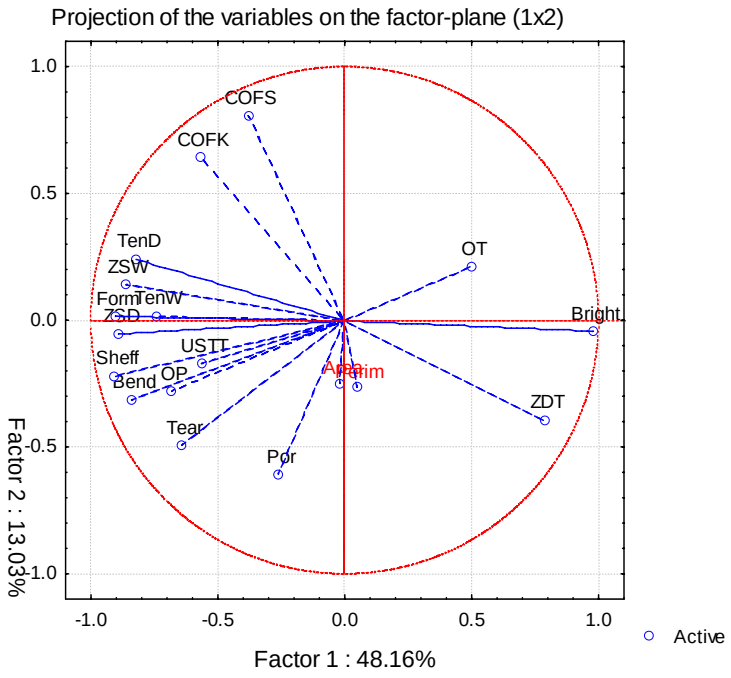

Figure 4-23: Case II PCA Projection on Factor Plane 1 and 2

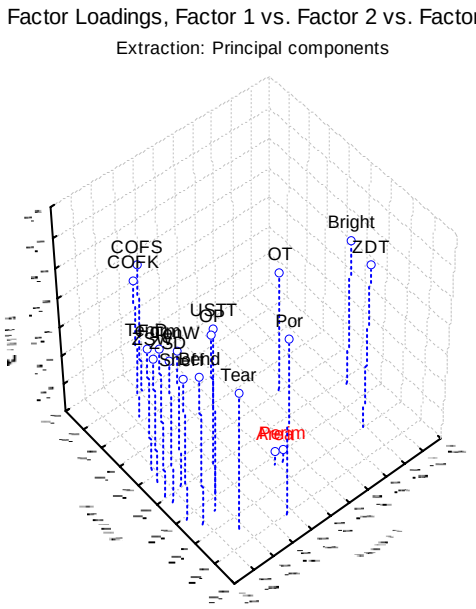

Figure 4-24: Case II 3-D Plot of the first Three Factors

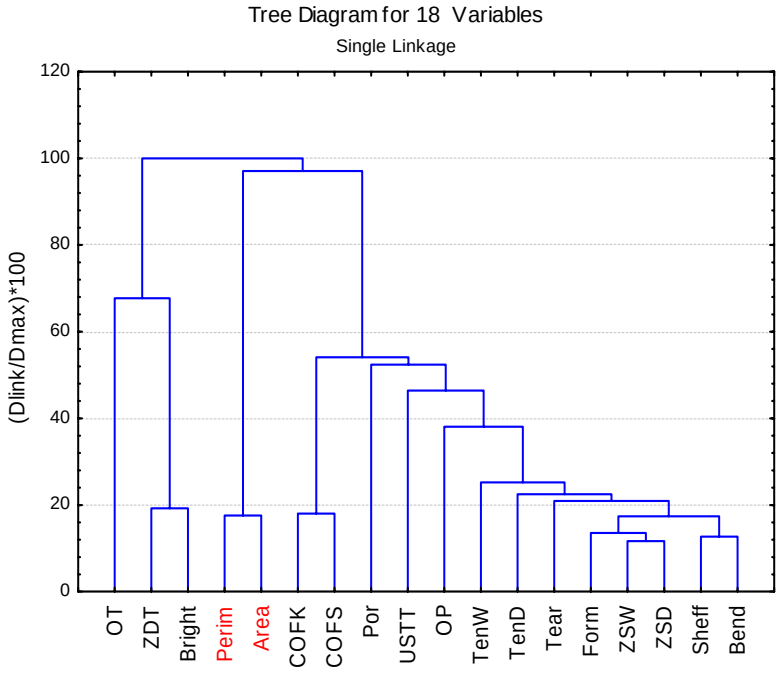

Figure 4-25: Case II Tree Diagram

4.4.3 Case III

Case III has six significant eigenvalues, such that the data can be reduced to six factors, which account for a total of 82.44% of the total variation of the original data (see Table 4-16). Factors 1, 2 and 3 contain 27.28%, 19.40% and 13.36% of the total variation respectively. Factors 1, 2 and 3 account for a total of 60.03% of the total variation of the original data. Area and Perim are both highly correlated with factor 1 (see Table 4-17). They are also closely related to COFK, COFS, OP, Bright, Form, TenW and OT. From the tree diagram is it clear that Area and Perim are closely related to COFS, COFK, OT, OP and Bright and the related to TenW, ZDT, ZSW and Form.

Table 4-16: Case III Eigenvalues

Eigenvalues of correlation matrix, and related statistics (PCA All in PCA All) Active variables only				
	Eigenvalue	% Total Variance	Cumulative Eigenvalue	Cumulative %
1	4.91	27.28	4.91	27.28
2	3.49	19.40	8.40	46.67
3	2.40	13.36	10.81	60.03
4	1.80	10.01	12.61	70.04
5	1.23	6.83	13.84	76.87
6	1.00	5.58	14.84	82.44
7	0.79	4.41	15.63	86.85
8	0.68	3.75	16.31	90.60
9	0.49	2.73	16.80	93.34
10	0.38	2.13	17.18	95.46
11	0.32	1.78	17.50	97.24
12	0.23	1.28	17.73	98.52
13	0.16	0.86	17.89	99.38
14	0.05	0.25	17.93	99.63
15	0.03	0.16	17.96	99.79
16	0.03	0.16	17.99	99.95
17	0.01	0.05	18.00	100.00
18	0.00	0.00	18.00	100.00

Table 4-17: Case III: Factors 1, 2 and 3

Factor Loadings Extraction: Principal components (Marked loadings are >.30)			
Variable	Factor 1	Factor 2	Factor 3
Bend	0.01	0.64	0.10
Bright	-0.60	0.15	-0.42
COFS	-0.81	0.30	0.35
COFK	-0.88	0.06	0.12
OT	-0.28	-0.02	-0.57
OP	-0.71	0.16	-0.48
Por	0.36	0.82	-0.19
Sheff	0.46	0.30	-0.43
Tear	-0.09	0.84	-0.19
TenD	-0.03	0.28	-0.71
TenW	-0.35	0.08	0.45
ZDT	0.32	0.14	0.16
USTT	-0.16	-0.90	-0.20
ZSD	0.56	0.60	0.18
ZSW	-0.17	0.32	0.53
Form	-0.52	-0.01	-0.37
Area	-0.81	0.13	0.15
Perim	-0.82	0.25	0.17

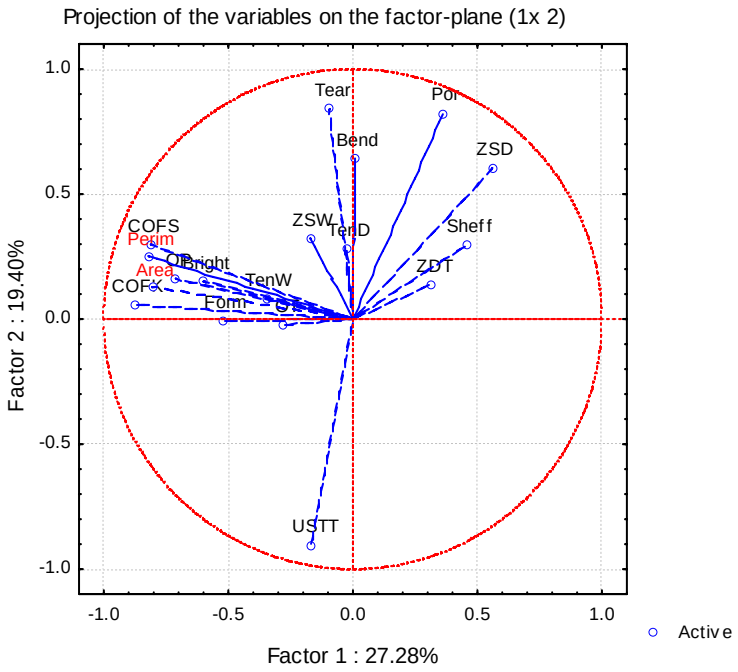

Figure 4-26: Case III PCA Projection on Factor Plane 1 and 2

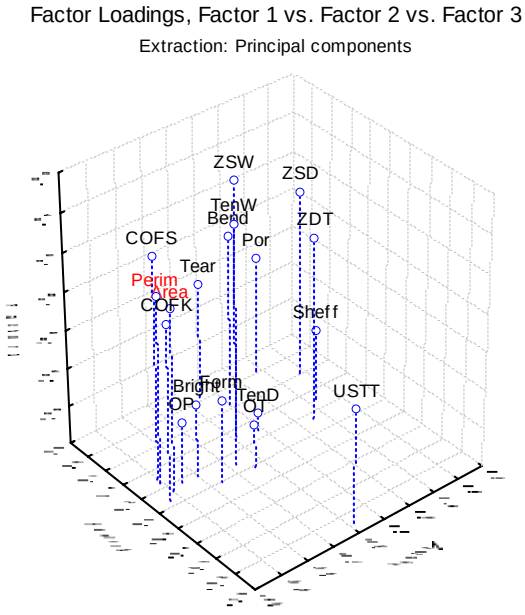

Figure 4-27: Case III 3-D Plot of the first Three Factors

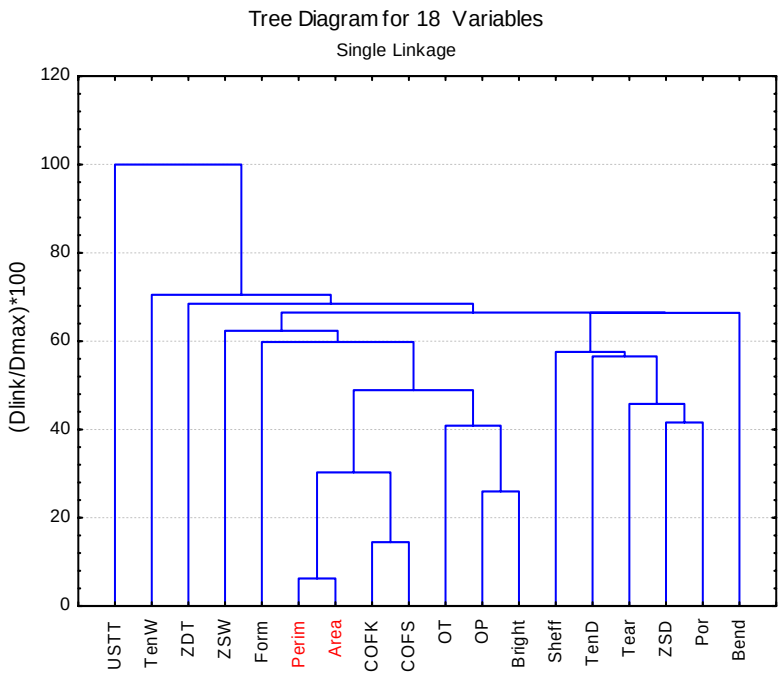

Figure 4-28: Case III Tree Diagram

4.4.4 Case IV

Case IV has six significant eigenvalues, which means the data can be reduced to six factors, which account for a total of 82.74% of the total variation of the original data (see Table 4-18). Factors 1, 2 and 3 contain 33.33%, 14.01% and 12.19% of the total variation respectively. Factor 1 and factor 2 account for a total of 52.62% of the total variation of the original data. Area and Perim are most highly correlated with Factor 3 (see Table 4-19). Case IV has a correlation with ZSD and Sheff but none of the other variables. According to the tree diagram, Area and Perim are not closely related with any variable in particular.

Table 4-18: Case IV Eigenvalues

Eigenvalues of correlation matrix, and related statistics (PCA All in PCA All) Active variables only				
	Eigenvalue	% Total Variance	Cumulative Eigenvalue	Cumulative %
1	6.00	33.33	6.00	33.33
2	2.52	14.01	8.52	47.34
3	2.19	12.19	10.72	59.53
4	1.56	8.69	12.28	68.22
5	1.35	7.52	13.63	75.74
6	1.26	7.00	14.89	82.74
7	0.77	4.25	15.66	86.99
8	0.66	3.69	16.32	90.68
9	0.48	2.69	16.81	93.37
10	0.39	2.14	17.19	95.51
11	0.34	1.88	17.53	97.40
12	0.15	0.85	17.68	98.24
13	0.12	0.68	17.81	98.92
14	0.09	0.48	17.89	99.40
15	0.04	0.25	17.94	99.65
16	0.03	0.18	17.97	99.83
17	0.02	0.12	17.99	99.96
18	0.01	0.04	18.00	100.00

Table 4-19: Case IV: Factors 1, 2 and 3

Factor Loadings Extraction: Principal components (Marked loadings are >.30)			
Variable	Factor 1	Factor 2	Factor 3
Bend	0.55	0.55	-0.07
Bright	-0.82	0.01	0.25
COFS	0.93	0.12	0.07
COFK	0.89	0.17	-0.01
OT	0.53	0.60	-0.20
OP	0.45	0.68	-0.13
Por	0.67	-0.59	-0.15
Sheff	0.48	-0.38	-0.44
Tear	0.82	0.18	0.15
TenD	0.78	-0.07	0.21
TenW	-0.38	0.22	-0.01
ZDT	0.33	-0.23	-0.07
USTT	0.35	-0.64	-0.19
ZSD	-0.21	0.25	-0.32
ZSW	-0.31	0.46	0.12
Form	-0.48	0.15	0.24
Area	-0.29	0.08	-0.88
Perim	-0.31	0.11	-0.89

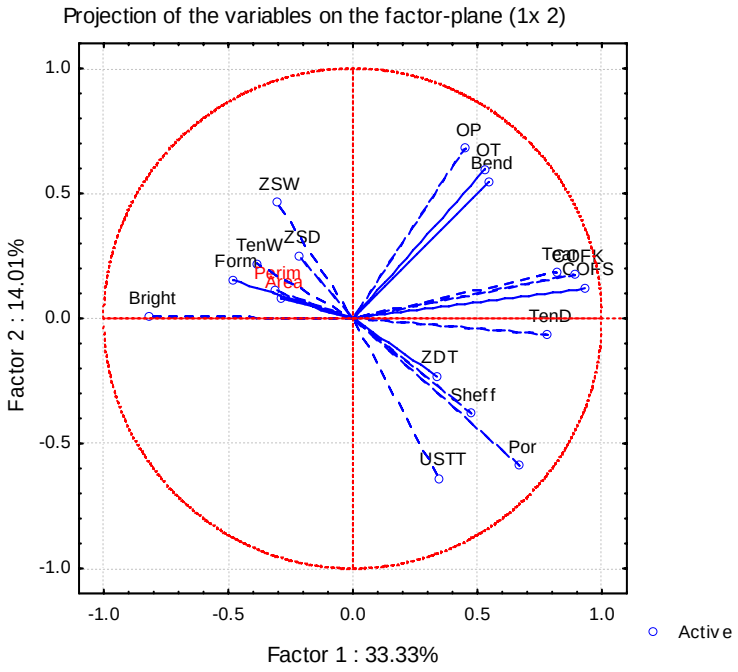

Figure 4-29: Case IV PCA Projection on Factor Plane 1 and 2

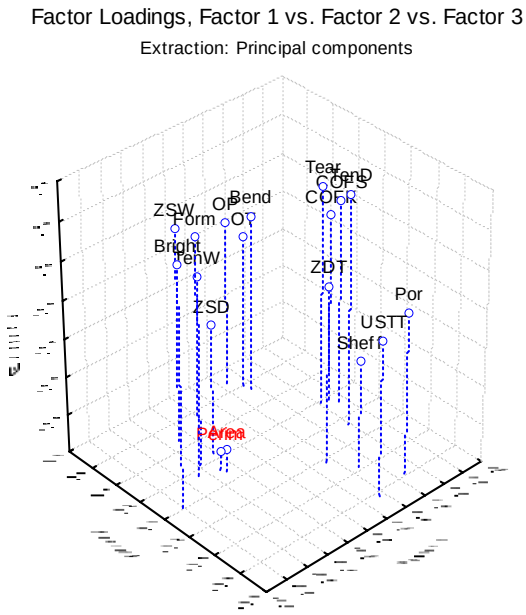

Figure 4-30: Case IV 3-D Plot of the first Three Factors

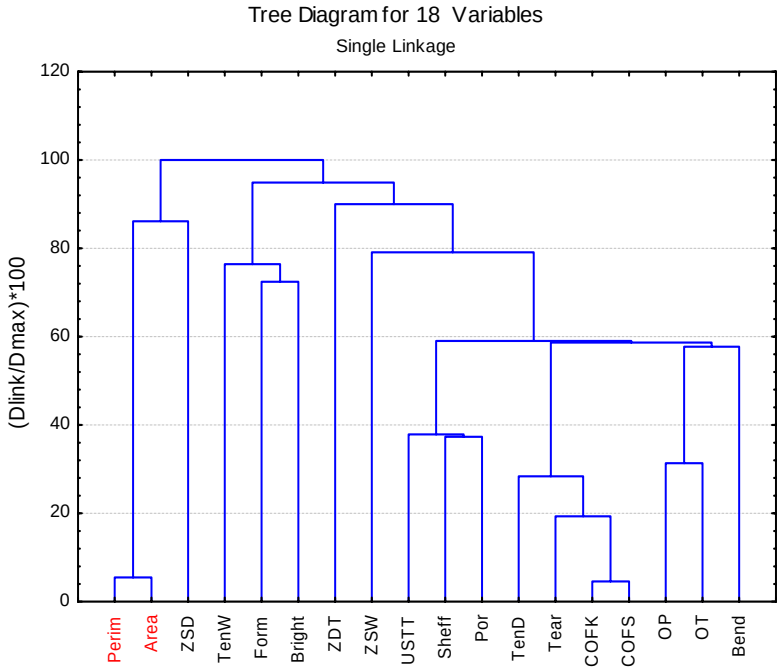

Figure 4-31 Case IV Tree Diagram

4.4.5 Case V

Case V has five significant eigenvalues, such that the data can be reduced to five factors, which account for a total of 79.06% of the total variation of the original data (see Table 4-20). Factors 1, 2 and 3 contain 30.80%, 18.65% and 12.17% of the total variation respectively. Factors 1, 2 and 3 account for a total of 61.62% of the total variation of the original data. Area and Perim are both highly correlated with factors 2 and 3. Are and Perim are highly correlated with OT, OP, Por, ZSW and Form (see Table 4-21). They are also correlated to Bright, Tear and USTT. According to the tree diagram, Area and Perim are most related to USTT, ZSD, TenD, COFK, COFS and Bend.

Table 4-20: Case V Eigenvalues

Eigenvalues of correlation matrix, and related statistics (PCA All in PCA All) Active variables only				
	Eigenvalue	% Total Variance	Cumulative Eigenvalue	Cumulative %
1	5.54	30.80	5.54	30.80
2	3.36	18.65	8.90	49.45
3	2.19	12.17	11.09	61.62
4	1.80	9.99	12.89	71.61
5	1.34	7.44	14.23	79.06
6	0.84	4.64	15.07	83.70
7	0.74	4.13	15.81	87.83
8	0.56	3.12	16.37	90.95
9	0.49	2.70	16.86	93.65
10	0.39	2.18	17.25	95.83
11	0.29	1.61	17.54	97.44
12	0.21	1.15	17.75	98.59
13	0.11	0.63	17.86	99.22
14	0.06	0.36	17.92	99.57
15	0.05	0.25	17.97	99.83
16	0.02	0.12	17.99	99.95
17	0.01	0.05	18.00	99.99
18	0.00	0.01	18.00	100.00

Table 4-21: Case V: Factors 1, 2 and 3

Factor Loadings Extraction: Principal components (Marked loadings are >.30)			
Variable	Factor 1	Factor 2	Factor 3
Bend	-0.87	-0.12	-0.08
Bright	0.34	0.01	-0.82
COFS	-0.85	-0.11	-0.03
COFK	-0.93	-0.18	-0.05
OT	-0.33	0.67	-0.10
OP	-0.35	0.71	-0.29
Por	0.42	-0.68	0.48
Sheff	0.75	-0.18	-0.06
Tear	-0.07	0.04	-0.40
TenD	-0.64	-0.27	-0.11
TenW	0.62	-0.01	-0.12
ZDT	0.81	-0.05	-0.06
USTT	-0.41	0.20	0.62
ZSD	-0.29	0.07	-0.09
ZSW	0.61	0.47	0.07
Form	0.11	0.71	-0.37
Area	-0.02	-0.74	-0.42
Perim	-0.19	-0.68	-0.53

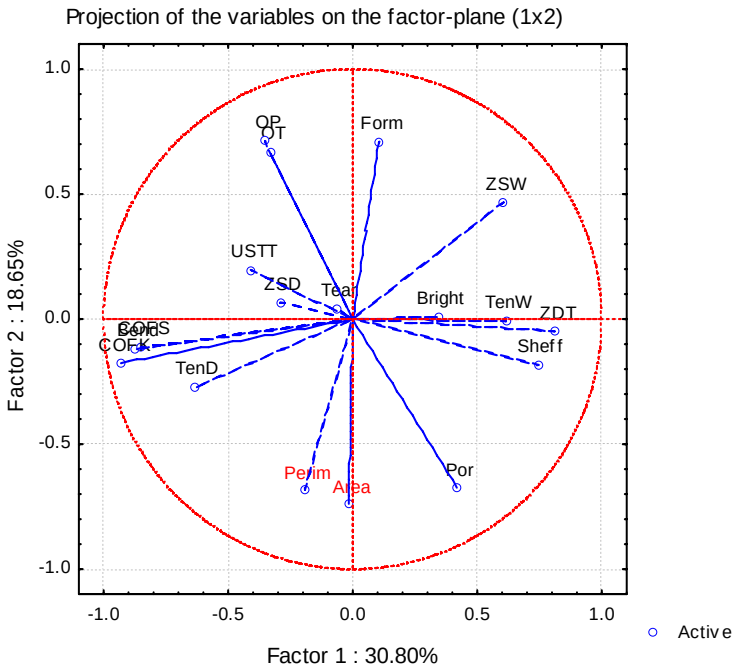

Figure 4-32: Case V PCA Projection on Factor Plane 1 and 2

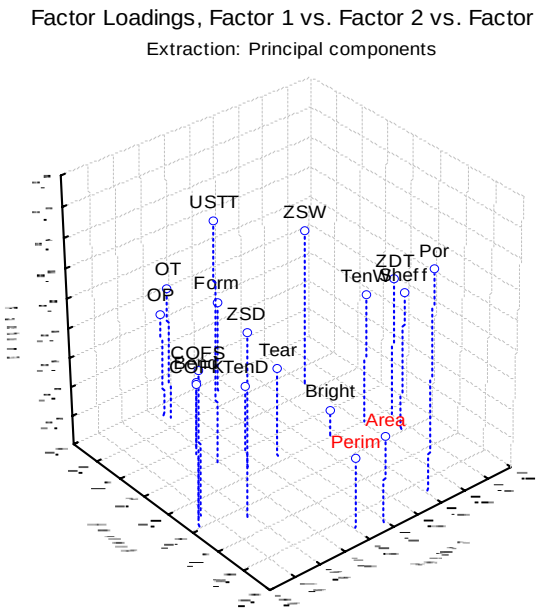

Figure 4-33: Case V 3-D Plot of the first Three Factors

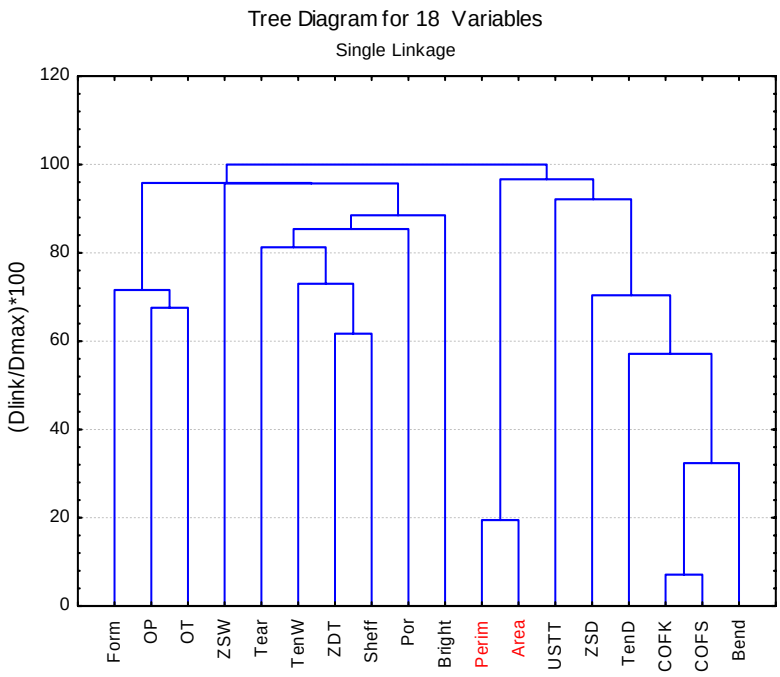

Figure 4-34: Case V Tree Diagram

5 DISCUSSION

The results presented in Chapter 4 will now be discussed. Important information concerning physical attributes of the filler, fiber, polymers, or physical properties may be mentioned again for clarity or emphases. The ash contents and some of the physical testing results for the sheets will be looked at in greater detail. The PASS test in the SEM methods was a key component to the success of the method. The one-way ANOVA is the statistical foundation of the SEM method and is the reason more powerful statistical methods, such as PCA are needed. PCA will be further discussed in terms of the physical test results and what the implications are for the designed structures. A closer looked will be taken at some of the actual SEM images and how they may reveal what the designed structures may look like. Conclusions will be presented throughout the discussion.

5.1 Comparison of Physical and SEM based Analyses

After reviewing the data in Chapter 4, two ways of grouping the data will help facilitate the discussion, by filler delivery method and by designed structure case. The *filler delivery method* group coincides more closely with the image analysis data and the *designed structure case* group coincides more closely with the physical testing data.

Designed structure cases were originally described as having three delivery methods:

1. Control → without and with solvent (Case I and Case V)
2. Pre-Flocculation → with and without starch (Case II and Case III)
3. Conventional → PEO (Case IV)

The particle data results show that each delivery method affected particle size and location and contributed to some differences in the physical testing. It was unclear at the beginning that the data would reveal a difference between the two polymer methods, pre-flocculation and conventional. The image analysis data of the particles clearly showed a difference between the pre-flocculation and the conventional PEO. However, the physical testing data did not always suggest a difference between the two polymer methods

Evidence from the physical testing indicates there are two distinct groups within the five cases.

1. Non-polymer → Case I (control) and Case V (ethanol)
2. Polymer → Case II (pre-flocc with starch), Case III (pre-flocc dual polymers) and Case IV (PEO)

This is not surprising since typically filler retention improves with polymer addition. This shows a general correlation between two of the components of the FFP polymer structures; the filler and polymers. Physical tests in which there were differences in the non-polymer group and the polymer group were brightness, opacity, basis weight, ultrasonic specific stiffness, ultrasonic velocity, wet tensile index and porosity. There were also many physical tests where all five cases exhibited similar behavior. One exception to this grouping was that on occasion Case II did not following the same behavior as any of the other cases.

5.1.1 SEM Particle Data

The image analysis process was able to differentiate subtle differences in fiber and filler particle areas and perimeters for each different handsheet compositions. The quantitative statistical-based data for the particles could then be compared with bulk physical testing data.

Case I and V had roughly the largest area and particle data except for the 15% filler sample of Case V (see Table 4-1). This is somewhat unfortunate since the 15% filler level was chosen and used for all the SEM analysis. As filler content was increased the particle area and perimeter increased steadily in Case I and fluctuated in Case V. It appears that the filler particles would agglomerate in one place and be more spread out in other places with little consistency. The filler particles themselves may have been influenced by local changes in pH, salt content or other phenomenon causing localized changes in the surface charge of the particles. This variation in surface charge density would cause the filler particles to vary considerably in size, which would be detected by the image analysis process. The ethanol may be affecting the filler particles by coating smaller filler particles or preventing filler particles from agglomerating in one location, while doing just the opposite in other locations. Since the ethanol molecule is bigger than the water molecule and only a portion of the molecule contributes to hydrogen bonding, it

is possible that steric hindrance also plays a role. This is a significant difference between the control case and the ethanol case.

Case II and Case III have roughly medium values for area and particle data, the particles were smaller than Case I and Case V, but larger than Case IV. This result is interesting because these are the two cases where the filler was pre-flocced with polymer prior to addition to the fiber furnish. It appears that the size of the particles had less variation from filler level to filler level (with the exception in 0% filler level as noted in Chapter 4). This may be explained by the pre-floccing of the filler particles creating an even distribution of filler particle size and the ability to maintain that distribution would increase in filler content.

Case IV was unique to the other cases because the clay was not pre-flocced, rather a polymer (PEO) was used for this case. Case IV had the smallest values for particle area and perimeter. Also, particle size was fairly constant, which is in line with Case II and Case III that also indicated polymer addition leads to uniform particle size at all filler levels.

5.1.2 Physical Testing Data

There were several physical properties where Cases I and V (no polymer) were similar, but different from Case2 II, III and IV (polymer), including opacity, brightness, ultrasonic specific stiffness, ultrasonic velocity and porosity, (see Table 5-1, Chapter 3). These differences may be indicative of structural differences between Cases I and V and Cases II, III and IV. Recall Table 5-1 from Chapter 3 Since it is labeled Table 5-1 you might just want to say the non-polymer and polymer cases The discussion will follow the table headings: surface characteristics, optical properties, 3-D structure, stiffness, and tensile.

Table 5-1: Grouping of Physical Tests into Fundamental Properties

Fundamental Properties	
Surface Characteristics	
Sheffield Roughness	Print-Surf
Static COF	Kinetic COF
Optical Properties	
Printing Opacity	TAPPI Opacity
Brightness	
3-D Structure	
Formation	US* Thickness
Stiffness, E	
Tear	Bending Stiffness
US* Elastic Stiffness	US* Specific Stiffness
US*Travel Time	US* Velocity
Tensile	
Tensile Index (Dry & Wet)	
Z-Directional Tensile	Porosity
Zero-Span (Dry & Wet)	
* = Ultra Sonics	

5.1.3 Surface Characteristics

Coefficient of friction is a measure of the friction of the paper surface, which may increase or decrease with filler addition. Friction occurs from the adhesion of the two surfaces which is highly dependent on surface chemistry and surface physical characteristics. Static COF is the friction caused when motion is just initiated and kinetic COF is the friction measured when the sample is kept in motion. What the results of the COF testing reflects is the difference in surface characteristics between the five cases (see Figure 4-3). Both static and kinetic COF are highest for Case V, which was the only case to use the ethanol coated filler. Case I contained only filler and fiber and is the second highest static COF, but still lower than Case V. This shows that the ethanol coated filler greatly affected the surface chemistry and/or physical characteristics.

Case IV is unique because PEO has a significantly different chemical composition than polyamine, PAM and cationic starch. Polyamines, PAM and cationic starch contain nitrogen groups as the source of cationic or anionic charge, while PEO does not contain nitrogen. This may be why Case II and Case III COF are different from Case IV (see Figure 1-12, Figure 1-13, and Figure 1-14). Case II and Case III have identical static COF. This makes sense because the surface chemistry is likely to be similar. It is

possible that the starch in Case II causes the difference in kinetic COF between Case II and Case III, because it could cause a difference in friction not noticed by the static measurement, but with continuous motion the starch could affect the adhesion between the sample. Case IV is the only case to have a negative correlation with COF. This is most likely to due the difference in chemical composition between Cases II and III and Case IV.

The Parker Print-Surf results are somewhat unclear (see Figure 4-4). Each case follows a different pattern though the overall trend for all cases (expect Case III) is a negative correlation with filler level. A stronger negative correlation with filler level was expected because typically as ash content is increased, surface smoothness increases.

Sheffield roughness had a much stronger negative correlation with ash content, which was expected (see Figure 4-5). Sheffield roughness is a better for the surface smoothness of these designed structure cases. As the paper surface becomes smoother, Sheffield roughness decrease, indicating less air escapes from under the rubber seal on the paper surface. It was expected that Case I and Case V would have the highest surface roughness because of their lower filler content. However, Case V data showed that its roughness was much lower, being lower than both Case I and Case III. Since there was such a dramatic difference from the COF testing, this would indicate that the COF results for Case V were due to surface chemistry rather than surface physical characteristics.

Both Cases II and III were smoother than were expected. Case III consistently had higher ash content than any other handsheet, but it does not have the smoothest surface. Case II may be smoother than Case III because of better formation or from the starch addition. Case IV has the smoothest surface. When a surface is smoother it usually has a smaller pore volume. PEO could affect the structure of the FFP (fiber/filler/polymer) structure so that the pore volume is reduced, giving a smoother surface.

5.1.4 Optical Properties

Case I and Case V had the greatest opacity losses as ash content increased, compared to the other cases. This could be due to the lower filler content of Case I and

V. The object of increasing opacity is to prevent images on one side of the sheet from showing through on the other side. This is very important for newsprint. It was disappointing that opacity did not increase with filler content, in fact for most cases opacity went down.

The mechanical pulp used in this research was not brightened to a high degree during its production at the mill. The starting brightness was between 59 and 60.5% and the brightness of the kaolin clay was 83.3% (see Table 2-3). Thus, it seems reasonable that the increase in brightness is from the addition of the kaolin clay since there is a great than 20% brightness difference between the pulp and the clay. From the brightness data, it is clear that brightness increased for each case (see Figure 4-6). This makes sense because ash content increase for all cases at all filler levels (see Figure 4-2).

Brightness overall did not increase at the same rate for Cases I and V, as it did for Cases II, III and IV. The filler retention for the non-polymer cases leveled off at higher ash contents due to lack of retention causing the brightness to level off as well. Brightness continued to increase at all filler levels for handsheets with polymer because the ash retention increased at a fairly constant rate. Brightness increased at a faster rate for Case II and Case IV after the 5% filler level despite similar retention through 15% filler level. However, at the 20% filler level, the retention for Case II and Case IV drops slightly but the increase in brightness remains constant and surpasses Case III. This indicates a secondary factor to explain these brightness results. Recall the following equation for brightness from the Kubelka-Monk theory:

$$R_\infty = 1 + \frac{K}{S} - \sqrt{\frac{K^2}{S^2} + 2\frac{K}{S}}$$

Since it has been previously noted that K (absorption coefficient) is primarily a function of bleaching conditions, it is the scattering coefficient, S, that could be affecting the brightness of Case II and Case IV. Note that Case IV (PEO) starts with the lowest brightness at 0% filler and reached the highest brightness level at 20% filler content. It is known that the maximum light scattering (S) coefficient for a given pigment is obtained at a particular optimum particle size (ref). Therefore, it is possible that because the PEO case had the highest brightness, it also has the highest value of S and thus the particle size of the kaolin clay is optimized. The particle area and perimeter measurements, (Table

5-2) indicate significant differences between Case IV and either Case II or III.. Therefore, based on the optimal brightness of Case IV the optimal particle size characteristics as given by the SEM data appear to be an area of 0.897 mm^2 and a perimeter of 2.71 mm.

Table 5-2: Area and Perimeter Data for each case at 15% FillerLevels

15% Filler	Case I	**Case II**	**Case III**	**Case IV**	Case V
Area (mm^2)	1.547	**1.633**	**1.444**	**0.897**	0.361
Perimeter (mm)	3.035	**3.630**	**3.505**	**2.704**	1.510

For Cases II, III and IV, the average brightness increase was 1% for each additional filler level. This is a promising result because just a 1% increase in brightness is generally considered a valuable increase.

Opacity is the ability of a paper sheet to absorb or reflect light and filler particles help to scatter more light to increase opacity. Instead, opacity was inconsistent across all filler levels and all cases (see Figure 4-7). Ash content did increase over every filler level for each case. Therefore, secondary factors must be influencing opacity. In can be described by the following two empirical equations.

$$Opacity = \frac{R_0}{R_\infty} \cdot 100$$ (Printing Opacity)

and

$$TAPPI\ Opacity = \frac{R_0}{R_{0.89}} \cdot 100$$ (TAPPI Opacity)

Typically, as filler levels increased, opacity should increase. Instead, opacity was inconsistent across all filler levels and all cases (see Figure 4-7). Ash content did increase over every filler level for each case. Therefore, secondary factors must be influencing opacity. Figure 4-6 shows that R_∞ did increases with each filler level increase for each case. Therefore, the value for R_0, must be influencing opacity in an unexpected manner. What this suggests is that the individual handsheets had significant variation in basis weight, even though the physical testing results were normalized to basis weight (where applicable). One physical attribute of the handsheets that could have

a negative impact on opacity is poor formation. As previously discussed, the formation decreased in all cases as the filler levels increased.

Another explanation could be that the handsheets with 0% filler already had a high opacity and so the addition of fillers had little effect on opacity. Some industry standards consider 94% opacity acceptable (Freeman, 1994), (Sharkey, 1989). For the handsheets used in this study, the opacity range was 93.5%-95.5% (printing) and 95.25%-97% (TAPPI). The handsheets were likely very bulky due to a lack of calendaring or other pressing after formation. The thickness of the sheets ranged from 183 μm to 153 μm.

5.1.5 3-D Structure

Basis weight is expected to decrease as filler addition increased due to less than 100% retention. Cases II and III maintained basis weight well despite being made from thick stock. It was expected that Cases II, III and IV would not decrease in basis weight to as great a degree as the cases without polymer, and this is what was observed (see Figure 4-8). Case V had the greatest variation in basis weight, most likely caused by poor flocculation. Another possibility is that the ethanol adversely affected fines retention due to solvent interaction.

The Formation OpTester is an optical measurement of formation and is highly correlated with basis weight. The basis weight and formation plots for each case look relatively similar (see Figure 4-9). Poor flocculation can also result in poor formation. Case IV had the best formation, although it did drop off at the 15% filler level, however, it still remained better than the other cases. Case IV (PEO) may have better formation due to PEO's affinity for lignin, which could create an optimum flocc size. Case III also had good formation, especially since it had the highest ash content. It is unclear why Case II had the worst formation, but it may have been caused by over flocculation of the furnish. The main difference between Case II and Case III was the addition of starch to Case II. Since starch can act like a polymer it is possible that Case II may have been overdosed resulting in poor flocculation.

The thickness as measured by ultrasonic waves appears to have some sort of systematic error associated with it (see Figure 4-10). It could be there was some malfunction with the ultrasonic tester or a bad calibration. Since Cases I and III were measured on the same day and Case II was measured on a different day from any of the other cases, it is also possible it was operator error. By comparing the bending stiffness data and the ultrasonic specific stiffness data it was concluded that the data for Cases I and II was incorrect and thus it will difficult to draw conclusions from Cases I and II ultrasonic data. Data for Cases I and II should be much closer to that of Cases III, IV and V. During ultrasonic testing, the measured thickness is used to calculate velocity, elastic stiffness and specific stiffness. Hence data from each of these tests will also have the same error as the thickness measurement.

5.1.6 Stiffness, E:

It is well accepted that strength properties decrease with higher filler content. Tear indices for the five handsheets have negative correlations with ash content (see Figure 4-11), as was expected. Cases I and V had relatively high tear strengths which most likely was due to the low ash content. Case II had the highest tear strength, despite having a high ash content reflecting the addition of starch as a dry strength agent. Case II also had the highest filler content. Case III had good tear strength, higher than Case IV. One of the differences between Cases III and IV was the pre-flocculation of the clay. Pre-flocculated clay may have interacted with fiber-to-fiber bonding in a positive way, either by less disruption of bonding or increased hydrogen bonding. From the following equation for tear strength:

$$G = \frac{\beta \sigma^2 a}{E}$$

The only parameters that could change are σ^2 (tensile stress) and E. The crack length, a, is constant for all tear tests (see Figure 3-4). Therefore since Case IV had a lower tensile index, that might influence the tear strength here, causing Case IV to have a lower tear index than Case II.

Bending stiffness was expected to decrease with filler content and all cases did have negative correlations between ash content and bending stiffness although Cases I

and V decreased faster than did Cases II, III and IV. Despite their rapid rate of decrease, Cases I and V had relatively high basis weights compared to the other cases between 0 to 15% filler levels. This is expected because Cases I and V have no polymer and hence lower ash contents than the other cases. There is a significant difference in the bending stiffness between Cases II and III. This result is somewhat unexpected because of the make-up similarity of the cases and the starch addition in Case II would be expected to increase bending stiffness. However bending stiffness is highly correlated with basis weight and Case II had the lowest basis weight as can be seen from the following equation:

$$s_b = \frac{Ed^2}{12}$$

Since E is relatively constant for all the cases, thickness (d) or basis weight is primarily responsible for changes in bending stiffness. Therefore, it seems reasonable that Case II would have a lower bending stiffness. In fact, if the graphs for basis weight and bending stiffness are compared, they look very similar, with each case following a similar pattern.

It was noted earlier that the apparent error in the ultrasonic could be clarified by looking and the specific stiffness and the bending stiffness. The range in values for bending stiffness within all five cases are between 0.10 km^2/s^2 and 0.04 km^2/s^2. The range in values for ultrasonic specific stiffness are between 0.14 km^2/s^2 and 0.12 km^2/s^2 for Case III, Case IV and Case V. The results for bending stiffness should be close to the results for ultrasonic specific stiffness. These two physical tests that actually measure the same paper property in different ways. The data for Cases III, IV and V match and the data for Case I and Case II ado not. Therefore, it is likely that the ultrasonic results for Case I and II are incorrect and the correct data is more likely similar to the other cases.

Ultrasonic velocity is also related to thickness and thus has the same error pattern as all the previous ultrasonic tests. However, ultrasonic travel time is not affected by thickness and thus does not contain the error. Travel time has a negative correlation with ash content. This makes sense because basis weight decreases with ash content, therefore there is less physical material through which the ultrasonic waves to propagate. Travel time also decreases as a function of increasing filler content to a greater extent in Case II, III and IV suggesting that increased filler content affects the travel time

5.1.7 Tensile

All the tensile properties gave results that were expected and both dry and wet tensile followed the same trend. This supports the generally accepted conclusion that increasing filler content decreases tensile strength. There are, however, a few unexpected observations. The dry tensile data for the 10% filler level of Case III is inconsistent with the rest of Case III and the wet tensile of Case III. Therefore, it is likely that the 10% filler level data for Case III is in error. Also it is strange that Case II has some of the lowest dry tensile indices even though starch was added to the furnish. Starch is used as dry strength agent so it was expected that Case II would have a higher tensile index. Case II has the same or lower ash content as Case III and yet its tensile index is lower. One possible explanation is that the lower basis weight of Case II was the main cause for the lower tensile index even though it was normalized by basis weight. Another factor could be that Case II had poor formation, where some areas of the sampler were affected by localized basis weight variation and thus some areas of the sample failed first, perhaps causing the entire sample to fail prematurely. The Page equation:

$$\frac{1}{T} = \frac{9}{8 \cdot Z} + \frac{3 \cdot w_f}{\tau_b \cdot l_f \cdot RBA}$$

where

T = *tensile strength*
Z = *zero span strength*
w_f = *fiber width*
τ_b = *breaking force of bond over bond area*
l_f = *fiber length*
RBA = *relative bonded area*

Ideally, they only factors in the equation that should vary between the samples would be RBA and τ_b, which is the breaking force over bond area. Therefore, if localized basis weight or formation caused any negative change to RBA or τ_b then, it would affect tensile index in a negative correlation as well. It seems reasonable that localized variation in basis weight or formation would impact both RBA and τ_b.

The wet tensile index results were similar to the dry tensile index data. This is what should happen if all the samples were re-wetted under the same conditions. Therefore, the data support that the samples were tested correctly by re-wetting the sample for the same amount of time. One exception to this is Case V. Due to the

evidence from previous data that the surface chemistry of Case V was different compared to the other cases, it is not surprising that Case V would be unlike the other cases. Here, Case V had lower wet tensile index compared to dry tensile index. It is likely that the ethanol coated filler was the cause, whether the ethanol made it easier to further saturate the sample or if when the ethanol coated filler was re-wetted it negatively impacted bonding more so than in the dry state.

Every case had a negative correlation with Z-directional tensile (ZDT). This correlation was anticipated because filler typically interrupts fiber-to-fiber bonding in all directions. In this experiment, ZDT may be one of the better indicators of sheet bond strength. Filler distribution in the thickness direction of the sheet greatly influences the physical properties of the paper. Here Case II has the highest ZDT perhaps due to the added starch. It could also be that the filler distribution is constant in the Z-direction, so that the bonding is equally affected by the filler in all layers. This would make no layer weaker than any other. Such an even distribution is likely to be caused by the pre-flocculation of the filler because the only other pre-flocced sample, Case III, also has high ZDT. Case IV shows an interesting pattern in that ZDT drops at 5% filler level and then remains constant until the 20% filler level where it drops again. There could be something in the FFP structure where the filler does not impact ZDT until it gets to the 20% filler level. Case V had the lowest ZDT, despite the low ash content. The ethanol may have some effect on the z-directional distribution of the filler causing the filler to agglomerate more locally causing weak areas that failed first. This hypothesis is supported by the variation in particle size.

Zero-span should be governed primarily by fiber strength. Zero-span can be affected by poor bonding if the zero-span results are caused by fiber pull out instead of fiber breakage. The rapid decrease as ash content increased was expected because as filler content was increased, the amount of fibers in the sheet decrease. This meant there were fewer fibers supporting the sheet. Even Cases I and V were similar to Cases III and IV, while Case II had significantly lower zero span tensile than any of the other cases. Case II had poor formation and low basis weight and these factors could be impacting the zero span tensile. Wet zero span tensile appears to accentuate the results for the dry zero span. Here Case V is lower than Cases I, III and IV. This result for Case V is similar to

the wet tensile index and could be related to the re-wetting phenomenon being affected by the ethanol coated filler.

One of the main objectives in creating the FFP structures was to keep the filler off the fiber so that it would not disrupt fiber-to-fiber bonding. Fillers typically decrease porosity because they can fill the void areas between the fibers as well as be between the fibers. The porosity results are different for the polymer cases versus the non-polymer cases. Cases II, III and IV all have negative correlations with ash content meaning that pore size is decreasing with increased filled retention. It is not descernable whether filler is only filling the void spaces and not lodging in between the fibers. However, Cases I and V both have a positive correlation between ash and porosity indicating that the pore volume is increasing. This could be the result of filler between the fibers, thereby creating a more bulky and porous structure. These trends are consistent with the objective in creating the designed structures whereby cases with polymer (II, III and IV) were intend to keep filler off the fibers and in the void spaces and where cases with no polymer (I and V) could have filler in void spaces as well as between fibers.

5.2 SEM Method: One-Way ANOVA & PASS

Overall, Cases I and V, and Cases II and III often had similar means. Case VI was often similar to Cases II and III. These results were encouraging because it was showing both differences and similarities between specific cases, which could lead to information about the differences in the FFP structures.

The main goal of using the one-way ANOVA was to determine if statistical significance was determined from the quantitative data from the image analysis of the SEM micrographs. So complete a method for obtaining quantitative data from SEM micrographs had not yet been developed before this research.

Before it was determined that the data from the image analysis did not fit a normal distribution, it was very discouraging to analyze the data because the results made no sense. At first, with so much data, it was not obvious that the data was non-normal. All the statistical analysis techniques were failing and it was fear that it would not be possible to obtain quantitative data from the SEM micrographs. This was where the non-

parametric statistical techniques brought new life into the research. Once it was realized that the data was non-normal and non-parametric statistical methods were used, the data was looking very promising.

However, as promising as the data was, the time and resources it took to obtain and analyze all the image data was of concern from a practical point of view. If this method was to be useful to other research and applications, there had to be a way to determine if the same statistical differences could be determined from a smaller sample size. Power analysis and sample size (PASS) analysis made it possible to determine that a 5 x 5 grid samples procedure that gave 25 images per stub gave a sample size approximately five times larger than was needed. Imagine the time and effort that could be put to other uses. Now that the PASS procedure has been combined with the SEM method, the next researcher to use this technique can perform the PASS analysis even before the research is begun and develop an experimental plan that is statistically and economically sound.

5.3 Principal Components Analysis

The PCA results showed that when the physical tests were correlated with the particle areas and perimeters different physical properties were correlated only with certain structures. This indirectly supports the conclusion that the designed structures were different. By relating difference physical and optical properties, with the PCA results it is possible to gain insight into the characteristics of the different fiber/fill/polymer structures. What would potentially influence a structure would be if a physical test, identified by PCA, was an extreme for that physical test. In other words that physical property was indentified from both physical testing and PCA analysis to be unique to that structure.

Case I was highly correlated with the following variables: Bright, COFK, Sheff, TenD, TenW, ZDT, USTT and ZSW. The only optical property identified by PCA was brightness and Case I had the lowest brightness at the 15% filler level (see Figure 4-6). Thus this structure may indicative of poor optical properties due to lower light scattering from a sheet with lower bulk, less surfaces to scatter light and lower porosity. Case I did

have the most porous sheet of any of the cases (see Figure 4-17). Case I was highly correlated with Sheffield roughness according to the PCA results and Case I did have the highest Sheffield roughness of any of the cases (see Figure 4-5). Roughness and porosity are linearly related, as roughness increases so does porosity and vice versa. The strength results from the PCA analysis were inconclusive as the physical testing results for Case I were somewhere in the middle compared to the other cases.

Case II was an odd case because Area and Perim were not highly correlated with any other variables according to the PCA results. This is not surprising because as previously discussed, Case II consistently gave inconsistent results. There was little explanation for the wide variation in physical testing results. Therefore, it is understandable that the PCA analysis did not find any significant correlations. This also implies that PCA may not be suitable for some data sets.

Case III was highly correlated with Bright, COFS, COFK, OP, Por, Sheff, TenW, ZDT, ZSD and Form. One aspect that was interesting was that Case III has the least porous sheet but still had the second highest surface roughness and the highest opacity, which was the opposite of what was expected. What these results could suggest is that the structure of Case III is still somewhat bulky (high opacity) and what the porosity could suggest is that the filler particles are mostly contained in the void spaces, thus maintaining bulk and opacity and decreasing sheet porosity. There are other aspects of the data that support this. Ash content was high and strength properties, including TenW, ZDT and ZSD were high as well. Case III also had the second highest formation. From all the physical testing results and the PCA analysis, it appears that Case III may have produced the desired structure of keeping the filler off the fibers and into the void spaces.

Case IV was the opposite of Case II, because Area and Perim were correlated with all the variable, especially ZSD and Sheff. In some ways this is understandable because Case IV physical testing results consistently fell in the middle of the results. Therefore, it makes sense that there were not many strong correlations as determined by PCA. There were a few exceptions where Case IV fell on the extreme of physical testing results including Sheff, Form, COFS and COFK. Case IV seems to have produced a structure with low surface toughness, good formation and low surface friction. Of these physical tests only a correlation with Sheff was detected by PCA. From Cases II and IV

it can be said that PCA was not always sensitive to small trends in the physical testing data, i.e. if the data being compared was to similar to the other data or too different, PCA could not form strong correlations.

Case V was highly correlated with OT, OP, Por, ZSW and Form. It was also weakly correlated with USTT, ZSD, TenD, COFK, COFS and Bend. As has been note previously, Case V was considered the worst-case scenario and was presumed to have the worst physical testing results. However, the correlations derived by the PCA analysis were not very descriptive because the physical testing results were typically in the middle of the results for the other cases. Therefore, it is difficult to assign structural characteristics to the PCA results for Case V.

The results of the strength and optical data together with paper physics can support where the filler was located and how much filler was in the sheet for example. If the results of the correlations are examined by thinking of the fiber and the filler, general conclusions can be drawn based on the testing and imaging data. For example high strength and high filler content imply that fiber was being incorporated into the sheet without disrupting fiber-to-fiber bonding, suggesting something about the structure was like the *Ball and Chain* or *Barbell* structures. Next, if the different types are polymers are figured into the correlation results, additional conclusions can be drawn. Starch imparts strength in paper sheets, therefore when starch was used, increased strength could mean that the fiber was being kept off the fiber or the starch was helping the filler bond with the fiber, so that even if the filler was on the fiber, bonding could occur. By combining the PCA results with the PT data more valuable relationships are revealed for further study.

5.4 SEM Micrographs

The actual SEM micrographs help support most of the results and discussions. Cases I and V look very similar and look nothing like Cases II, III or IV. Two images from each case at the 15% filler level were selected and can been seen below. These particular images were chosen because they seemed to be representative of the designed structure cases.

5.4.1 Cases without Polymer(s): Case I and Case V

What is readily apparent from these images is that Case I (control case) and Case V (ethanol coated filler) have a few "large" filler particles, and very few "small" filler particles. The ash content of the 15% filler level for Case I was only 6.855% and Case V was only 8.59%, half of the actual filler content of Case II, Case III and Case IV. Compared to Case II, Case III and Case IV, the lack of smaller filler particles is most likely due to the smaller filler particles getting through the fiber mat and going out with the white water. Since there are no polymers to help retain the smaller filler particles, this would seem to make sense.

The filler particle themselves appear to be both on the fibers and in the void areas. There appears to be no logical pattern to where they are in the sheet. Also, the orientation appears to be somewhat random, as some filler particles lie in the plane of the paper and some appear to be more perpendicular.

The only difference between the control case (Case I) and the solvent coated case (Case V) was the ethanol coated filler. From these images (see Figure 5-1 and Figure 5-2) there is no discernable difference between the two cases.

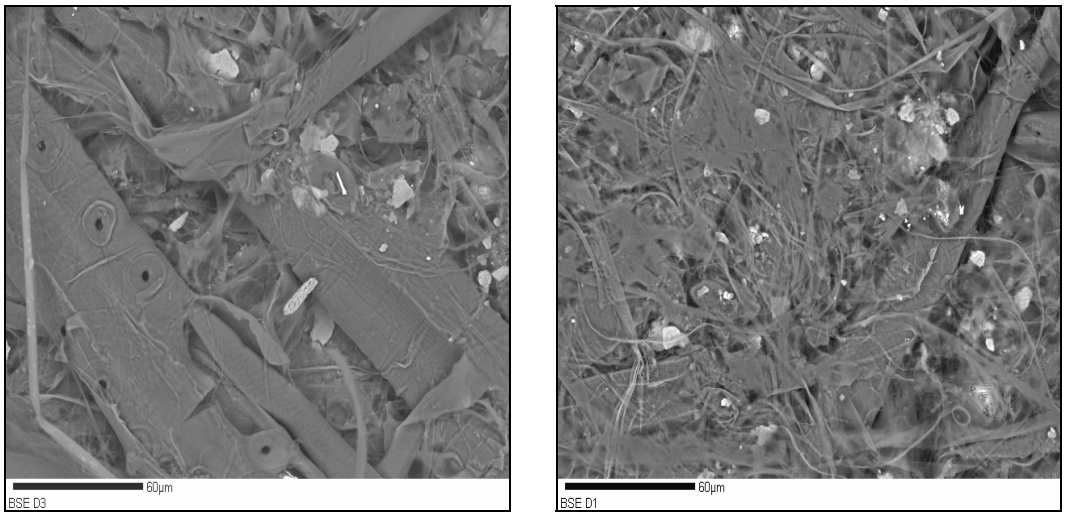

Figure 5-1: Two SEM Micrographs of Case I: Control

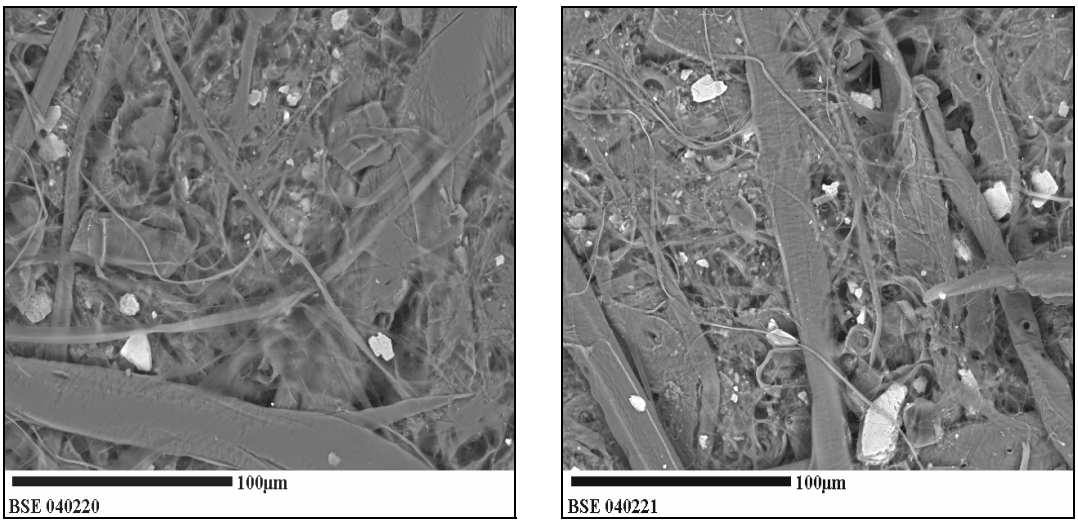

Figure 5-2: Two Micrographs of Case V: Solvent Coated Filler

5.4.2 Cases with Polymers :Case II, Case III and Case IV

The visual difference between the cases with and without polymer is readily apparent. While there are roughly the same number of "large" filler particles, there are many more "small" filler particles in these cases. This supports the current state of the art that states polymer additional improves filler retention. In addition, the ash content of these cases was much higher; Case II 14.58%, Case III 14.55%, and Case IV 12.89%.

From the images, it seems that filler particles are on the fibers themselves. However, a closer examination shows that the filler particles are really on top of fines or fibrils that in turn are on the fibers. Most of the filler particles are in the void areas away from the fibers as was hypothesized by the idealized structures *Barbell* and *Ball and Chain*. This is a very exciting result supporting the original hypothesis that a structure could be designed to keep filler off the fibers.

There is a minor difference in the Case IV (PEO) images, where it looks like there is filler directly on the fiber. This could be from filler that was attracted to the PEO which was already adsorbed onto the fibers. This is due to PEO's affinity for lignin. This was a difference that was discussed in the designed structures and it was believed that filler could be both on the fibers and in the void spaces of Case IV and still maintain

desirable strength and optical properties. Since Case IV did maintain strength properties it is possible that the PEO case

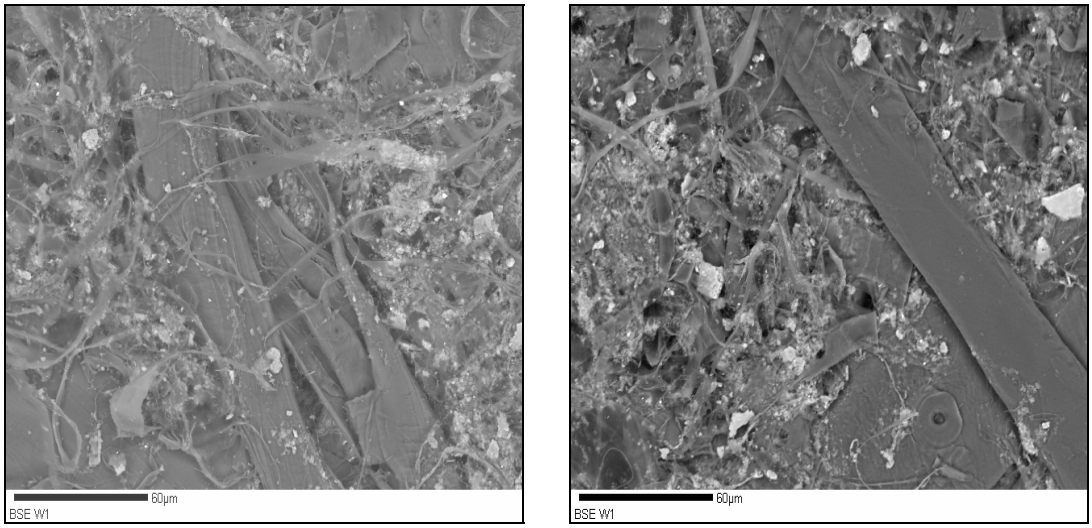

Figure 5-3: Two SEM Micrographs of Case II: Pre-flocculation with Starch

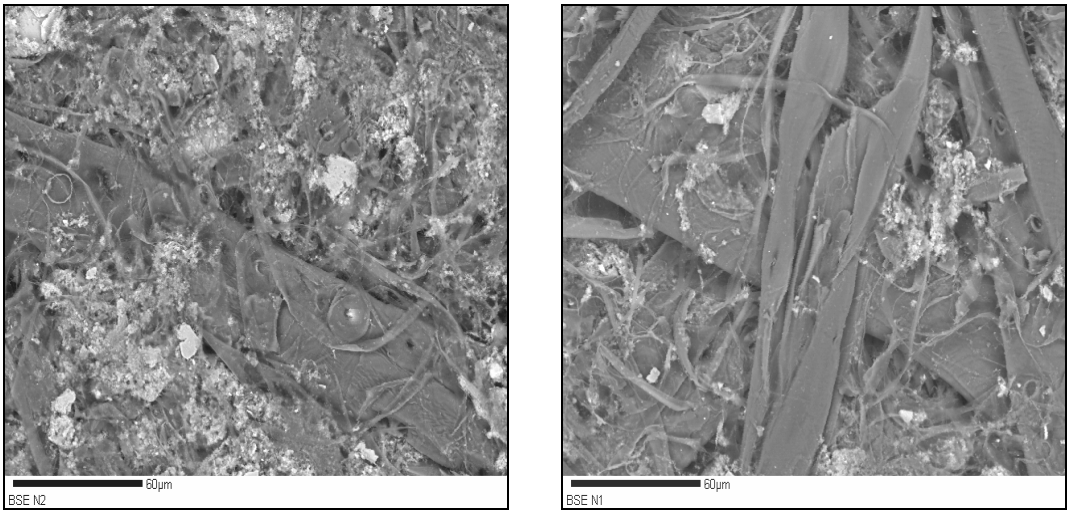

Figure 5-4: Two SEM Micrographs of Case III: Pre-flocculation Dual Polymer

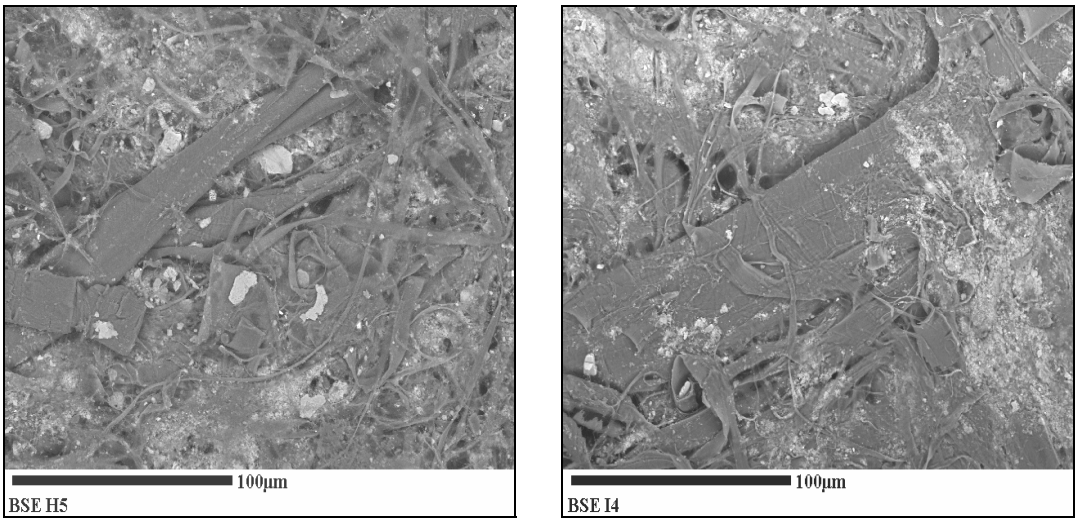

Figure 5-5: Two SEM Micrographs of Case IV: Conventional PEO

6 ADDITIONAL PARTICLE-BASED OPPORTUNITIES-TEM

6.1 TEM-Preliminary Work

Transmission electron microscopes have not been widely used within the paper industry. As of yet this is an unused tool for understanding the bonding and surface properties of paper. In transmission electron mission microscopes (TEMs), the image is formed by electrons passing through the sample. The sample must be thin enough to allow sufficient electron transmission without affecting the sample by heat absorption of the electrons (Rochow, 1994). There must be sufficient sample to show differential absorption, where electrons pass though some areas and are absorbed in other areas. The TEM image cannot be directly view by the eye; it must be projected onto a fluorescent screen where it can be transferred to photographic plates or films (Rochow, 1994).

TEM has a resolution of between 4 Å and 3 Å. Tilting the sample can improve the resolution. Contrast in the TEM depends on many factors, including adjustments to the electron beam voltage and stains. Focus depth is not an issue as it is with SEM. The magnification of a TEM depends on its resolving power. Particulate samples such as dusts, precipitates and fillers must be dispersed well enough to differentiate units from aggregates (Rochow, 1994).

The scattering of the electrons in TEM is directly proportional to the mass density of the specific area of the sample (Wischnitzer, 1970). Since different parts of the sample absorb electrons differentially, the resulting image on the fluorescent screens is darker where the sample has absorbed more electrons and lighter where the sample has absorbed less electrons. Different "stains" have been developed to enhance the electron density of components in the sample, thereby making the image easier to see. Colloidal gold staining is one such stain (Rochow, 1994).

Gold (atomic number 79) is sufficiently electron dense to be viewed with various microscopic techniques. The main function of using colloidal gold is in the in situ localization of cellular moacromolecules. Gold colloid can be prepared in a wide range of sizes from 2-150 nm, with 20-40 nm being ideal for SEM. Because the colloid is so dense, quantification of labeling can be carried out by direct counting of the number of particles in a given area. Colloidal gold particles have been used most commonly and

effectively for transmission electron microscopy (Hayat, 2000). Gold particles of ~ 3 nm in diameter can be visualized without any form of enhancement. Colloidal gold can also be used in scanning electron microscopy for both secondary and back-scattered electron imaging. Horisberger et al. introduced immunogold staining method for SEM (Horisberger, 1975). Trejdosiewicz et al. reported first imagining of colloidal gold in back-scattering (BSE) mode for SEM (Trejdosiewicz, 1981). Typically colloidal god particles > 15 nm in diameter can be imaged in secondary electron mode. Smaller particles need to be silver-enhanced for imaging purposes (Hayat, 1995). Colloidal gold has been used for detection of cellulose on nitrocellulose paper (Hsu, 1984).

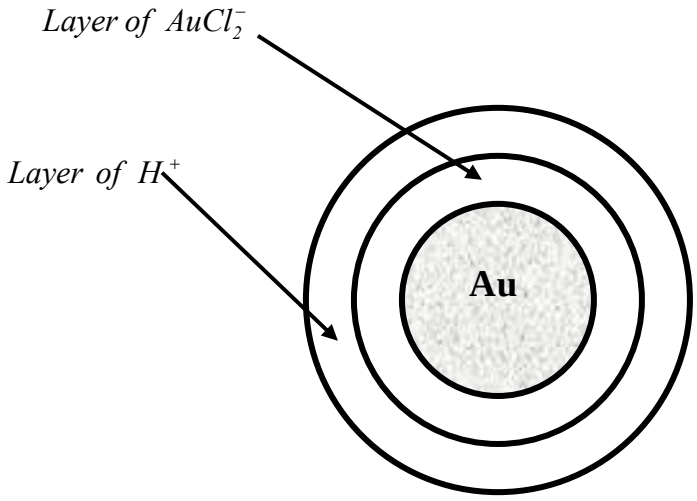

Figure 6-1: Representation of Gold Colloid (Hayat, 1989)

The basis for this TEM method was to introduce the gold colloid into the fiber slurry during the sheet making process. The addition point was in the handsheet mold, after all other components were added. The reason for this was to incorporate the colloid into the sheet. Other methods have including soaking, coating or otherwise trying to get the gold colloid into the sheet after it is formed. When the fiber slurry is in the handsheet mold, micro-flocs are formed and the interactions between the fiber, polymer and filler has already happened. As the handsheet drains, there was a consolidation of the fiber slurry, which included mechanical entrapment/entanglement of fibers, filler and polymers. If the gold colloid was added to the handsheet mold, it could interact directly

with the FFP structure in the dilute environment and interact with the fiber furnish. One other method tried at IPST saw most of the polymers visualized as long stands all flowing in the same direction. This is due to the application of gold colloid to a few fibers. The excess colloid is then pulled off the TEM grid with blotter paper, causing a flow which then is seen in the TEM and gives an unrealistic picture of the polymer.

A select group of cases and filler levels used a gold colloid technique developed for this thesis. These SEM and TEM images were taken at the Georgia Technology Research Institute (GTRI). Samples prepared for TEM used the same gold colloid technique plus a staining technique also developed at IPST and GTRI.

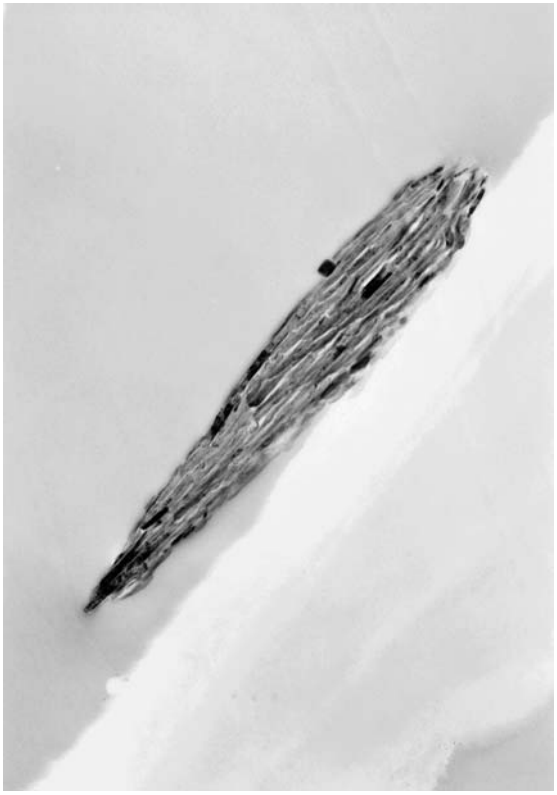

Figure 6-2: TEM image of fiber (light) and filler particle (dark)

Figure 6-3: TEM image of paper with clay and polyamine. The small round dots are the gold colloid

7 CONCLUSIONS

This thesis developed a method for correlating SEM observations of filler containing sheets with the corresponding physical properties as measured using standard physical tests. The significant aspect of this method is that it eliminates the subjective qualities usually associated with microscopy observation by employing statistical methods to determine the number and type of required SEM images, computer based image analysis techniques to identify pertinent image features, and further application of statistical techniques to establish correlations between SEM observations and physical test data.

One goal of the work was to develop fiber/filler/polymer structures that would allow for greater levels of filler content in newsprint without a significant reduction in sheet strength, optical properties or surface properties. Evaluation of these structures required the development of a method for relating macroscopic physical properties to microscopic fiber/filler and filler size/shape structural properties. Thus, there was a need for an objective and statistically sound method for obtaining the required microscopic structural information. Development of such a methodology was made more difficult because the filler distribution data proved to be non-normal data with an unknown distribution. The developed method allowed the sample size to be reduced and statistically compared the means of the data points using non-parametric methods.

The following general conclusions can be drawn about the thesis as a whole:

* **A successful method for obtaining statistically significant, objective data from Scanning Electron Microscopy micrgraphs was developed in this thesis**

* **This method was the first to bridge the gap between statistical procedures and SEM imaging, combing them in a new and unique method**

* **This thesis provided a successful example using SEM method by analyzing physical testing data and particle data from SEM micrographs of five different paper samples with different designed fiber/filler/polymer structures**

* **Case III came closest to producing the desired structure where the filler was kept off the fiber and in the void spaces.**

7.1 Hypotheses

The following hypotheses were studied in this thesis:

1. *Fiber/filler/polymer structures can be designed where the filler material is kept off the fiber material*

2. *Fiber/filler/polymer structures can be designed by using different polymers and different filler/polymer addition processes*

3. *Quantitative data can be obtained from SEM micrographs using objective and statistically sound processes*

4. *By comparing image data and physical testing data, differences in fiber/filler/polymer structures can be detected or inferred*

The thesis yielded the following conclusions about the hypotheses:

* **Designed structures Case II and Case III did keep the majority of the filler off the fiber even at high ash content**

* **Case I (filler no polymer), Case II and Case III (pre-flocculation of filler with polymer), Case IV (filler and polymer w/o pre-flocc) and Case V (ethanol coated filler produced different structures using different filler/polymer addition processes**

* **Objective, quantitative data was obtained from SEM micrographs and the data on the filler particles was statistically different in each case**

* **Comparing the image particle data and the physical testing data with statistical techniques including one-way analysis of variance and principal**

components analysis physical differences in the five designed structures were inferred

7.2 Designed Structures

Designed structures based on polymer chemistry, retention and flocculation mechanisms and paper physics were developed. The designed structures were based on two conceptually designed structures, the *Ball and Chain* and the *Barbell* structures. The structure created by either design would form a complex where the filler was in contact with the polymer and bonded to the fiber through the polymer. There were five different fiber/filler/polymer designed structures created for this study. In summary, the components of the five structures were:

1. Case I: Control → Fiber and filler only, no polymers
2. Case II: Pre-flocculation with starch → Dual polymer system with starch
3. Case III: Pre-flocculation with dual polymer system → Dual polymer system
4. Case IV: Conventional → One of the most common polymers used for NP
5. Case V: Solvent coated → Fiber and solvent coated filler only, no polymers

SEM images of each structure were discussed in the thesis. There was a dramatic difference between Case I and Case V vs. Case II, Case III and Case IV. The following conclusions of the five designed structures were drawn:

- **Five different designed fiber/filler/polymer structures were created successfully**

- **Case II and Case III were most like the bar bell and ball and chain structures**

- **Polymer addition greatly affected the five designed structures based on physical testing and image particle data**

- **Case I and Case V produced poor structures for paper making**

- **Case V was unsuccessful due to the fluctuation of filler particle size**

- **Case IV (PEO) did not produce the best strength or optical properties overall**

- **Case II and Case III produced the best strength and optical properties overall, with Case III resulting the ideal structure (of the five structures here)**

7.3 Physical Properties

As stated previously, the basis for study in this project was to relate macroscopic properties to microscopic properties. Physical testing provided the macroscopic properties used in conjunction with the SEM particle data. Many strength and optical properties were studied with all five cases, resulting in 21 physical tests in total. Physical testing results indicated similarities in Cases I and V and also in Cases II, III and IV. The physical testing results were consistent with current state of the art, with a few minor exceptions. This was important because the physical testing was partially intended as a tool to measure the new techniques against, not as a new tool itself.

The physical testing data yielded the following conclusions:

- **Physical testing results contributed to determining that five different fiber/filler/polymer structures were created**

- **Physical testing data provided the macroscopic data on the fiber/filler/polymer structures**

- **Differences in filler particle data from image analysis, area and perimeter, were detected in the physical testing results**

- **Physical testing results showed that Case I and Case V had similar structural components.**

- **Physical testing restuls showed that Case II, Case III and Case IV had similar structural components in common, although Case IV was often different from all other cases**

- **Physical testing results showed that the surface chemistry of Case V was different from the other cases due to the ethanol coated filler**

- **Physical testing data analysis is not straight forward and often there is more than one factor that contributes to the outcome of the test**

7.4 SEM Method

This work developed a method for obtaining statistically significant, objective data from SEM images. The specific application was imaging filler particles in paper, but the method can be applied to images with similar contrast levels. The significant aspect of this method was that it eliminated the subjective qualities usually associated with microscopy observation by employing (1) statistical methods to determine the number and type of required SEM images and (2) computer based image analysis techniques to quantify the size/shape characteristics of pertinent image features. This data can then be correlated with other sample data, such as physical testing data. The data base for developing the method consisted of five different fiber/filler/polymer "structures." Each structure was assumed, and later shown, to produce different filler distributions.

The image analysis process was very successful. It was able to differential each case and filler level, giving a wide range of results. It is important for this method to be able to detect subtly differences in the particles being studied. This ability of the image analysis process enabled the collection of statistical quantitative data for comparison with physical testing data. This was a great success of part of the SEM method.

Power analysis and sample size (PASS) analysis made it possible to determine that a 5 X 5 grid samples procedure that gave 25 images per stub gave a sample size approximately five times larger than was needed. PASS justified reducing the sample

size to a 3 X 3 grid by calculating the new sample size would still be statistical significant. This was a critical component to the SEM method because it made the method more practical by reducing time and resources. This was important if the method was to be used elsewhere. The next researcher to use this technique can perform the PASS analysis even before the research is begun and develop an experimental plan that is statistically and economically sound.

The development of the SEM method yielded the following conclusions:

* **New SEM grid method makes it possible to acquire objective micrographs**

* **Unique computer based image analysis procedure extracts quantitative data from the particle images visualized in the SEM micrographs**

* **Given the necessary equipment, SEM image capture could be automated**

* **The SEM method is not limited to analyzing filler particles in paper and will be useful for other areas of research**

* **Using PASS to reduce the SEM grid size from a 5 X 5 grid to a 3 X 3 grid was critical step that made the method applicable to other research.**

* **The data produced is non-normal and requires using statistical methods appropriate for such data.**

* **Using ANOVA techniques for non-normal data it was shown that the five structures had both differences and similarities in filler area and perimeter characteristics.**

* **The SEM method is repeatable based on objective and statistical procedures**

* **The SEM method appears to be the most complete method todate**

7.5 Principal Components Analysis

When the physical testing and particle image data were complied and analyzed with Principal Components Analysis (PCA), different correlations for the different cases were noted. It is believed that differences in the structures may be indicated by these unique correlations. Physical properties appear to be different and this can be directly related back to the structural differences in those structures.

Using PCA on both particle data and physical testing data can be a useful tool. PCA points out which physical properties are important for that structure. PCA picked out different relationships for each filler case. The correlations PCA found aligned with the physical testing data a lone for the most part.

The following conclusions can be drawn concerning the use of PCA:

* **Principal Components Analysis is a successful statistical technique for data analysis of combined physical testing data and image analysis data**

* **Principal Components Analysis should be used in conjunction with the SEM method developed in this thesis**

* **PCA was used to determine how each of the five designed structures were related**

* **PCA was used to determine what physical and image properties were related within each designed structure (at 15% filler level)**

* **PCA has shown that it is possible to use a statistical procedure to draw conclusions about fiber/filler/polymer structures**

* **If the data being compared was to similar to the other data or too different, PCA could not form strong correlations**

7.6 TEM Method

The basis for this TEM method was to introduce the gold colloid into the fiber slurry during the sheet making process. The addition point was in the handsheet mold, after all other components were added. The reason for this was to incorporate the colloid into the sheet. Other methods have including soaking, coating or otherwise trying to get the gold colloid into the sheet after it is formed. By adding the gold colloid to the handsheet mold, it could interact directly with the FFP structure in the dilute environment and interact with the fiber furnish.

This technique needs further study as it should have great potential. Do to the technique being in early stages it did not contribute significantly to this thesis. However, the following conclusion can be drawn:

* **TEM Method developed for this thesis can provide further insight into fiber/filler/polymer structures**

7.7 Implications for Newsprint

The PEO case (Case IV) that was used to simulate the current newsprint production was not the best process for newsprint. The pre-flocculation case without starch (Case III) may be a better choice fore newsprint. The filler level attained by Case III was greater than for Case IV at all filler levels but especially at the higher filler levels. Also, many of the strength properties were higher for Case III than Case IV even with Case III having a higher filler level. The PEO case did produce a sheet with higher brightness, but the opacity values were lower and the formation was poorer than the pre-flocculation case without starch. The pre-flocculation of fillers may prove beneficial for newsprint manufacture. If inexpensive filler material can be used to replace more costly fiber furnish, the pre-flocculation method may prove more cost effective.

This research yielded the following conclusions concerning newsprint:

* **Filler pre-flocculation would benefit newsprint properties and economics**

* **Case III is best suited for use in newsprint as it has the best combination of strength and optical properties**

7.8 Final thoughts

Despite the obstacles overcome, the results of this work were successful. The SEM method was developed and used here to gain valuable new insight into aspects of fiber/filler/polymer structures. Up until now, there has not been anobjective, statistical method for farthing the understanding of these structures. Understanding these and other designed structures is going to be important for the future of the paper industry. The paper industry must become smarter at making paper, not just faster. One way to achieve this would be to be able to design or engineer paper at its microscopic level to produce desirable properties. These structures will differ, as different properties are important for difference paper grades. Case V would be good for a paper grade in need to particular high surface friction, but probably not well suited for grease paper. Case V would may be acceptable for copy paper providing good smoothness and brightness but not good for newsprint because of its low opacity. Case II might be suitable for paper board graded because it has many favorable strength and optical properties but not well suited for fines papers due to its poor formation.

The main thrust of this thesis was developing a new and comprehensive microscopy technique. By no means is this technique limited to the study of paper. It has potential applications in areas of material science, biological science and more. This technique is more comprehensive than previous techniques, allowing a researcher to use this from start to finish.

8 FUTURE WORK

There are many areas in this thesis to expand on and explore for future research work. This thesis provides a good starting platform from where good scientific work can be pursued. Below is a listing of possible future work. It is like that not all possibilities have been thought of here, but it is a good start.

8.1 Designed Structures

- Additional fiber furnishes and/or fiber fractionation
- Additional basis weights
- Additional polymer variation including length (MW), charge density, dosage and addition processes
- Altering the pre-flocculation process so that the filler particle size can be controlled, thus allowing tailoring of particle size and potentially sheet characteristics

8.2 Physical Testing

- Cut out physical tests that did not produce useful results and add different test for ink adsorption and others related to printing issues

8.3 SEM Method

- Cross-sectional SEM work

8.4 Statistical Methods

- Complete PCA analysis on the other filler levels
- Find additional statistical methods to better correlate physical properties

8.5 TEM

- Develop TEM methods further-huge potential to further develop this method

8.6 Other Future Work

- Economic studies of implementing pre-flocc technology to newsprint.
- Use actual NP paper from various mills to see if this technique is useful for mill produced paper, not just laboratory samples
- Use additional pressing/calendaring to better reproduce end paper products

9 APPENDICES

9.1 Appendix 1: Physical Testing Data

Table 9-1: Summary of physical testing results for Case I: Control

Physical Test	Measure	0%	5%	10%	15%	20%
Ash Content	Average	0.93%	2.97%	6.20%	7.79%	11.45%
Filler Content	Average	0.00%	2.04%	5.27%	6.86%	10.52%
Basis Wieght (g/m^2)	Average	63.65	59.59	59.04	57.73	58.14
Bending	Average	0.092	0.082	0.075	0.060	0.056
	Std. Dev.	0.008	0.011	0.005	0.006	0.006
Brightness	Average	60.36	60.19	60.77	61.25	61.16
	Std. Dev.	0.39	0.39	0.45	0.45	0.58
COF-Static, m_s	Average	0.825	0.885	0.826	0.917	0.977
	Std. Dev.	0.086	0.137	0.061	0.102	0.096
COF-Kinetic, m_k	Average	0.458	0.453	0.423	0.475	0.513
	Std. Dev.	0.040	0.048	0.040	0.073	0.046
Formation Index	Average	108	104	95	93	84
	Std. Dev.	11	6	5	7	8
TAPPI Opacity	Average	95.28	94.57	94.43	94.36	94.64
	Std. Dev.	0.41	0.43	0.36	1.03	0.77
Printing Opcaity	Average	96.98	96.41	96.59	95.70	95.66
	Std. Dev.	0.36	0.48	0.71	0.93	0.47
Air Permeance (Porosity)	Average	3.58	4.07	3.89	5.04	4.79
	Std. Dev.	0.41	0.28	0.36	1.01	0.41
Print-Surf	Average	5.53	5.45	5.09	5.39	5.12
	Std. Dev.	0.32	0.46	0.47	0.49	0.47
Sheffield	Average	319	317	310	310	303
	Std. Dev.	17	11	15	17	11
Tear	Average	89	74	69	66	64
	Std. Dev.	11	3	3	2	3
Tensile Strength-dry	Average	29.437	28.850	27.466	24.872	23.630
	Std. Dev.	0.873	0.895	1.143	1.822	1.736
Tensile Strength-wet	Average	3.200	2.879	2.527	2.242	1.999
	Std. Dev.	0.177	0.090	0.080	0.151	0.134
Breaking Length-dry	Average	3.001	2.941	2.800	2.535	2.409
	Std. Dev.	0.089	0.091	0.117	0.186	0.177
Breaking Length-wet	Average	0.325	0.293	0.258	0.229	0.204
	Std. Dev.	0.018	0.009	0.008	0.015	0.014
Tensile Index-dry	Average	29.417	28.831	27.448	24.857	23.617
	Std. Dev.	0.875	0.892	1.142	1.820	1.737
Tensile Index-wet	Average	3.441	2.970	2.564	2.241	1.997
	Std. Dev.	0.199	0.090	0.080	0.152	0.135
ZDT	Average	54.28	58.87	61.41	49.74	53.38
	Std. Dev.	14.10	9.90	13.60	11.23	13.00

Table 9-1: Summary of physical testing results for Case I: Control

Physical Test	Measure	0%	5%	10%	15%	20%
Ultra Sonics-Thickness	Average	347.2628	323.7660	308.0686	298.2078	292.0195
	Std. Dev.	11.6004	0.0231	14.8568	0.0188	4.2270
Ultra Sonics-Travel Time	Average	0.5447	0.5036	0.4709	0.4758	0.4608
	Std. Dev.	10.2760	0.0210	13.7228	0.0175	4.4684
Ultra Sonics-Velocity	Average	638.0270	642.6056	654.5140	626.7388	633.8397
	Std. Dev.	6.4096	0.0117	12.7204	0.0167	3.3154
Ultra Sonics-Specific Stiffness	Average	0.4072	0.4138	0.4287	0.3930	0.4018
	Std. Dev.	9.7413	0.0146	16.7700	0.0209	3.7169
Ultra Sonics-Elastic Stiffness	Average	70.4545	76.8048	83.4829	79.0996	82.7440
	Std. Dev.	14.0764	0.0232	7.6425	0.0098	4.5601
Zero-Span (dry)	Average	22.9	22.0	21.4	20.7	19.7
	Std. Dev.	1.2	0.9	1.4	0.9	0.9
Zero-Span (wet)	Average	17.1	17.4	16.8	16.1	15.6
	Std. Dev.	0.5	1.4	0.9	0.5	0.9

Table 9-2: Summary of physical testing results for Case II: Pre-flocculation with dual polymer system

Physical Test	Measure	0%	5%	10%	15%	20%
Ash Content	Average	0.92%	6.34%	10.95%	15.50%	17.80%
Filler Content	Average	0.00%	5.42%	10.03%	14.58%	16.88%
Basis Wieght (g/m^2)	Average	56.90	56.57	56.87	57.80	59.67
Bending	Average	0.065	0.059	0.055	0.048	0.056
	Std. Dev.	0.010	0.010	0.006	0.008	0.005
Brightness	Average	59.17	60.66	62.78	63.65	64.35
	Std. Dev.	0.40	0.33	0.43	0.39	0.26
COF-Static, m_s	Average	0.628	0.726	0.770	0.883	0.854
	Std. Dev.	0.049	0.032	0.030	0.050	0.032
COF-Kinetic, m_k	Average	0.376	0.421	0.424	0.453	0.467
	Std. Dev.	0.018	0.021	0.033	0.036	0.021
Formation Index	Average	81	79	79	72	75
	Std. Dev.	5	5	6	4	4
TAPPI Opacity	Average	93.50	93.88	94.26	95.17	95.52
	Std. Dev.	0.79	0.40	0.50	0.42	0.39
Printing Opcaity	Average	95.29	95.28	95.53	95.47	96.38
	Std. Dev.	0.84	0.51	0.39	0.35	0.36
Air Permeance (Porosity)	Average	8.63	8.12	6.69	5.96	5.37
	Std. Dev.	1.30	0.49	0.90	0.45	0.44
Print-Surf	Average	4.78	4.54	4.68	4.47	4.43
	Std. Dev.	0.40	0.40	0.27	0.35	0.33
Sheffield	Average	265	259	243	237	226
	Std. Dev.	16	15	13	9	13
Tear	Average	74	80	71	60	61
	Std. Dev.	3	4	8	3	3

Table 9-2: Summary of physical testing results for Case II: Pre-flocculation with dual polymer system

Physical Test	Measure	0%	5%	10%	15%	20%
Tensile Strength-dry	Average	26.115	24.866	22.760	21.228	20.545
	Std. Dev.	1.41553	1.31815	0.78142	1.48572	1.45715
Tensile Strength-wet	Average	2.725	2.162	1.548	1.694	1.436
	Std. Dev.	0.06082	0.14164	0.13885	0.16856	0.15282
Breaking Length-dry	Average	2.662	2.535	2.320	2.164	2.094
	Std. Dev.	0.14439	0.13454	0.07961	0.15153	0.1488
Breaking Length-wet	Average	0.278	0.220	0.158	0.173	0.146
	Std. Dev.	0.00621	0.01444	0.01416	0.01718	0.01559
Tensile Index-dry	Average	26.101	24.851	22.745	21.214	20.530
	Std. Dev.	1.41554	1.31899	0.78045	1.48562	1.45879
Tensile Index-wet	Average	2.725	2.115	1.474	1.693	1.435
	Std. Dev.	0.06089	0.14154	0.13878	0.16845	0.15282
ZDT	Average	60.08	60.99	64.30	55.40	51.54
	Std. Dev.	7.83	8.34	2.69	7.25	8.34
Ultra Sonics-Thickness	Average	330.0247	335.5121	318.6869	299.9062	297.4533
	Std. Dev.	18.0610	14.0648	22.7641	14.3139	12.7826
Ultra Sonics-Travel Time	Average	0.5094	0.5118	0.4745	0.4345	0.4280
	Std. Dev.	0.0396	0.0325	0.0421	0.0302	0.0290
Ultra Sonics-Velocity	Average	649.1347	656.5652	672.6828	691.3802	696.1538
	Std. Dev.	21.3628	19.3994	18.4333	22.7411	22.4485
Ultra Sonics-Specific Stiffness	Average	0.4219	0.4314	0.4528	0.4784	0.4852
	Std. Dev.	0.0275	0.0252	0.0249	0.0315	0.0312
Ultra Sonics-Elastic Stiffness	Average	77.0431	77.3757	85.7881	96.0753	98.1778
	Std. Dev.	8.0293	6.7332	8.9302	9.7088	9.4134
Zero-Span (dry)	Average	16.5	17.3	16.5	14.6	14.0
	Std. Dev.	1.4	1.4	2.1	1.4	1.1
Zero-Span (wet)	Average	13.8	13.5	13.0	12.4	12.7
	Std. Dev.	1.0	0.7	1.2	1.0	1.5

Table 9-3: Summary of physical testing results for Case III: Pre-flocculation with starch

Physical Test	Measure	0%	5%	10%	15%	20%
Ash Content	Average					
Filler Content	Average					
Basis Wieght (g/m^2)	Average	60.69	60.83	60.21	60.90	59.18
Bending	Average	0.084	0.079	0.065	0.065	0.050
	Std. Dev.	0.011	0.010	0.014	0.009	0.008
Brightness	Average	58.94	60.50	61.53	62.84	63.86
	Std. Dev.	0.48	0.52	0.36	0.62	0.50
COF-Static, m_s	Average	0.704	0.754	0.777	0.886	0.882
	Std. Dev.	0.072	0.026	0.071	0.058	0.054

Table 9-3: Summary of physical testing results for Case III: Pre-flocculation with starch

Physical Test	Measure	0%	5%	10%	15%	20%
COF-Kinetic, m_k	Average	0.449	0.462	0.469	0.500	0.500
	Std. Dev.	0.038	0.028	0.029	0.032	0.018
Formation Index	Average	97	92	94	93	90
	Std. Dev.	10	7	10	8	7
TAPPI Opacity	Average	94.36	95.07	94.98	95.20	94.99
	Std. Dev.	0.66	0.41	0.71	0.53	0.57
Printing Opcaity	Average	96.94	96.07	96.05	96.13	96.09
	Std. Dev.	0.54	0.48	0.77	0.64	0.68
Air Permeance (Porosity)	Average	10.19	10.29	9.45	8.16	8.09
	Std. Dev.	1.81	1.63	1.23	1.32	1.40
Print-Sufr	Average	5.34	5.26	5.05	5.34	5.41
	Std. Dev.	0.40	0.44	0.51	0.38	0.39
Sheffield	Average	287	286	271	259	251
	Std. Dev.	36	17	15	13	11
Tear	Average	76	74	71	65	59
	Std. Dev.	4	6	4	3	3
Tensile Strength-dry	Average	29.504	27.030	31.196	23.202	21.927
	Std. Dev.	2.164	1.790	3.031	2.406	2.072
Tensile Strength-wet	Average	2.713	2.328	2.109	1.875	1.575
	Std. Dev.	0.232	0.226	0.305	0.209	0.121
Breaking Length-dry	Average	3.008	2.756	3.180	2.365	2.235
	Std. Dev.	0.220	0.183	0.309	0.245	0.212
Breaking Length-wet	Average	0.277	0.237	0.215	0.191	0.161
	Std. Dev.	0.024	0.023	0.029	0.021	0.012
Tensile Index-dry	Average	29.488	27.016	31.176	23.190	21.912
	Std. Dev.	2.159	1.791	3.028	2.406	2.074
Tensile Index-wet	Average	2.732	2.324	2.144	1.874	1.574
	Std. Dev.	0.232	0.226	0.288	0.209	0.120
ZDT	Average	57.59	58.46	60.43	47.86	51.73
	Std. Dev.	14.96	9.83	13.38	10.80	12.60
Ultra Sonics-Thickness	Average	173.0059	168.2170	162.3589	155.4732	158.1842
	Std. Dev.	8.5107	7.2263	5.2319	6.2687	5.9185
Ultra Sonics-Travel Time	Average	0.4942	0.47536	0.45671	0.42483	0.4266
	Std. Dev.	0.0346	0.02741	0.02629	0.02018	0.0163
Ultra Sonics-Velocity	Average	350.644	354.197	355.968	366.167	370.6844
	Std. Dev.	10.1281	7.2757	11.5868	6.73988	5.3066
Ultra Sonics-Specific Stiffness	Average	0.12307	0.1255	0.12686	0.13417	0.1374
	Std. Dev.	0.00701	0.00526	0.0082	0.00506	0.0039
Ultra Sonics-Elastic Stiffness	Average	42.8361	44.8861	46.9679	51.8494	52.1901
	Std. Dev.	4.0873	3.3890	4.0556	3.0566	2.2789
Zero-Span (dry)	Average	21.1	21.2	19.4	19.1	17.0
	Std. Dev.	1.0	1.4	1.7	0.9	0.9
Zero-Span (wet)	Average	17.1	16.4	15.7	14.3	13.7
	Std. Dev.	1.4	0.8	1.5	0.7	0.6

Table 9-4: Summary of physical testing results for Case IV: PEO

Physical Test	Measure	0%	5%	10%	15%	20%
Ash Content	Average	1.02%	5.81%	10.20%	14.90%	20.30%
Filler Content	Average	0.90%	5.58%	9.72%	14.55%	19.50%
Basis Wieght (g/m^2)	Average	57.59	59.66	58.83	56.63	56.28
Bending	Average	0.071	0.057	0.063	0.058	0.044
	Std. Dev.					
Brightness	Average	58.88	59.80	61.31	62.89	64.92
	Std. Dev.	0.65	0.45	0.71	0.60	0.45
COF-Static, m_s	Average	0.858	0.759	0.713	0.628	0.649
	Std. Dev.	0.106	0.054	0.092	0.034	0.020
COF-Kinetic, m_k	Average	0.406	0.403	0.396	0.431	0.441
	Std. Dev.	0.027	0.026	0.020	0.020	0.011
Formation Index	Average	108	110	110	99	96
	Std. Dev.	8	9	12	8	9
TAPPI Opacity	Average	94.25	94.84	94.68	94.52	94.33
	Std. Dev.	0.48	0.34	0.42	0.63	0.69
Printing Opcaity	Average	95.19	95.66	95.53	95.50	95.19
	Std. Dev.	0.44	0.38	0.34	0.77	0.55
Air Permeance (Porosity)	Average	5.73	5.07	4.88	4.83	4.70
	Std. Dev.	0.42	0.39	0.60	0.52	0.54
Print-Sufr	Average	4.90	4.88	4.85	4.86	4.81
	Std. Dev.	0.15	0.18	0.14	0.24	0.28
Sheffield	Average	239	236	222	221	202
	Std. Dev.	17	23	25	25	18
Tear	Average	66	66	61	59	54
	Std. Dev.	7	5	2	4	4
Tensile Strength-dry	Average	27.057	25.185	23.964	22.541	20.420
	Std. Dev.	1.349	1.559	1.101	1.175	0.865
Tensile Strength-wet	Average	3.435	2.105	2.103	2.081	1.916
	Std. Dev.	0.183	0.107	0.115	0.110	0.085
Breaking Length-dry	Average	2.761	2.568	2.443	2.297	2.081
	Std. Dev.	0.139	0.159	0.112	0.120	0.088
Breaking Length-wet	Average	0.345	0.215	0.214	0.212	0.195
	Std. Dev.	0.018	0.011	0.012	0.011	0.009
Tensile Index-dry	Average	27.065	25.174	23.948	22.524	20.405
	Std. Dev.	1.364	1.559	1.101	1.173	0.865
Tensile Index-wet	Average	3.313	2.216	2.197	2.079	1.915
	Std. Dev.	0.153	0.107	0.115	0.110	0.085
ZDT	Average	51.15	43.93	43.20	43.86	37.64
	Std. Dev.	18.00	12.16	11.00	9.51	9.23
Ultra Sonics-Thickness	Average	183.6371	180.1447	171.0689	160.9938	153.1610
	Std. Dev.	5.8928	4.9892	5.8550	5.2088	4.8956
Ultra Sonics-Travel Time	Average	0.5354	0.5113	0.4847	0.438	0.4099
	Std. Dev.	0.02357	0.01792	0.02158	0.02278	0.0151

Table 9-4: Summary of physical testing results for Case IV: PEO

Physical Test	Measure	0%	5%	10%	15%	20%
Ultra Sonics-Velocity	Average	343.233	352.447	353.146	368.055	373.9550
	Std. Dev.	8.36756	6.17616	9.79013	11.3752	11.2017
Ultra Sonics-Specific Stiffness	Average	0.11785	0.12425	0.1247	0.1355	0.1399
	Std. Dev.	0.00581	0.00433	0.00702	0.00842	0.0085
Ultra Sonics-Elastic Stiffness	Average	38.5651	41.4209	43.8238	50.6139	54.8538
	Std. Dev.	2.5041	1.9740	2.9036	4.0336	3.2541
Zero-Span (dry)	Average	22.7	20.6	20.7	19.3	18.0
	Std. Dev.	1.5	1.2	1.4	1.3	1.1
Zero-Span (wet)	Average	17.4	16.7	15.6	15.0	14.4
	Std. Dev.	1.3	0.9	0.8	0.5	1.1

Table 9-5: Summary of physical testing results for Case V: Solvent coated filler

Physical Test	Measure	0%	5%	10%	15%	20%
Ash Content	Average	0.93%	3.17%	6.56%	8.04%	11.80%
Filler Content	Average	0.00%	2.97%	6.00%	7.79%	11.45%
Basis Wieght (g/m^2)	Average	63.65	56.08	53.53	59.25	54.42
Bending	Average	0.092	0.067	0.063	0.069	0.054
	Std. Dev.	0.008				
Brightness	Average	60.36	59.80	59.99	60.89	61.21
	Std. Dev.	0.39	0.41	0.59	0.62	0.80
COF-Static, m_s	Average	0.825	0.972	1.119	1.170	1.132
	Std. Dev.	0.086				
COF-Kinetic, m_k	Average	0.458	0.561	0.575	0.581	0.564
	Std. Dev.	0.040				
Formation Index	Average	108	92	82	88	81
	Std. Dev.	11	7	11	8	9
TAPPI Opacity	Average	95.28	94.23	94.08	95.04	94.31
	Std. Dev.	0.41	0.46	0.76	0.66	0.86
Printing Opcaity	Average	96.98	95.28	95.32	95.82	95.41
	Std. Dev.	0.36	0.43	0.79	0.59	0.88
Air Permeance (Porosity)	Average	3.58	6.76	7.66	6.09	6.62
	Std. Dev.	0.41	0.72	1.99	1.65	1.82
Print-Sufr	Average	5.53	4.91	5.01	4.97	4.93
	Std. Dev.	0.32	0.16	0.12	0.12	0.11
Sheffield	Average	319	258	265	247	240
	Std. Dev.	17	20	27	14	16
Tear	Average	89	72	67	62	60
	Std. Dev.	11	4	5	3	4
Tensile Strength-dry	Average	29.437	26.121	24.604	23.661	22.584
	Std. Dev.	0.873	0.941	1.896	1.634	1.166

Table 9-5: Summary of physical testing results for Case V: Solvent coated filler

Physical Test	Measure	0%	5%	10%	15%	20%
Tensile Strength-wet	Average	3.200	2.257	2.019	1.882	1.638
	Std. Dev.	0.177	0.136	0.178	0.095	0.128
Breaking Length-dry	Average	3.001	2.660	2.508	2.412	2.302
	Std. Dev.	0.089	0.099	0.194	0.167	0.119
Breaking Length-wet	Average	0.325	0.230	0.206	0.192	0.167
	Std. Dev.	0.018	0.014	0.018	0.010	0.013
Tensile Index-dry	Average	29.417	26.083	24.590	23.644	22.570
	Std. Dev.	0.875	0.971	1.900	1.636	1.166
Tensile Index-wet	Average	3.441	2.135	1.984	1.881	1.637
	Std. Dev.	0.199	0.135	0.178	0.096	0.128
ZDT	Average	54.28	38.90	34.32	32.95	31.01
	Std. Dev.	14.10	11.21	10.25	4.90	3.89
Ultra Sonics-Thickness	Average	347.2628	182.2152	176.7395	184.0588	168.7390
	Std. Dev.	11.6004	5.3595	5.9016	3.6860	4.6099
Ultra Sonics-Travel Time	Average	0.5447	0.5404	0.52495	0.53415	0.4942
	Std. Dev.	10.2760	0.0194	0.028	0.02207	0.0188
Ultra Sonics-Velocity	Average	638.0270	337.3302	337.284	344.976	341.6366
	Std. Dev.	6.4096	5.4040	11.8712	10.6996	10.6733
Ultra Sonics-Specific Stiffness	Average	0.4072	0.1139	0.11385	0.11925	0.1168
	Std. Dev.	9.7413	0.0037	0.00803	0.0073	0.0073
Ultra Sonics-Elastic Stiffness	Average	70.4545	37.5157	38.7224	38.8566	41.5576
	Std. Dev.	14.0764	1.7744	3.2063	2.6892	2.6278
Zero-Span (dry)	Average	22.9	20.8	20.5	18.4	18.2
	Std. Dev.	1.2	1.3	1.9	1.6	1.8
Zero-Span (wet)	Average	17.1	15.7	15.3	13.6	13.8
	Std. Dev.	0.5	1.4	1.1	1.1	0.8

9.2 Appendix 2: Testing Procedures

Table 9-6: List of Procedures and Physical Tests

Procedures/Physical Tests	TAPPI Test Method	Instrument
Air resistance of paper (Gurley method)	T 460 om-96	
Bending Stiffness	T 489 om-99	Teledyne Taber 150-D
Coefficients of Static and Kinetic Friction of Uncoated Writing and Printing Paper by the use of the Horizontal Plane Method (COF)	T 549 pm-90	
Diffuse Brightness of Pulp (d/0º)	T 525 om-92	
Diffuse Opacity of Paper (d/0º paper backing)	T 519 om-96	
Fines Fraction by Weight of Paper Stock by Wet Screening (Britt Jar)	T 261 cm-00	
Formation		Formation OPTester
Forming Handsheets for the Physical Tests of Pulp	T 205 sp-95	
Grammage of paper and paperboard (weight per unit area)	T 410 om-98	
Internal Bond Strength of Paperboard (Z-direction Tensile)	T 541 om-99	
Internal tearing resistance of paper (Elmendorf-type method)	T 414 om-98	
Klason Lignin	T 222	
Opacity of paper (15/d geometry, illuminant A/2º, 89% reflectance backing and paper backing)	T 425 om-96	
Roughness of Paper and Paperboard (Print-Surf Method)	T 555 om-99	
Roughness of paper and paperboard (Sheffield method)	T 538 om-96	
Tensile properties of paper and paperboard (using constant rate of elongation apparatus)	T 494 om-99	
Ultra Sonics		
Wet Tensile Breaking Length of Paper and Paperboard	T 456	
Wet zero-span tensile strength of pulp	T 273 om-95	
Wood, Pulp, Paper and Paper Board Combustion at 525ºC (Ash)	T 211 om-93	
Wood, Pulp, Paper and Paper Board Combustion at 900ºC (Ash)	T 413 om-93	
Zero-span breaking strength of pulp (dry zero-span tensile)	T 231 om-96	

9.3 Appendix 3: Gold Colloid Procedure

Gold Colloid Preparation Procedure (100 mL):

Au Solution
Chemicals: 1 mL of 1% $HAuCl_4$
79 mL of distilled H_2O

Reducing Mixture
Chemicals: tri-sodium citrate dihydride ($Na_3C_6H_5O_7 \bullet 2\ H_20$) (4 mL of 1%)
tannic acid [$(c_{14}H_{10}O_9)_n$] (5 mL of 1 %)
potassium carbonate (K_2CO_3) (5 mL of 25 mM)
distilled H_2O (6 mL)
1% $Na_3C_6H_5O_7 \bullet 2\ H_2O$ → 0.50 grams dissolved in 50 grams water
1% $(C_{14}H_{10}O_9)_n$ → 0.50 grams dissolved in 50 grams water
25 mM K_2CO_3 (FW: 138.21g/mol) → 0.1728 grams in 50 mL

The reducing mixture will require filtration through a membrane to remove any undissolved solids that may interfere with TEM visualization. Both the Au solution and the reducing mixture are heated on a hot plate to 60°C (this temperature is critical) with constant rapid agitation. The reducing mixture is then added quickly to the Au solution. The formation of Au colloid occurs within seconds. Bring the mixture to a boil.

Equipment:
- Balance capable of reading to four decimal places
- Weighing boats/paper
- Balance for taring the mixing beakers
- 5 cc sterile syringes
- Magnetic stir bars (2) and hot plate (2), for a water bath that includes agitation
- Thermometers (2)

(Hayat, 1989)

9.4 Appendix 4: NCSS Reports

Analysis of Variance Report
Database C:\Documents and Settings\fm ... 5% Filler\Case II 15%-500.S0
Response Area

Tests of Assumptions Section

Assumption	Test Value	Prob Level	Decision (0.05)
Skewness Normality of Residuals	8.1121	0.000000	Reject
Kurtosis Normality of Residuals	6.5054	0.000000	Reject
Omnibus Normality of Residuals	108.1262	0.000000	Reject
Modified-Levene Equal-Variance Test	0.4095	0.801541	Accept

Box Plot Section

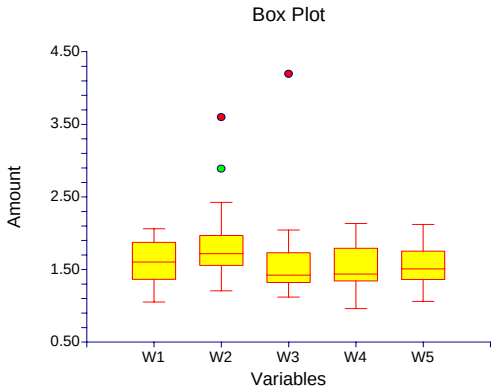

Expected Mean Squares Section

Source Term	DF	Term Fixed?	Denominator Term	Expected Mean Square
A: Sample	4	Yes	S(A)	S+sA
S(A)	119	No	S(A)	

Note: Expected Mean Squares are for the balanced cell-frequency case.

Analysis of Variance Table

Source Term	DF	Sum of Squares	Mean Square	F-Ratio	Prob Level	Power (Alpha=0.05)
A: Sample	4	1.525778	0.3814445	2.260.066932		0.645296
S(A)	119	20.10608	0.1689586			
Total (Adjusted)	123	21.63186				
Total	124					

* Term significant at alpha = 0.05

Kruskal-Wallis One-Way ANOVA on Ranks
Hypotheses
Ho: All medians are equal.
Ha: At least two medians are different.

Test Results

Method	DF	Chi-Square (H)	Prob Level	Decision(0.05)
Not Corrected for Ties	4	11.85614	0.018454	Reject Ho
Corrected for Ties	4	11.85614	0.018454	Reject Ho

Number Sets of Ties 0
Multiplicity Factor 0

Group Detail

Group	Count	Sum of Ranks	Mean Rank	Z-Value	Median
W1	25	1654.00	66.16	0.5699	1.6136
W2	25	2048.00	81.92	3.0237	1.7275
W3	25	1236.00	49.44	-2.0334	1.4323
W4	25	1426.00	57.04	-0.8501	1.4498
W5	24	1386.00	57.75	-0.7210	1.5185

Means and Effects Section

Term	Count	Mean	Standard Error	Effect
All	124	1.632677	6.580913E-02	
A: Sample				
W1	25	1.618428	8.220915E-02	1.552619
W2	25	1.848392	8.220915E-02	1.782583
W3	25	1.584176	8.220915E-02	1.518367
W4	25	1.55304	8.220915E-02	1.487231
W5	24	1.556296	8.390437E-02	1.490487

Plots of Means Section

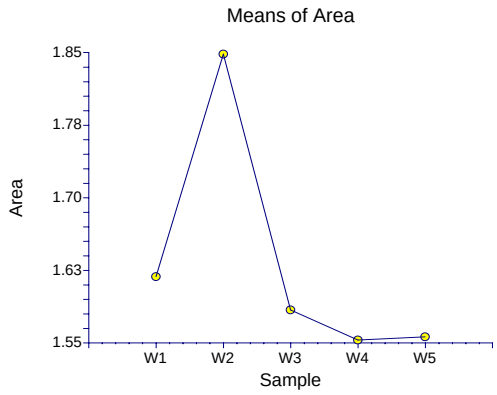

Tukey-Kramer Multiple-Comparison Test

Response: Area
Term A: Sample

Alpha=0.050 Error Term=S(A) DF=119 MSE=0.1689586 Critical Value=3.9175

Different From

Group	Count	Mean	Groups
W4	25	1.55304	
W5	24	1.556296	
W3	25	1.584176	
W1	25	1.618428	
W2	25	1.848392	

Notes:
This report provides multiple comparison tests for all pairwise differences between the means.

Analysis of Variance Report
Database C:\Documents and Settings\fm ... a\Image\15%-500-All Cases.S0
Response Area

Tests of Assumptions Section

Assumption	Test Value	Prob Level	Decision (0.05)
Skewness Normality of Residuals	9.3742	0.000000	Reject
Kurtosis Normality of Residuals	7.7514	0.000000	Reject
Omnibus Normality of Residuals	147.9598	0.000000	Reject
Modified-Levene Equal-Variance Test	10.2272	0.000000	Reject

Expected Mean Squares Section

Source Term	DF	Term Fixed?	Denominator Term	Expected Mean Square
A: Case	4	Yes	S(A)	S+sA
S(A)	299	No		S(A)

Note: Expected Mean Squares are for the balanced cell-frequency case.

Analysis of Variance Table

Source Term	DF	Sum of Squares	Mean Square	F-Ratio	Prob Level	Power (Alpha=0.05)
A: Case	4	64.39541	16.09885	101.74	0.000000*	1.000000
S(A)	299	47.31374	0.1582399			
Total (Adjusted)	303	111.7091				
Total	304					

* Term significant at alpha = 0.05

Kruskal-Wallis One-Way ANOVA on Ranks
Hypotheses
Ho: All medians are equal.
Ha: At least two medians are different.

Test Results

Method	DF	Chi-Square (H)	Prob Level	Decision(0.05)
Not Corrected for Ties	4	178.4046	0.000000	Reject Ho
Corrected for Ties	4	178.4048	0.000000	Reject Ho

Number Sets of Ties 4
Multiplicity Factor 24

Group Detail

	Sum of	Mean

Group	Count	Ranks	Rank	Z-Value	Median
Case I	45	8028.50	178.41	2.1423	1.3816
Case II	124	25592.50	206.39	8.8722	1.5764
Case III	45	7958.50	176.86	2.0137	1.435
Case IV	45	3667.50	81.50	-5.8702	0.8422
Case V	45	1113.00	24.73	-10.5637	0.3327

Means and Effects Section

Term	Count	Mean	Standard Error	Effect
All	304	1.294848		1.934592E-02
A: Case				
Case I	45	1.547351	0.0592996	1.528005
Case II	124	1.632677	3.572294E-02	1.613332
Case III	45	1.443518	0.0592996	1.424172
Case IV	45	0.8966111	0.0592996	0.8772652
Case V	45	0.3610022	0.0592996	0.3416563

Kruskal-Wallis Multiple-Comparison Z-Value Test

Area	Case I	Case II	Case III	Case IV	Case V
Case I	0.0000	1.8291	0.0839	5.2296	8.2929
Case II	1.8291	0.0000	1.9307	8.1641	11.8750
Case III	0.0839	1.9307	0.0000	5.1457	8.2090
Case IV	5.2296	8.1641	5.1457	0.0000	3.0633
Case V	8.2929	11.8750	8.2090	3.0633	0.0000

Regular Test: Medians significantly different if z-value > 1.9600
Bonferroni Test: Medians significantly different if z-value > 2.8070

Tests of Assumptions Section

Assumption	Test Value	Prob Level	Decision (0.05)
Skewness Normality of Residuals	-2.4511	0.014241	Reject
Kurtosis Normality of Residuals	4.4288	0.000009	Reject
Omnibus Normality of Residuals	25.6219	0.000003	Reject
Modified-Levene Equal-Variance Test	2.3153	0.057436	Accept

Expected Mean Squares Section

Source Term	DF	Fixed?	Denominator Term	Expected Mean Square
A: Case	4	Yes	S(A)	S+sA
S(A)	299	No	S(A)	

Note: Expected Mean Squares are for the balanced cell-frequency case.

Analysis of Variance Table

Source Term	DF	Sum of Squares	Mean Square	F-Ratio	Prob Level	Power (Alpha=0.05)
A: Case	4	162.9092	40.72731	275.34	0.000000*	1.000000
S(A)	299	44.22724	0.1479172			
Total (Adjusted)	303	207.1365				
Total	304					

* Term significant at alpha = 0.05

Kruskal-Wallis One-Way ANOVA on Ranks
Hypotheses
Ho: All medians are equal.

Ha: At least two medians are different.

Test Results

Method	DF	Chi-Square (H)	Prob Level	Decision(0.05)
Not Corrected for Ties	4	201.1012	0.000000	Reject Ho
Corrected for Ties	4	201.1013	0.000000	Reject Ho

Number Sets of Ties 2
Multiplicity Factor 12

Group Detail

Group	Count	Sum of Ranks	Mean Rank	Z-Value	Median
Case I	45	5836.00	129.69	-1.8860	2.9705
Case II	124	26713.00	215.43	10.3599	3.59595
Case III	45	8880.00	197.33	3.7068	3.518
Case IV	45	3886.00	86.36	-5.4688	2.6666
Case V	45	1045.00	23.22	-10.6886	1.54

Means and Effects Section

Term	Count	Mean	Standard Error	Effect
All	304	3.072335		4.731366E-02
A: Case				
Case I	45	3.034693	5.733279E-02	2.98738
Case II	124	3.629607	0.0345381	3.582294
Case III	45	3.504653	5.733279E-02	3.45734
Case IV	45	2.704349	5.733279E-02	2.657035
Case V	45	1.510051	5.733279E-02	1.462737

Kruskal-Wallis Multiple-Comparison Z-Value Test

Perimeter	Case I	Case II	Case III	Case IV	Case V
Case I	0.0000	5.6047	3.6503	2.3384	5.7452
Case II	5.6047	0.0000	1.1828	8.4374	12.5644
Case III	3.6503	1.1828	0.0000	5.9887	9.3955
Case IV	2.3384	8.4374	5.9887	0.0000	3.4069
Case V	5.7452	12.5644	9.3955	3.4069	0.0000

Regular Test: Medians significantly different if z-value > 1.9600
Bonferroni Test: Medians significantly different if z-value > 2.8070

9.5 Appendix 5: Kruskal-Wallis Multiple-Comparison Z-Value Test

Appendix 6: Kruskal-Wallis Multiple-Comparison Z-Value Test

Area 0% Filler Level					
Area	Case I	Case II	Case III	Case IV	Case V
Case I	0.0000	**3.2154**	**5.0156**	**3.1028**	0.0000
Case II	**3.2154**	0.0000	**2.8733**	0.5513	**3.2154**
Case III	**5.0156**	**2.8733**	0.0000	1.9127	**5.0156**
Case IV	**3.1028**	0.5513	1.9127	0.0000	**3.1028**
Case V	0.0000	**3.2154**	**5.0156**	**3.1028**	0.0000
Perimeter 0% Filler Level					
Perimeter	Case I	Case II	Case III	Case IV	Case V
Case I	0.0000	**3.3656**	**5.1372**	**3.1560**	0.0000
Case II	**3.3656**	0.0000	**2.8707**	0.4657	**3.3656**
Case III	**5.1372**	**2.8707**	0.0000	**1.9811**	**5.1372**
Case IV	**3.1560**	0.4657	**1.9811**	0.0000	**3.1560**
Case V	0.0000	**3.3656**	**5.1372**	**3.1560**	0.0000
Area 5% Filler Level					
Area	Case I	Case II	Case III	Case IV	Case V
Case I	0.0000	**3.8862**	0.5737	**3.8070**	**2.1300**
Case II	**3.8862**	0.0000	**4.5820**	**8.5029**	1.3033
Case III	0.5737	**4.5820**	0.0000	**3.2332**	**2.7037**
Case IV	**3.8070**	**8.5029**	**3.2332**	0.0000	**5.9369**
Case V	**2.1300**	1.3033	**2.7037**	**5.9369**	0.0000
Perimeter 5% Filler Level					
Perimeter	Case I	Case II	Case III	Case IV	Case V
Case I	0.0000	**5.7130**	1.3453	**2.1097**	**3.1233**
Case II	**5.7130**	0.0000	**4.0816**	**8.2714**	1.9255
Case III	1.3453	**4.0816**	0.0000	**3.4550**	1.7780
Case IV	**2.1097**	**8.2714**	**3.4550**	0.0000	**5.2329**
Case V	**3.1233**	1.9255	1.7780	**5.2329**	0.0000
Area 10% Filler Level					
Area	Case I	Case II	Case III	Case IV	Case V
Case I	0.0000	**2.9416**	1.1516	**5.7707**	**5.6930**
Case II	**2.9416**	0.0000	**4.3382**	**9.9396**	**3.9621**
Case III	1.1516	**4.3382**	0.0000	**4.6190**	**6.8446**
Case IV	**5.7707**	**9.9396**	**4.6190**	0.0000	**11.4636**
Case V	**5.6930**	**3.9621**	**6.8446**	**11.4636**	0.0000
Perimeter 10% Filler Level					
Area	Case I	Case II	Case III	Case IV	Case V
Case I	0.0000	**5.5568**	1.6273	**3.8451**	**7.4333**
Case II	**5.5568**	0.0000	**3.5834**	**10.2197**	**3.4573**
Case III	1.6273	**3.5834**	0.0000	**5.4725**	**5.8059**
Case IV	**3.8451**	**10.2197**	**5.4725**	0.0000	**11.2784**
Case V	**7.4333**	**3.4573**	**5.8059**	**11.2784**	0.0000
Area 15% Filler Level					
Area	Case I	Case II	Case III	Case IV	Case V
Case I	0.0000	1.8291	0.0839	**5.2296**	**8.2929**
Case II	1.8291	0.0000	1.9307	**8.1641**	**11.8750**

Case III	0.0839	1.9307	0.0000	**5.1457**	**8.2090**
Case IV	**5.2296**	**8.1641**	**5.1457**	0.0000	**3.0633**
Case V	**8.2929**	**11.8750**	**8.2090**	**3.0633**	0.0000
Perimeter 15% Filler Level					
Area	Case I	Case II	Case III	Case IV	Case V
Case I	0.0000	**5.6047**	**3.6503**	**2.3384**	**5.7452**
Case II	**5.6047**	0.0000	1.1828	**8.4374**	**12.5644**
Case III	**3.6503**	1.1828	0.0000	**5.9887**	**9.3955**
Case IV	**2.3384**	**8.4374**	**5.9887**	0.0000	**3.4069**
Case V	**5.7452**	**12.5644**	**9.3955**	**3.4069**	0.0000
Area 20% Filler Level					
Area	Case I	Case II	Case III	Case IV	Case V
Case I	0.0000	0.1250	**4.8097**	**8.4958**	0.5247
Case II	0.1250	0.0000	**5.7076**	**10.1777**	0.7613
Case III	**4.8097**	**5.7076**	0.0000	**3.6862**	**5.3344**
Case IV	**8.4958**	**10.1777**	**3.6862**	0.0000	**9.0206**
Case V	0.5247	0.7613	**5.3344**	**9.0206**	0.0000
Perimeter 15% Filler Level					
Area	Case I	Case II	Case III	Case IV	Case V
Case I	0.0000	**6.3835**	0.6245	**4.5593**	**2.8214**
Case II	**6.3835**	0.0000	**5.6261**	**11.9124**	**2.9620**
Case III	0.6245	**5.6261**	0.0000	**5.1838**	**2.1969**
Case IV	**4.5593**	**11.9124**	**5.1838**	0.0000	**7.3807**
Case V	**2.8214**	**2.9620**	**2.1969**	**7.3807**	0.0000
Regular Test: Medians significantly different if z-value > 1.9600					

REFERENCES

Au, C. O., Johansson, K. and Thron, I. (1995). The Use of Retention and Drainage Aids in the Wet-End. Applications of Wet-End Paper Chemistry. C. O. Au and I. Thorn. New York, Blackie Academic & Professional**:** 13-26.

Bauch, A. J. (1992). Pigments and Fillers. Chemical Processing Aids in Papermaking: A Practical Guide. K. J. Hipolit. Atlanta, TAPPI Press**:** 93-101.

Beauchemin, S., D. Hesterbery, et al. (2002). "Principal Component Analysis Approach for Modeling Sulfur K-XANES Spectra of Humic Acids." Soil Sci. Soc. Am. J. **66**: 83-91.

Beazley, K. M. and House, L. W. (1998). Retention Properties of Clay. Retention of Fines and Fillers During Papermaking. J. M. Gess. Atlanta, TAPPI Press**:** 333-345.

Biermann, C. J. (1996). Handbook of Pulping and Papermaking. San Diego, Academic Press.

Bristow, J. A. (1986). The Pore Structure and the Sorption of Liquids. Paper: Structure and Properties. J. A. Bristow and P. Kolseth. New York, Marcel Dekker, Inc. **8:** 183-201.

Bronze, M. R. and L. F. V. Boas (1998). “Characterisation of brandies ansd wood extracts by capillary electrophesis.” Analusis **26**: 40-47.

Brouwer, P. H., Johnson, M. A. and Olsen, R. H. (1998). Starch and Retention. Retention of Fines and Fillers During Papermaking. J. M. Gess. Atlanta, TAPPI Press**:** 197-242.

Doiron, B. E. (1998). Retention Aid Systems. Retention of Fines and Fillers During Papermaking. J. M. Gess. Atlanta, TAPPI Press**:** 157-176.

Drage, G. and Tamms, O. (2000). Kaolin. Pigment Coating and Surface Sizing of Paper. E. Lehitnen. Helsinki, Finland, Fapet Oy. **11:** 68-93.

Eklund, D. and Lindstrom, T. (1991). Paper Chemistry: An Introduction. Grankulla, Finland, Hango Tryckeri.

Fielding, Alan (2004). http://149.170.199.144/multivar/pca.htm. Manchester Metropolitan University, Manchester UK.

Freeman, J. D. (1994). Newsprint: End Use Requirements & Experiences. TAPPI Papermakers Conference: Proceedings, TAPPI Press.

Georgeson, M. (1995). Starch in Papermaking. Applications of Wet-End Paper Chemistry. C. O. Au and I. Thorn. New York, Blackie Academic & Professional**:** 76-90.

Gibbons, J. D. (1976). Nonparametric methods for quantitative analysis. Atlanta; Holt, Rinehart and Winston.

Gill, R. A. (1995). Fillers for Papermaking. Applications of Wet-End Paper Chemistry. C. O. Au and I. Thorn. New York, Blackie Academic & Professional**:** 54-75.

Halverson, F. (1992). Retention Aids, Drainage Aids, and Flocculants. Chemical Processing Aids in Papermaking: A Practical Guide. K. J. Hipolit. Atlanta, TAPPI Press**:** 103-127.

Hayat, M. A. (1989). Colloidal Gold: Principals, Methods, and Applications. San Diego, California, Academic Press, Inc.

Hayat, M. A. (1995). Immunogold-Silver Staining: Principles, Methods and Applications. Boca Raton, FL, CRC Press.

Hayat, M. A. (2000). Prinicples and Techniques of Electron Microscopy: Biological Applications. Cambridge, United Kingdom, Cambridge Universtiy Press.

Hintze, J., L. (2000). PASS User's Guide. Kaysville, UT

Horisberger, M., J. Rosset, et al. (1975). "Colloidal godl granules as markers for cell surface receptors in the scanning electron micriscope." Experientia **31**: 1147.

Hostetter, D. W. (1991). Driving Forces for Change in the 1990's. TAPPI International Mechanical Pulping Conference: Proceedings, TAPPI Press.

Hsu, Y. H. (1984). "Immunogold for detection of antigen on nitrocellulose paper." Anal. Biochem. **142**: 221.

Kajanto, I., Laamanen, J. and Kainulainen, M. (1998). Paper Bulk and Surface. Paper Physics. K. Niskanen. Helsinki, Finland, Fapet Oy. **16:** 88-115.

Ketola, H. and Andersson, T. (1999). Dry-Strength Additives. Papermaking Chemistry. L. Neimo. Helsinki, Finland, Fapet Oy. **4:** 268-287.

Khantayanuwong, S. (2003). "Determination of the Effect of Recycling Treatment on Pulp Fiber Porperties by Principal Component Analysis." Kasetsart J. (Nat. Sci.) **37**: 219-223.

Leskela, M. (1998). Optical Properties. Paper Physics. K. Niskanen. Helsinki, Finland, Fapet Oy. **16:** 54-87.

Levlin, J.-E. (1999). General Physical Properties of Paper and Board. Pulp and Paper Testing. J.-E. Levlin and L. Sodrehjelm. Helsinki, Finland, Fapet Oy. **17:** 136-161.

Lindholm, C.-A. and Kurdin, J. A. (1998). Chemimechanical Pulping. Mechanical Pulping. J. Sundholm. Helsinki, Finland, Fapet Oy. **5:** 222-249.

McDonough, T. (2003). Personal Conversation, Institute of Paper Science and Technology, Atlanta, GA.

Nesbakk, T., K. Morseburg, et al. (2001). Relationships between Fibre Properties and Cross-sectional Paper Characteristics of Mechanical Pulp Handsheets. TAPPI International Mechanical Pulping Conference Proceedings, TAPPI Press.

Niskanen, K., Kajanto, I. and Pakarinen, P. (1998). Paper Structure. Paper Physics. K. Niskanen. Helsinki, Finland, Fapet Oy. **16:** 13-53.

Norell, M., Johansson, K. and Persson, M. (1999). Retention and Drainage. Papermaking Chemistry. L. Neimo. Helsinki, Finland, Fapet Oy. **4:** 42-81.

Norton, P. (2003). Personal Conversation, Institute of Paper Science and Technology, Atlanta, GA.

Page, D. H. (1969). "A Theory for the Tensile Strength of Paper." TAPPI **52**(4): 674-681.

Palmer, M. (2004). Principal Component Analysis. http://www.okstate.edu/artsci/botany/ordinate.PCA.htm

Pauler, N. (1986). Opacity and Reflectivity of Multilayer Sheets. Paper: Structure and Properties. J. A. Bristow and P. Kolseth. New York, Marcel Dekker, Inc. **8:** 203-224.

Pauler, N. (2000). Paper Optics. Ostervala, Sweden, AB Lorentzen & Wettre.

Retulainen, E., Niskanen, K. and Nilsen, N. (1998). Fibers and Bonds. Paper Physics. K. Niskanen. Helsinki, Finland, Fapet Oy. **16:** 54-87.

Rochow, T. G. and Tucker, P. A. (1994). Introduction to Microscopy by Means of Light, Electrons, X-rays or Acoustics. New York, Plenum Press.

Scallan, A. M. and Borch, J. (1972). "An Interpretation of Paper Reflectance Based Upon Morphology: I. Initial Considerations." TAPPI Journal **55**(4): 583-588.

Scott, W. E. (1996). Principals of Wet End Chemistry. Atlanta, TAPPI Press.

Scott, W. E. and Abbott, J. C. (1995). Properties of Paper: An Introduction. Atlanta, TAPPI Press.

Sharkey, W. A. (1989). Newsprint From a Producer's Viewpoint. Expo Paper Asia: Second International Asian Conference for the Paper Industry, E. J. Krasue & Associates, Inc.

Sheskin, D. J. (2000). Handbook of Parametric and Nonparametric Statistical Procedures. Boca Raton, FL, CRC Press.

Smook, G. A. (1997). Handbook for Pulp & Paper Technologists. Bellingham, Angus Wilde Publications.

Sundholm, J. (1998). What is Mechanical Pulping? Mechanical Pulping. J. Sundholm. Helsinki, Finland, Fapet Oy. **5:** 16-21.

Tienvieri, T., Huusari, E., Sundholm, J., et al. (1998). Thermomechanical Pulping. Mechanical Pulping. J. Sundholm. Helsinki, Finland, Fapet Oy. **5:** 158-221.

Trejdosiewicz, L. K. (1981). "Cell surface distribution of fobronectin in cultures if fibroblasts and bladder derivde epithelium: SEM-immunogold localization compared to immunoperoxidase and immunoflurescence." J. microsc. **123**: 227.

Vaarasalo, J. (1999). Optical Properties of Paper. Pulp and Paper Testing. J.-E. Levlin and L. Sodrehjelm. Helsinki, Finland, Fapet Oy. **17:** 162-181.

Vinson, K. D. (1998). Process for Making Smooth Uncreped Tissue Paper Containing Fine Particulate Fillers. USA, The Proctor & Gamble Company.

Vinson, K. D., Bourbon, R. M., Deason, H. T., et al. (1999). Soft Filled Tissue Paper with Biased Surface Properties. USA, The Proctor & Gamble Company.

Vinson, K. D. and Deason, H. T. (1997). Process for Including a Fine Particulate Filler into Tissue Paper Using an Anionic Polyelectrolyte. USA, The Proctor & Gamble Company.

Vinson, K. D., Erspamer, J. P., Neal, C. W. and Halter, J. P. (1997). Tissue Paper Containing a Fine Particulate Filler. USA, The Proctor & Gamble Company.

Vinson, K. D., Erspamer, J. P., Neal, C. W., et al. (1997). Process for Including a Fine Particulate Filler into Tissue Paper Using Starch. USA, The Proctor & Gamble Company.

Vinson, K. D. and Ficke, J. A. (1998). Soft Tissue Paper with Biased Surface Properties Containing Fine Particulate Fillers. USA, The Proctor & Gamble Company.

Wischnitzer, S. (1970). Introduction to Electron Microscopy. New York, Pergamon Press.

Wise, B. M., and Ricker, N. L. (1991). "Recent Advances in Multivariate Statistical Process Control: Improving Robustness and Sensitivity," IFAC Symposium on Advanced Control of Chemical Processes, pps. 125-130, Toulouse, France.

Xiao, H., Pelton, R., Hamielec, A.. (1996). Tappi J. 79(4):129